

Copyright
by
Sarah Rose van Tol
2022

**The Dissertation Committee for Sarah Rose van Tol Certifies that this is the
approved version of the following dissertation:**

Proviral Roles of Ebola virus VP35 Ubiquitination

Committee:

Alexander N. Freiberg, PhD,
Chair and Co-Mentor

Ricardo Rajsbaum, PhD,
Co-Mentor

Dennis Bente, DVM, PhD

Alexander Bukreyev, PhD

Vineet D. Menachery, PhD

Benhur Lee, MD

Dean, Graduate School

Proviral Roles of Ebola virus VP35 Ubiquitination

by

Sarah Rose van Tol, BS, MS

Dissertation

Presented to the Faculty of the Graduate School of

The University of Texas Medical Branch

in Partial Fulfillment

of the Requirements

for the Degree of

Doctor of Philosophy in Microbiology and Immunology

The University of Texas Medical Branch

April 21, 2022

Dedication

To Sarina van Tol and Rosalyn Croy: the women who gave me everything from my name
to my love for learning, music, and animals

Acknowledgements

To my co-mentors Dr. Alexander Freiberg and Dr. Ricardo Rajsbaum, your mentorship has guided me through a unique predoctoral career. You both have been supportive of my goals from the beginning. Even though my intended dissertation project was filled with challenges, you have been encouraging to me throughout the years. I am grateful to you both for the opportunity to be your graduate student.

Thank you to all the members of the Freiberg lab: Dr. Colm Atkins, Dr. Olivier Escaffre, Dr. Birte Kalveram, Kendra Johnson, Terry Juelich, Jacob Nelson, Jennifer Smith, and Dr. Lihong Zhang; and the Rajsbaum lab: Dr. Preeti Bharaj, Dr. Maria I. Giraldo, Dr. Maria Gonzalez-Orozco, Dr. Leopoldo Aguilera-Aguirre, Karl M. Valerdi, and Abbey N. Warren, I have enjoyed working with all of you over the years. Thank you for all your helpful discussions and encouragement over the years. A special thank you to Terry and Jennifer for being my BSL-4 trainers. Thank you to Dr. Philip Iliny, Dr. Kai Huang, and Dr. Adam Ronk in Dr. Bukreyev's lab for making the recombinant viruses used for these experiments. Thank you to Dr. Maki Wakamiya for generating the knockout mice. Thank you to Dr. Christopher Basler, Dr. Michaela Gack, Dr. Adolfo García-Sastre, and Dr. Gijs Versteeg for generously sharing various reagents.

Thank you to my committee: Dr. Dennis Bente, Dr. Alexander Bukreyev, Dr. Benhur Lee, and Dr. Vineet Menachery your collective expertise in virology, immunology, biochemistry, molecular biology, pathology, and biodefense were invaluable in the success of this project. Thank you to Dr. Lynn Soong for all your support during my time in the Microbiology and Immunology program. Thank you to Andrew Kanost in UTMB's

Molecular Genomics Core for sequencing innumerable plasmid constructs and your kindness over the years.

Thank you to Michelle Vu, Abbey Warren, Scott Segura, Dr. Adam Hage, and Karl Valerdi for being excellent mentees and being patient with me as I gained confidence in a mentorship role. I hope that you all will love molecular cloning as much as I do one day.

Thank you to my former mentors Dr. Stephanie Allard, Dr. Susan Carpenter, Dr. Alyssa Evans, Dr. Sarah Short, Dr. George Dimopoulos, Dr. Alan Scott, and Dr. Andrew Pekosz. I am grateful to each of you everything you have taught me and encouraging me to study what I love. To my good friends Chelsea Hunt, Meaghan Plumb, Renuka Joseph, Megan Weitner, Katherine DuPuis, and Dr. Stephanie Foster, thank you all for your advice, support, and keeping me sane.

Thank you to my family and to my best friend Dr. Adam Hage for their endless love, encouragement, and for always believing in me. Finally, to my beloved cat Mr. Darcy, thank you for reminding me to take a break from studying every now and then.

Proviral Roles of Ebola virus VP35 Ubiquitination

Publication No. _____

Sarah R. van Tol, PhD

The University of Texas Medical Branch, 2022

Co-Supervisors: Alexander Freiberg and Ricardo Rajsbaum

Ebola virus' structural protein VP35 is polyfunctional and plays vital roles in Ebola's life cycle from antagonizing the host's type I interferon pathway to acting as the polymerase co-factor. The mechanisms that regulate which function any given VP35 molecule engages remains unknown. Previously, we observed the host E3 ubiquitin ligase TRIM6 conjugates ubiquitin onto VP35 at lysine (K) 309. This post-translational modification was found to be proviral, but we did not know which VP35 role(s) ubiquitination regulated. We generated recombinant EBOVs encoding glycine (G) or arginine (R) mutations at VP35/K309 (rEBOV-VP35/K309G/-R) and show that both mutations prohibit VP35/K309 ubiquitination. The rEBOV-VP35/K309G mutant loses the ability to efficiently antagonize the IFN-I response, while the rEBOV-VP35/K309R mutant's suppression is enhanced. The replication of both mutants was significantly attenuated in both IFN-competent and -deficient cells due to impaired interactions with the viral polymerase. The lack of ubiquitination on VP35/K309 or TRIM6 deficiency disrupts viral transcription with increasing severity along the transcriptional gradient. This dysregulation of the transcriptional gradient results in unbalanced viral protein production, including reduced synthesis of the viral transcription factor VP30. Blocking VP35/K309 ubiquitination enhanced interaction with the viral nucleoprotein and may trigger premature

nucleocapsid packaging. Prior work also showed that at least one lysine residue other than K309 is ubiquitinated and that VP35 non-covalently interacts with ubiquitin. We observed that multiple residues in VP35's N-terminus can receive covalent ubiquitin, including K119, 126, and 141. Substitution of K119-, 126-, and/or 141-to-R significantly attenuates VP35's polymerase co-factor activity, but their mutation does not alter interactions with the viral polymerase or nucleoprotein. When looking into VP35's non-covalent ubiquitin interaction, we found that VP35 specifically binds K63-linked ubiquitin chains via its C-terminus. The specific cleavage of unanchored ubiquitin chains, using the deubiquitinase isopeptidase T, impedes VP35's non-covalent binding to ubiquitin and stunts EBOV's polymerase activity. Finally, we also found that TRIM25, TRIM6's relative, facilitates ubiquitin ligation onto VP35 and enhances VP35's non-covalent interaction with ubiquitin. EBOV replication is attenuated 100-10,000 fold in cells lacking TRIM25. Overall, our data support that TRIM6- and TRIM25-mediated VP35 ubiquitination and VP35's non-covalent interaction with unanchored ubiquitin is proviral.

This dissertation is based in part on the previously published and submitted manuscripts listed below. I have permission from my co-authors and publishers to use the works listed below in this dissertation. Figures and tables from the listed manuscript which have been used in full or part in this dissertation include a citation in the figure legend. Dissertation sections which have been based on the works listed below include:

Chapter 1: Introduction – Ebola virus and the Ubiquitin System

Chapter 2: Methods for Studying Ebola virus VP35 and its Effects on Replication

Chapter 3: Ubiquitination of Ebola virus VP35 at Lysine 309 Regulates Viral Transcription and Assembly

Chapter 7: Discussion

van Tol, S., Hage, A., Giraldo, M. I., Bharaj, P., Rajsbaum, R. (2017). The TRIMendous Role of TRIMs in Virus-Host Interactions. *Vaccines*, 5(3): E23. doi: 10.3390/vaccines5030023.

van Tol, S., Kalveram, B., Ilinykh, P.I., Ronk, A., Huang, K., Aguilera-Aguirre, L., Bharaj, P., Hage, A., Atkins, C., Giraldo, M. I., Wakamiya, M., Gonzalez-Orozco, M., Warren, A. N., Bukreyev, A., Freiberg, A. N., Rajsbaum, R. (2022). Ubiquitination of Ebola virus VP35 at Lysine 309 Regulates Viral Transcription and Assembly. (Provisionally Accepted 18 April 2022: PLoS Pathogens)

TABLE OF CONTENTS

List of Tables	xiii
List of Figures	xiv
List of Abbreviations	xvii
Chapter 1: Introduction – Ebola virus and the Ubiquitin System	1
<i>Ebolaviruses</i>	1
VP35 as the Polymerase Co-Factor	3
VP35 in Assembly	4
VP35 as a Type-I Interferon Antagonist.....	5
The Host’s Type-I Interferon Pathway	5
VP35-Mediated dsRNA-dependent IFN-I Antagonism.....	7
VP35-Mediated dsRNA-dependent IFN-I Antagonism.....	8
Regulation of VP35’s Functions.....	8
Ubiquitin Post-translational Modifications.....	9
Ubiquitin and Ebola virus	11
Tripartite Motif E3 Ubiquitin Ligases	12
TRIM6.....	13
TRIM25.....	14
Hypothesis & Specific Aims.....	20
Chapter 2: Methods for Studying Ebola virus VP35 Ubiquitination and its Effects on Replication.....	23
Cells and Viruses	23
Generation of <i>Trim6</i> ^{-/-} mice.....	24
Virus Infections and Plaque Assays.....	24
Plasmids	25
Transfections and Immunoprecipitations.....	26
Protein Purification	27
<i>In vitro</i> Ubiquitin Binding Assay.....	27
IFNβ Luciferase Promoter Assay	28
Biotin poly(I:C) Binding.....	29

Minigenome Assay	29
IFN β ELISA.....	29
Western Blots.....	30
RNA Extractions and Quantitative PCR.....	31
Virus Purification.....	32
ATPase Assay	33
Statistics	33
 Chapter 3: Ubiquitination of VP35 at Lysine 309 Regulates Viral Transcription and Assembly	 43
A Basic Residue and Lack of Ubiquitination at VP35/309 is required for efficient IFN-I antagonism	 43
Impairment of TRIM6-mediated VP35/K309 Ubiquitination attenuates EBOV replication	 48
Ubiquitination of VP35/K309 enhances viral transcriptase activity.....	59
Mutation of VP35/309 dysregulates VP35's interaction with EBOV proteins but not binding with TRIM6 or itself	 67
Lack of ubiquitination and a basic residue at VP35/309 dysregulates virus assembly	 76
 Chapter 4: VP35's N-terminus can be Ubiquitinated and Mutation of the K119.126.141 Cluster Attenuates VP35's Polymerase Co-Factor Activity	 141 79
Multiple lysine residues in VP35's N-terminus are ubiquitinated.....	79
Mutation of VP35's lysine residues at positions 119,126, and 141 to arginine impairs VP35's polymerase co-factor activity	 84
Mutation of VP35's N-terminal lysine residues to arginine does not alter IFN- I inhibition, homo-oligomerization, or interaction with other viral proteins	 87
 Chapter 5: VP35 and NP's Interaction with Unanchored, K63-linked Polyubiquitin Enhances Polymerase Activity	 90
VP35 interacts with unanchored ubiquitin.....	90
VP35's C-terminus and NP interact with K63-linked polyubiquitin.....	93
Cleavage of unanchored ubiquitin blocks Ebola virus' polymerase activity.	97
Free ubiquitin is packages in to Ebola virus particles.....	99

Chapter 6: TRIM25 is Proviral and can Ubiquitinate VP35	101
Trim25 Interacts with VP35's C-terminus.....	101
TRIM25 can facilitate VP35 ubiquitination and VP35's non-covalent interaction with ubiquitin.....	104
TRIM25 is a proviral factor for Ebola virus replication	106
Chapter 7: Discussion	109
Ubiquitination of Ebola virus VP35 at Lysine 309 Regulates Viral Transcription and Assembly	109
VP35's N-terminal K119, 126, and 141 can be Ubiquitinated and Facilitate VP35's Polymerase Co-factor Activity	119
Unanchored Ubiquitin Regulates EBOV Polymerase Activity	120
TRIM25 is Proviral During EBOV Infection and can Ubiquitinate VP35	122
Limitations of the Study.....	125
Chapter 8: Conclusions and Future Perspectives	128
Conclusions.....	128
Conservation of VP35 Ubiquitination Across <i>Filoviridae</i>	129
Blocking VP35 Ubiquitination	130
Packaging of Free Ubiquitin into EBOV Particles	131
References	133
VITA	148
Education	149
Publications.....	150

List of Tables

Table 2.1 Oligonucleotides for introducing VP35/K309 mutations into pcDNA3 ...	34
Table 2.2 sgRNA and screening primers for Trim6 ^{-/-} mice	35
Table 2.3 List of plasmids used	37
Table 2.4 Oligonucleotides to generate mutants.....	39
Table 2.5 Oligonucleotides for standard quantitative PCR	40
Table 2.6 Oligonucleotides to assess synthesis of Ebola virus RNA species.....	41

List of Figures

Figure 1.1. Ebola virus transcription and VP35.....	17
Figure 1.2 VP35 antagonism of type-I interferon induction.....	19
Figure 2.1 Validation of Ebola virus strand-specific quantitative PCR.....	42
Figure 3.1 A basic residue and lack of ubiquitination at VP35/309 is required for most efficient IFN-I antagonism.....	46
Figure 3.2 The replication of rEBOV-VP35/K309R and -G mutants is attenuated in IFN-competent cells.....	51
Figure 3.3 The rEBOV-VP35/K309G mutant is impaired in IFN-I antagonism during infection	53
Figure 3.4 TRIM6-mediated VP35/K309 ubiquitination is required for efficient replication	55
Figure 3.5 Attenuation of the rEBOV-VP35/K309R mutant is TRIM6-dependent in primary dendritic cells	56
Figure 3.6 The replication of rEBOV-VP35/K309R and -G mutants is attenuated in IFN-incompetent cells.....	57
Figure 3.7 Ubiquitination of VP35/309 enhances viral transcriptase function.....	63
Figure 3.8 TRIM6 regulates viral transcriptase function.....	65

Figure 3.9 Viral protein synthesis is dysregulated in the absence of VP35/K309 ubiquitination.....	66
Figure 3.10 Mutation of VP35 at K309 dysregulates VP35’s interaction with the EBOV polymerase but not TRIM6 or itself.....	71
Figure 3.11 Ubiquitination of VP35 at K309 impedes interaction with EBOV nucleoprotein	73
Figure 3.12 Lack of ubiquitination and a basic residue at VP35/309 dysregulates VP35’s interaction with viral proteins	75
Figure 3.13 Lack of ubiquitination and a basic residue at VP35/309 dysregulates virus assembly.....	78
Figure 4.1 Multiple lysine residues in VP35’s N-terminus are ubiquitinated	82
Figure 4.2 Mutation of VP35’s lysine residues at positions 119, 126, and 141 to arginine impairs VP35’s polymerase co-factor activity	85
Figure 4.3 Mutation of VP35’s N-terminal lysine residues to arginine does not alter IFN-I inhibition, homo-oligomerization, or interaction with other viral proteins.....	88
Figure 5.1 VP35 interacts with unanchored ubiquitin	92
Figure 5.2 VP35’s C-terminus and NP interact with K63-linked polyubiquitin	95
Figure 5.3 Cleavage of unanchored ubiquitin blocks Ebola virus’ polymerase activity	98

Figure 5.4 Free ubiquitin is packaged into Ebola virus particles.....	100
Figure 6.1 TRIM25 interacts with VP35's C-terminus	103
Figure 6.2 TRIM25 can facilitate VP35 ubiquitination and VP35's non-covalent interaction with ubiquitin.....	105
Figure 6.3 TRIM25 is a proviral factor for Ebola virus replication.....	107
Figure 7.1 A basic residue and ubiquitination capacity of VP35/K309 coordinates VP35's functions.....	115
Figure 7.2 Mutation of VP35 at K309 does not alter VP35's ATPase activity	117
Figure 7.3 A modified form of VP24 is present in rEBOV-eGFP-VP35/wild-type and K309R but not K309G particles	118
Figure 8.1 Alignment of Filovirus VP35	132

List of Abbreviations

A	Alanine
AP-1	Activatory protein 1
βME	β-mercaptoethanol
B	B-box domain
BDBV	<i>Bundibugyo ebolavirus</i>
BMDC	Bone marrow-derived dendritic cell
BOMV	<i>Bombali ebolavirus</i>
CARD	Caspase-activated recruitment domain
CBP	Central basic patch
CC	Coiled-coil domain
cRNA	Viral complementary/anti-genomic RNA
DCs	Dendritic cells
DUB	Deubiquitinating enzymes
dsRNA	Double-stranded RNA
E1	Ubiquitin activating enzyme
E2	Ubiquitin conjugating enzyme
E3	Ubiquitin ligating enzyme
EBOV	<i>Zaire ebolavirus</i>
FBP	First basic patch
G	Glycine
GFP	Green fluorescent protein
GP	Glycoprotein
HMW	high molecular weight
HMPV	Human metapneumonia virus
IA	Iotacetamide

IAV	Influenza A virus
IBV	Influenza B virus
IFN-I	Type I interferon
IID	Interferon inhibitory domain
IKK ϵ	Inhibitor of kappa light polypeptide gene enhancer
IP	Immunoprecipitation
IRF	Interferon regulatory factor
ISG	Interferon stimulated gene
ISGF3	ISG factor 3
IsoT	Isopeptidase T/Ubiquitin specific protease 5
ISRE	Interferon-stimulated response element
JAK1	Janus kinase 1
K	Lysine
K-to-R	Lysine-to-arginine
K48-polyUb	K48-linked poly-ubiquitin chains
K63-polyUb	K63-linked poly-ubiquitin chains
K-all-R	All lysine residues mutated to arginine
kb	Kilobase
KO	Knockout
L	Large polymerase subunit
LC8	Dynein light chain 8
LLOV	<i>Lloviu cuevavirus</i>
ma-EBOV	Mouse-adapted Ebola virus
MARV	<i>Marburg marburgvirus</i>
MAVS	Mitochondrial antiviral signaling protein
MDA5	Melanoma differentiation-associated protein
MEF	Murine embryonic fibroblast

MLAV	<i>Mengla dianlovirus</i>
mEFL35	Filovirus VP35-like element encoded by <i>Myotis</i>
MOI	Multiplicity of infection
MOM	Mitochondrial outer membrane
mRNA	Messenger RNA
NAP1	Nucleosome assembly protein 1
NEM	N-ethylmaleimide
NiV	Nipah virus
NF H ₂ O	Nuclease-free water
NP	Nucleoprotein
NP ^o	Free nucleoprotein
NPBP	Nucleoprotein-binding peptide
NP-RNA	Nucleoprotein-encapsidated RNA
NS1	Nonstructural protein 1
OTU	Ovarian tumor deubiquitinase
P	Phosphoprotein
PAMP	Pathogen-associated molecular pattern
PFU	Plaque forming-unit
polyUb	Poly-ubiquitin chains
PRR	Pattern recognition receptor
PTM	Post-translational modification
R	Arginine
RAVN	Ravn virus
RdRp	RNA-dependent RNA polymerase
RESTV	<i>Reston ebolavirus</i>
RSV	Respiratory syncytial virus
eEBOV-eGFP	Recombinant Ebola virus expressing enhanced GFP

RIG-I	Retinoic acid-inducible gene I
RING	Really interesting new gene E3 ligase domain
RLR	RIG-I-like receptor
S	Serine
sfRNA	sub-genomic flavivirus non-coding RNA
SFTSV	Severe fever with thrombocytopenia syndrome virus
ssRNA	Single-stranded RNA
STAT	signal transducer and activator of transcription
SUDV	<i>Sudan ebolavirus</i>
T	Threonine
TAFV	<i>Tai Forest ebolavirus</i>
TANK	TRAF family member-associated NF- κ B activator
TBK1	TANK binding kinase 1
TNF	Tumor necrosis factor
TRAF	TNF receptor-associated factor
TRIM	Tripartite motif E3 ubiquitin ligase
Tyk2	Tyrosine kinase 2
Ub	Ubiquitin
UBD	Ubiquitin-binding domain
ULM	Ubiquitin-like modifier
USP	Ubiquitin-specific protease
VLP	Virus-like particle
VP24	Nucleocapsid maturation factor; minor matrix protein
VP30	EBOV transcription factor
VP35	Structural protein VP35
VP40	Matrix protein
vRNA	Viral genomic RNA

WCE Whole cell extract

wt Wild-type

Chapter 1: Introduction – Ebola virus and the Ubiquitin System

EBOLAVIRUSES

Filoviruses are a family of non-segmented, negative-sense RNA viruses that include the genus *Ebolavirus*¹. Six *Ebolavirus* species have been identified: *Bombali ebolavirus* (BOMV), *Bundibugyo ebolavirus* (BDBV), *Reston ebolavirus* (RESTV), *Sudan ebolavirus* (SUDV), *Tai Forest ebolavirus* (TAFV), and *Zaire ebolavirus* (EBOV). Of these, four species, BDBV, SUDV, TAFV, and EBOV are virulent and cause lethal infection in humans. EBOV has been the most devastating of the six *Ebolavirus* species to humans causing over twenty known outbreaks and nearly 15,000 deaths^{2,3}. Despite the recent approval of an efficacious vaccine and two therapeutic monoclonal antibodies^{4,5}, an improved understanding of EBOV's replication cycle and interaction with the host is needed to broaden the treatments to additional targets.

The nearly 19 kilobase (kb) EBOV genome encodes seven structural proteins: nucleoprotein (NP), polymerase co-factor (VP35), matrix protein (VP40), glycoprotein (GP), transcription factor (VP30), nucleocapsid maturation factor (VP24), and the large polymerase subunit containing the RNA-dependent RNA polymerase (RdRp), polyribonucleotidyltransferase (PRNTase), and methyltransferase (MTase) enzymatic functions (L)^{6,7}. Upon entry into the cell, the virus undergoes primary transcription. The EBOV transcriptase, comprised of VP35, VP30, and L, loads onto the 3' end of the genome and initiates at the transcriptional start site of the first gene, NP⁶. The transcriptase navigates the transcriptional stop and start signals within the genome's intergenic regions without falling off to synthesize messenger RNA (mRNA) for each subsequent gene. If the

transcriptase is unable to read through these signals, the complex will dissociate from the genomic RNA (vRNA) template, re-load onto the 3' end, and initiate NP mRNA transcription. This discontinuous transcription produces a 3'-to-5' gradient of viral mRNAs with NP and L being the most and least abundant, respectively⁸⁻¹⁰ (Figure 1.1A). Following primary transcription, the viral proteins will be in sufficient abundance for replication. The viral replicase, L with VP35, works in cooperation with NP to generate the NP-encapsidated complementary/anti-genomic RNA (cRNA) from the NP-associated vRNA. Nascent genomes are then synthesized from the cRNA, and the vRNA serves as a template for secondary transcription or is packaged into progeny virus.

A mature nucleocapsid must be formed for EBOV vRNA to be packaged¹¹, and the components include the NP-vRNA, VP35, and VP24¹². Prior to being incorporated into virions, the nucleocapsid must be condensed. This maturation occurs once VP24 is recruited, and the rigidification of the mature nucleocapsid occludes the polymerase's access to vRNA^{13,14}. To this point, the signal(s) leading to VP24 recruitment remains unknown. Subsequently, the mature nucleocapsid interacts with VP40 to enable budding from GP-rich membranes¹¹.

Regulation of the events that initiate the polymerase replicase-transcriptase transition and the formation of a mature nucleocapsid is crucial to complete the viral life cycle efficiently and to produce infectious virus. The viral and host factors that coordinate these critical stages of viral replication are unknown beyond the need for dephosphorylated VP30 for transcription¹⁵⁻¹⁹ and VP24 for nucleocapsid maturation^{12,13}. VP35, a component of both the active polymerase complex⁶ and the mature nucleocapsid^{11,12}, is a potential regulator of the replicase-transcriptase transition and nucleocapsid formation. A review of

VP35 provides context for the experimental approach used to study this protein. The following is a discussion of VP35's characterized roles and associated functional regions (Figure 1.1B and 1.1C).

VP35 AS THE POLYMERASE CO-FACTOR

VP35's polymerase co-factor activity is required for the polymerase's transcriptase and replicase functions. This function relies on multiple interactions with both viral and host proteins. On the viral protein side, VP35 acts as bridge between L and the NP-vRNA template as NP and L do not interact in the absence of VP35^{7,20}. A region within VP35's N-terminus is required to bind the polymerase²¹, while the C-terminal first basic patch (FBP) facilitates interaction with NP²². The C-terminal-NP interacting region is predicted to bring NP-RNA into proximity of the polymerase²². VP35 also acts as a chaperone for RNA-free, monomeric nucleoprotein (NP^o). The N-terminal NP-binding peptide (NPBP) of VP35 is required to prevent NP's premature association with RNA^{23,24}. The NPBP is conserved among filoviruses and enables the coupling of viral replication and NP-vRNA and -cRNA encapsidation²³⁻²⁶. When the NPBP is deleted, VP35's polymerase co-factor activity is ablated²³. Of note, VP35 interacts indirectly with VP30 through L, NP, and RNA^{15,17}.

An important characteristic of filovirus VP35 is its ability to homo-oligomerize²⁷⁻³¹. The N-terminal coiled-coil region is required for self-interaction^{27,31}, and EBOV VP35 can form either trimers or tetramers while other *Ebolavirus* species' VP35 is predicted to form only asymmetric tetramers²⁸. When VP35 is mutated to ablate key leucine residues within the coiled-coil or the N-terminus is deleted, VP35 loses polymerase co-factor

activity³¹, interaction with L²¹, and type I interferon antagonism^{27,30,32}. Homooligomerization is also required for interaction with dynein light chain 8 (LC8) and the ablation of this interaction attenuates VP35's polymerase co-factor activity³³. Interestingly VP35's LC8 interacting peptide is located upstream of the coiled-coil region^{34,35} suggesting that VP35's ability to self-interact may impact binding affinity with partner proteins. Since VP35's interactions with itself, L, NP-RNA, NP°, and host proteins are required for efficient polymerase co-factor activity, different VP35 monomers within the asymmetric oligomer are hypothesized to perform different functions.

Recently, VP35 has been described to have ATPase- and helicase-like activities that are predicted to contribute toward its polymerase co-factor function. VP35 binds double-stranded RNA (dsRNA) and unwinds regions with a 5' overhang³⁶. Deletion of amino acids 137-173 or treatment with guanidine hydrochloride prohibits VP35's NTPase- and helicase-like activities and attenuates EBOV replication and transcription when using a minigenome system³⁶.

VP35 IN ASSEMBLY

Although the mechanisms have not been characterized, VP35 has also been indicated as a regulator of nucleocapsid maturation and incorporation into virions. When VP40 is co-expressed with the EBOV minigenome, NP, L, VP30, and VP35, the incorporation of EBOV minigenome vRNA into VP40 virus-like particles (VLPs) is VP35-dependent³⁷. Further, VP35 from both EBOV and Marburg virus (MARV) has been shown to increase VP24's recruitment to nucleocapsids to facilitate rigidification^{11,38}.

VP35 AS A TYPE-I INTERFERON ANTAGONIST

The most thoroughly studied VP35 function is antagonism of the host's antiviral immune response (Figure 1.2). Before describing the mechanisms of VP35-mediated type I interferon (IFN-I) inhibition, we will briefly overview the innate antiviral response.

The Host's Type-I Interferon Pathway

Cells identify pathogen invasion due to the presence of pathogen-associated molecular patterns (PAMPs) contained in viral components, which are recognized by host pattern recognition receptors (PRRs)³⁹. Examples of viral PAMPs include some envelope or capsid proteins, viral nucleic acid, or intermediates of genome replication³⁹. Upon PAMP engagement of a PRR, a signaling cascade is initiated that relies on post-translational modifications (PTMs) for proper coordination. These modifications include ubiquitination and phosphorylation, which facilitate the assembly of adaptor and enzymatic molecules needed to activate and inactivate transcription factors and other effector molecules³⁹⁻⁴¹. These transitions in the transcriptional profile and functional proteome enable the cell to respond optimally to the pathogen and to communicate (e.g., cytokine secretion) with neighboring cells to limit viral replication and promote clearance. Examples of pathways critical in response to viral infection include IFN induction and signaling and NF- κ B activation⁴².

A common pathway activated during virus infection is the retinoic acid-inducible gene I (RIG-I)-like receptor (RLR) pathway. Cytoplasmic viral dsRNA or single-stranded RNA (ssRNA) containing 5'-triphosphates produced during replication act as agonists for RLRs RIG-I and melanoma differentiation-associated protein (MDA5)⁴³⁻⁴⁶. RIG-I and

MDA5 bind distinct viral RNA agonists yet they induce similar downstream antiviral pathways ⁴⁷. RLRs are ATP-dependent RNA helicases that have two N-terminal caspase-activated recruitment domains (CARDs), a central DEAD box, and an auto-inhibitory C-terminal domain ⁴⁸. The unique PAMPs recognized by these receptors enable the host to respond to a broader range of pathogens ⁴⁷. Upon engagement of the PAMP with the RLR, a conformational shift exposes the CARDs, which allows homo-oligomerization and recruitment of the RLRs to their adaptor mitochondrial antiviral signaling protein (MAVS) at the mitochondrial outer membrane (MOM) ^{44,49-51}. A variety of factors influence the activation of RLRs downstream of PAMP recognition including ATP hydrolysis ^{44,52}, RLR oligomerization ^{49,50,52}, and PTMs ⁵³⁻⁵⁷. Interaction of the N-terminal CARDs of both the RLRs and MAVS induces the adaptor to form prion-like aggregates and exposes domains to recruit critical RING E3 ligases including tumor necrosis factor (TNF) receptor-associated factors (TRAFs) 3 and 6 ^{58,59}.

Downstream of TRAFs 3 and 6, both the NF- κ B and IFN-I arms of the innate antiviral response are activated. As VP35 is unable to inhibit NF- κ B, we will focus on the IFN-I pathway. TRAF3, in cooperation with NEMO, recruits and stabilizes TRAF family member-associated NF- κ B activator (TANK) or nucleosome assembly protein (NAP1) which are critical in linking TANK binding kinase 1 (TBK1), and in some cases inhibitor of kappa light polypeptide gene enhancer in B cells (IKK ϵ), to the MAVS signalosome ^{59,60}. Once activated, TBK1 and/or IKK ϵ phosphorylate the IFN regulatory factor (IRF) 3 and IRF7 ^{61,62}. Upon phosphorylation, the IRFs homodimerize and translocate to the nucleus where they bind to DNA regulatory regions ^{61,63}. To induce optimal IFN β transcription, activated IRF3, NF- κ B, and AP-1 (activator protein 1) must translocate to

the nucleus and bind to their respective regulatory regions of the *Ifnb1* promoter⁴². The resulting IFN β is then secreted and signals in a paracrine and autocrine manner. Binding of IFN β to its heterodimeric receptor results in the activation of tyrosine kinases, Janus kinase 1 (JAK1) and tyrosine kinase 2 (Tyk2), which phosphorylate signal transducer and activator of transcription (STAT) 1 and STAT2. Following phosphorylation, STAT1 and STAT2 heterodimerize and associate with IRF9 to form IFN-stimulated gene (ISG) factor 3 (ISGF3) and translocate to the nucleus⁶¹. Within the nucleus, ISGF3 binds to genes with an IFN-stimulated response element (ISRE) in their promoter to activate transcription⁶¹. The resulting proteins expressed from ISGs create a cellular environment that is prohibitive to viral entry and replication⁶¹. As with other immune pathways, ISGF3 also promotes the transcription of type-I IFN negative regulators to mitigate deleterious effects⁶¹.

VP35-Mediated dsRNA-dependent IFN-I Antagonism

Ebolavirus VP35 is able to suppress the RLR pathway both at and downstream of dsRNA recognition. VP35's C-terminal domain, also known as the IFN inhibitory domain (IID), mediates VP35's antagonism of the IFN-I induction pathway⁶⁴. Structurally, the IID is comprised of two basic residue clusters linked by two proline residues⁶⁵. The FBP, in addition to facilitating interaction with NP-RNA²², is required for proper folding of the dsRNA-binding central basic patch (CBP)⁶⁵. Mutation of residues that facilitate contact between the FBP- and CBP-containing sub-domains, such as isoleucine 340 and phenylalanine 239, destabilize the IID structure⁶⁵. The CBP has a large distribution of positive charge with several lysine (K) and arginine (R) residues that facilitate interaction with dsRNA. EBOV VP35's IID forms an asymmetric dimer on dsRNA due to some residues interacting with the dsRNA backbone, R312, R322, and K339, and the dsRNA

ends, F239 and H240 ⁶⁵. VP35's R305, K309, and K319 enhance interaction with the dsRNA backbone, but they are not required ^{65,66}. Binding to dsRNA allows VP35 to prevent the hosts' RLRs from recognizing viral RNA ^{67,68}. Substitution of the key dsRNA backbone-interacting basic residues for alanine (A) in recombinant EBOV results in significantly attenuated infection in rodent ^{69,70} and non-human primate ⁷¹ models of infection.

VP35-Mediated dsRNA-dependent IFN-I Antagonism

In addition to dsRNA-dependent IFN-I antagonism, VP35 is also able to antagonize through a dsRNA-independent route. VP35 is able to prevent both TBK1- and IKK ϵ -mediated IRF3 phosphorylation to prevent IFN-I production ^{67,68,72}. The mechanism underlying this route of inhibition remain enigmatic, but the inhibition takes place prior to IRF3 phosphorylation as VP35 cannot inhibit the constitutively active, phosphomimetic IRF3 construct (5D) ⁷³. VP35 can also block IRF7 through promoted PIAS1-mediated SUMOylation and is hypothesized to be important for antagonizing IFN-I induction in dendritic cells (DCs) ⁷⁴. Importantly, VP35 is linked to the impairment of DC maturation thus impeding the activation of the adaptive arm of the host's immune system ⁷⁵⁻⁷⁸. Mutations that block VP35's antagonism of IFN-I binding and IID intramolecular interactions suppress VP35's capacity to antagonize DC maturation suggesting a link between DC activation and IFN-I induction following EBOV infection ^{77,78}.

REGULATION OF VP35'S FUNCTIONS

Despite VP35 being known to participate in all of the functions described above, the mechanisms underlying the function that any given VP35 molecule may engage

remains unknown. Stochasticity likely contributes to VP35's functional flexibility, but specific signals could trigger VP35's capacity to engage in certain functions. Post-translational modifications, for example could modify the function(s) VP35 can participate. Importantly, PTMs on VP35, including phosphorylation and ubiquitination, have been described to enhance VP35's polymerase co-factor activity⁷⁹⁻⁸¹. VP35 phosphorylation at serine (S) 187⁸¹ and threonine (T) 210⁸⁰ have been described to promote VP35's polymerase co-factor activity. The mechanism for S187 has not been described, but T210 phosphorylation enhances binding with NP^{80,81}. We previously discovered VP35 ubiquitination at K309 via the host E3 ubiquitin ligase TRIM6⁷⁹. Ubiquitination at VP35/K309 facilitates polymerase co-factor activity and lack of TRIM6 impairs VP35 ubiquitination and virus replication⁷⁹. Although we observed a proviral phenotype for TRIM6-mediated VP35/K309 ubiquitination, we did not know which of VP35's functions this PTM regulates. Before delving into our hypothesized functions of VP35/K309 ubiquitination, we will briefly review ubiquitination and the TRIM family.

UBIQUITIN POST-TRANSLATIONAL MODIFICATIONS

Ubiquitin is a key protein in orchestrating cellular and viral functions including immune responses and viral budding. Ubiquitin (Ub) is a 76-amino-acid protein that associates either covalently or non-covalently with proteins^{40,82,83}. The addition of Ub to a protein target is catalyzed by three classes of Ub enzymes. The Ub activating enzyme (E1) binds the C-terminal glycine of Ub to its active-site cysteine in an ATP-dependent manner to form a high-energy thioester bond^{40,82}. Interaction of the E1 with Ub exposes a site to enable the recruitment of the next enzyme⁸⁴. Via a trans-thiolation reaction, the Ub is

transferred from the E1 to the Ub conjugating enzyme's (E2) active-site cysteine^{40,82}. Once the Ub is bound, an Ub ligating enzyme (E3) can interact with an E2-Ub conjugate and assist in the transfer of the Ub onto a target protein^{40,82}. When covalently attaching Ub to a protein, most often the Ub is covalently linked at a K's ϵ -amino group^{40,82}.

Since Ub has seven lysine residues itself, K6, 11, 27, 29, 33, 48, and 63, the Ub enzymes can coordinate the formation of covalently linked poly-ubiquitin chains (polyUb)^{40,82}. In addition, Ub molecules can be linked in a head-to-tail orientation in which the donor Ub's C-terminal glycine is linked to the acceptor ubiquitin's methionine-1 amino group^{40,82}. The E2 primarily determines the Ub chain topology^{84,85} while the E3 is more important in identification and recruitment of the appropriate target⁸⁴. Ubiquitin can be covalently linked to a protein as a single Ub at one site (mono-ubiquitination), single Ub molecules at multiple Ks of the same target protein (multi-mono-ubiquitination), or a covalently linked chain of Ub ligated onto a single K (covalent polyUb)⁸². Additionally, Ub cascade enzymes can synthesize unanchored polyUb (non-covalent polyUb) that act as a ligand for proteins containing an ubiquitin-binding domain (UBD)^{82,84,86,87}. The unique combination of polyUb chain topologies, covalent or non-covalent modifications, and chain length variation allows for precise signaling regulation.

The host encodes a variety of mechanisms to enact, regulate, and interpret this complex 'ubiquitin code.' Ubiquitin modification can directly influence the target molecule through induction of a conformational change. Such changes may recruit other molecules, expose a subcellular localization sequence, or alter protein stability^{82,83}. Recognition of Ub by UBD-containing proteins is analogous to a receptor binding its ligand. The UBD-containing proteins may recognize a specific polyUb topology (e.g.,

UBD specifically recognizing K48-linked polyUb chains (K48-polyUb)) and/or chain length (e.g., a UBD that interacts with mono-Ub) and then recruit specific molecules to create a signaling complex ^{82,83,88}. Although some exceptions exist, different polyUb topologies are associated with particular effector responses. The best-characterized examples include K48-polyUb, which stereotypically target proteins for proteasome-mediated degradation, or K63-linked polyUb (K63-polyUb), which generally coordinate cell signaling complexes and subcellular localization ^{82,83}. Despite the canonical roles of these chain topologies, K48-polyUb have been noted to be involved in promoting signaling complex assembly ⁸⁹ and K63-polyUb can mark protein targets for degradation ⁹⁰. To regulate the Ub response, the host also encodes deubiquitinating enzymes (DUB) or ubiquitin specific proteases (USP), which can disassemble polyUb or coordinate the removal of ubiquitinated enzymes ^{82,83}. Overall, the host encodes the enzymes necessary to generate, respond to, and eliminate Ub modifications.

Ubiquitin and Ebola virus

Several ubiquitin and ubiquitin-like proteins have been found to regulate the functions of EBOV proteins. EBOV's matrix protein, VP40, utilizes the host's E3 ubiquitin ligases SOCS3, SMURF2, WWP1, ITCH, and Nedd4 to facilitate egress of VLPs ⁹¹⁻⁹⁷. Inhibitors that block the WW domain, present in SMURF2, WWP1, ITCH, and Nedd4, from interacting with VP40's PPxY late domain impede the production of VLPs ^{98,99}. Interestingly, the ubiquitin-like modifier (ULM) ISG15 can also block VP40 ubiquitination to disrupt virus budding ¹⁰⁰. Modification of VP40 with ULM SUMO at K326 has also been reported to be incorporated into VLPs ¹⁰¹. VP24 is modified by covalent ligation ubiquitin and SUMO to regulate nuclear translocation and IFN-I signaling antagonism ¹⁰².

VP24 also contains a SUMO-interacting motif to enable non-covalent interactions ¹⁰². Treatment with USP7, which cleaves SUMO, prevents VP24's ubiquitin modification which enhances its IFN-I antagonism ¹⁰². The role of these VP24 PTMs on EBOV replication have not been investigated. The E3 ubiquitin ligase RBBP6 blocks NP-VP30 interaction by mimicking NP's binding motif, PPxPxY, but the potential role of RBBP6-mediated ubiquitination onto EBOV proteins has not been investigated ¹⁰³. The E3 ligase MARCH8 antagonizes budding of vesicular stomatitis virus pseudoparticles expressing EBOV's GP ¹⁰⁴ and blocks GP surface expression on transfected 293T cells through inhibition of furin cleavage which cause retention of GP in the Golgi ¹⁰⁵. As mentioned above, TRIM6 ubiquitinates VP35/K309 and EBOV replication is attenuated when TRIM6 is absent ⁷⁹.

TRIPARTITE MOTIF E3 UBIQUITIN LIGASES

Tripartite motif proteins (TRIMs) are an E3 ligase family critical in many cellular functions, including the regulation and coordination of innate immunity and antiviral responses ^{86,87,106-109}, but they can also be hijacked to facilitate viral replication ^{79,110}. The conserved RBCC domain gives TRIMs their name. The RBCC domain includes a really interesting new gene E3 ligase domain (R-RING), one or two B-box domains (B), and a coiled-coil domain (CC) ^{40,111}. Like other RING motif-containing E3 ligases, the RING domain of TRIMs usually mediates the interaction with Ub-bound E2 via the zinc finger motifs ^{40,84,112}. These motifs are comprised of key cysteine and histidine residues that coordinate binding to two zinc ions and facilitate protein–protein interactions ^{40,84,112}. The function of the B is less well characterized, however studies suggest that this domain is

important in coordinating TRIM self-association and protein–protein interactions, including higher-order TRIM oligomerization (reviewed in ¹¹²). The CC is a hyper-helical structure that allows for dimerization and self-association of TRIMs ¹¹¹⁻¹¹⁴. Often, dimerization of TRIMs via the CC domain and formation of higher order oligomerization through the B is critical for TRIM function and E3 ligase activity ^{112,113,115-119}. The variable C-terminal region of TRIMs is responsible primarily for interaction with target proteins and subcellular localization ^{40,111,120}. To date, 11 classes of TRIM C-terminal domains have been characterized ^{87,111,112}. The most prevalent TRIM C-terminal domain is the B30.2, or PRY-SPRY, domain with approximately 40 members identified in humans including TRIMs 6 and -25 ^{86,112,121}. TRIMs' PTMs ^{89,122-126}, alternatively spliced isoforms ^{109,127,128}, and heterodimerization ^{111,129} expand the diversity and functionality of this protein family.

In addition to differential mRNA expression upon viral infection, several TRIM family members are intimately involved in the antiviral response. Type-I IFNs and other cytokines have been noted to differentially regulate the expression of a significant population of TRIMs ^{87,130-136}. Likewise, TRIM overexpression influences the transcription of type-I IFN, pro-inflammatory cytokines, and ISGs ^{87,109}. The roles of TRIMs in viral infection include intrinsic restriction of viral pathogens, positive regulation of immune pathways that promote viral clearance, and negative regulation of antiviral pathways to limit immunopathology ^{86,87,137}. The incorporation of TRIM antagonists into viral genomes exemplifies the importance of TRIMs in antiviral responses ¹³⁸⁻¹⁴³.

TRIM6

TRIM6 has been described as a regulator of the IFN-I induction and signaling pathways, a target of viral-mediated antagonism, and a proviral factor. Initially, TRIM6

was observed to enhance the IFN β promoter activation following stimulation with constitutively active RIG-I¹⁰⁹, TBK1, or IKK ϵ ⁸⁹. Thorough molecular characterization, TRIM6 was found to facilitate IKK ϵ oligomerization and synthesis of IKK ϵ -dependent ISG's through the synthesis of unanchored, K48-linked poly-Ub in cooperation with E2 Ube2K⁸⁹. TRIM6 is needed for effective antiviral responses following infection including West Nile virus and Influenza A virus (IAV)^{141,144,145}. Further evidence of TRIM6 as an antiviral factor is highlighted by our findings that the Nipah virus (NiV) matrix protein facilitates TRIM6 degradation which impairs the hosts' IFN-I response¹⁴¹. In contrast to the antiviral role observed with other viruses, our EBOV infection studies clearly demonstrated that TRIM6's IFN-I regulatory roles were subverted, and VP35 appropriates TRIM6 to promote virus replication⁷⁹.

TRIM25

Several TRIMs positively regulate the receptors RIG-I and MDA5¹⁴⁶⁻¹⁴⁸. The best characterized example of TRIM-mediated RIG-I activation involves TRIM25. TRIM25 ligates K63-linked polyUb chains onto RIG-I's N-terminal CARD at K172, which induces downstream signaling¹⁴⁸. Additionally, TRIM25 catalyzes the synthesis of unanchored, non-covalent K63-polyUb, which facilitate RIG-I oligomerization and stabilization⁵⁵ to promote RIG-I CARDS' interaction with MAVS¹⁴⁹. TRIM25 has been implicated in the K48-polyUb of MAVS, which results in its proteasome-mediated degradation and release of downstream signaling molecules (TBK1, NEMO, and possibly TRAF3) to induce IFN-I production¹⁵⁰. Adding complexity to this system, TRIM25 can synthesize K48-polyUb to antagonize RLR activation. TRIM25 K48-linked polyubiquitination negatively regulates RLR activation, but USP15 can specifically disassemble these poly-Ub chains to stabilize

TRIM25¹⁵¹. The role of TRIM25 in the regulation of RLR pathways and/or type-I IFN induction has been shown to be conserved among different species including salmonids¹⁵², birds¹⁵³⁻¹⁵⁵, reptiles¹⁵⁶, and mammals¹⁵⁶.

Several viruses have been described to antagonize TRIM25's role in inducing the RLR pathway. The nonstructural protein 1 (NS1) of IAV and Influenza B virus (IBV) has been characterized as a viral antagonist of host innate immunity through interactions with TRIM25^{142,154,157,158}. The NS1 protein from IAV directly interacts with TRIM25's CC to impede its multimerization^{142,159}. Since dimerization is required for TRIM25 E3 ligase activity, NS1 binding to TRIM25 blocks RIG-I ubiquitination and downstream signaling, resulting in a reduced antiviral response^{142,159}. The TRIM25 interaction with IAV NS1 is virus strain and host species-specific. Human TRIM25 interacts with IAV strains isolated from many species, chicken TRIM25 binds only NS1 from avian strains, and murine TRIM25 does not bind any NS1¹⁵⁴. The nucleoprotein of SARS-CoV was demonstrated to interact with the SPRY domain of TRIM25, preventing the necessary interaction and subsequent ubiquitination of the RIG-I CARD domains¹⁶⁰. A similar loss of RIG-I-induced IFN β is achieved when MERS-CoV nucleoprotein associates with TRIM25¹⁶⁰. For DENV, Manokaran et al. compared two viral sequences (PR1 and PR-2B) and identified mutations that resulted in the increased production of sub-genomic flavivirus non-coding RNAs (sfRNAs) by the PR-2B strain¹⁴⁰. The PR 2B sfRNAs were capable of binding to host TRIM25 and prevented USP15-mediated deubiquitination¹⁴⁰, which is crucial for activation of RIG-I¹⁵¹. The NSs protein of severe fever with thrombocytopenia syndrome virus (SFTSV), a negative-sense RNA virus in the family *Bunyaviridae*, interacts directly with TRIM25, and indirectly with RIG-I and TBK1 to isolate these signaling molecules

from associating with MAVS ¹⁶¹. As with the other viral protein-TRIM25 interactions described above, downstream activation of IRF3 and subsequent IFN β production are impaired ¹⁶¹. The accessory protein V from NiV and other paramyxoviruses is capable of inhibiting TRIM25-dependent activation of RIG-I¹⁶². NiV-V interacts with both the SPRY domain of TRIM25 and the CARD domains of RIG-I¹⁶². The V protein is hypothesized to stabilize the TRIM25-RIG-I complex to impede the downstream steps of the IFN-I induction pathway including RIG-I ubiquitination ¹⁶². TRIM25 is a common target of a diverse group of RNA viruses, suggesting that other pathogens may also impair TRIM25-mediated stimulation of the RLR pathway. To this point, no proviral roles for TRIM25 have been described.

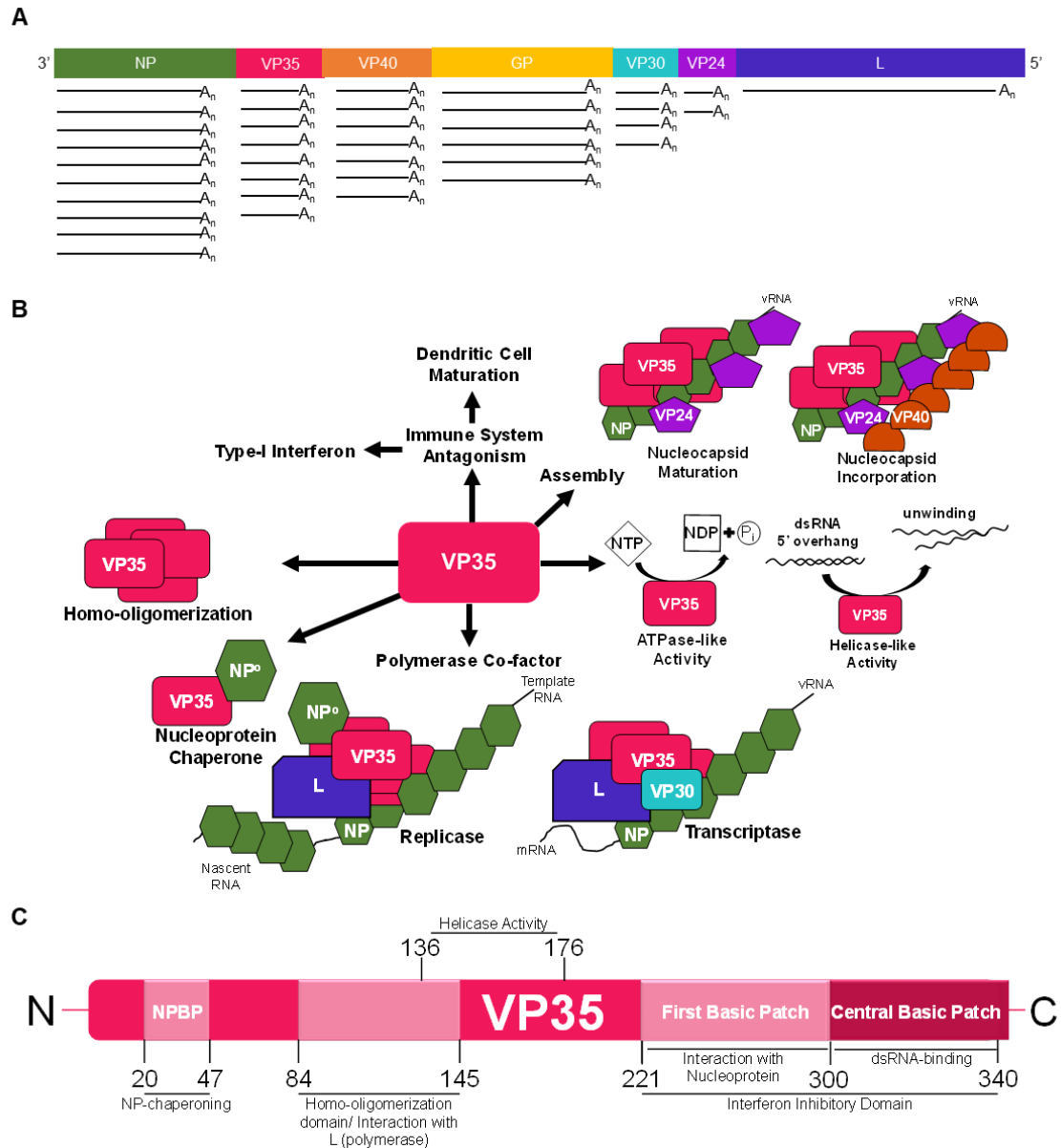


Figure 1.1. Ebola virus transcription and VP35

(A) A basic representation of Ebola virus' negative-sense genome to show gene order. Ebola virus (EBOV) discontinuously transcribes its genes, generation a transcriptional gradient. (B) A schematic reviewing EBOV VP35's diverse functions. VP35 (pink rectangle with 'VP35') is able to homo-oligomerize and is represented here as a tetramer. To prevent free nucleoprotein (green hexagon with 'NP^o') from prematurely binding to RNA, VP35 binds via its N-terminal NP binding peptide (NPBP). VP35 also acts as the essential polymerase co-factor. As part of the replicase, VP35 molecules interact with the large polymerase (indigo shape with 'L') subunit as well as NP^o and NP-encapsidated template viral RNA to facilitate the synthesis of nascent RNA. VP35 also acts as the co-factor for the polymerase's transcriptase function which also requires the transcription factor VP30 (light blue rectangle with 'VP30') to synthesize viral mRNAs from the

genomic RNA (vRNA). VP35 also has ATPase- and helicase-like activities which are expected to aid in its polymerase co-factor function. Studies have also implicated VP35 facilitating virus assembly through recruitment of the nucleocapsid maturation factor VP24 (purple pentagon with 'VP24') and promotes incorporation of the mature nucleocapsid into VP40 (orange half circle with 'VP40') rich membranes. VP35 is also an immune antagonist that suppresses the host's type I interferon induction pathway and dendritic cell maturation. (C) Linear representation of VP35 protein and its sub-domains with the associated amino acid boundaries indicated. (Figure created by Sarah van Tol)

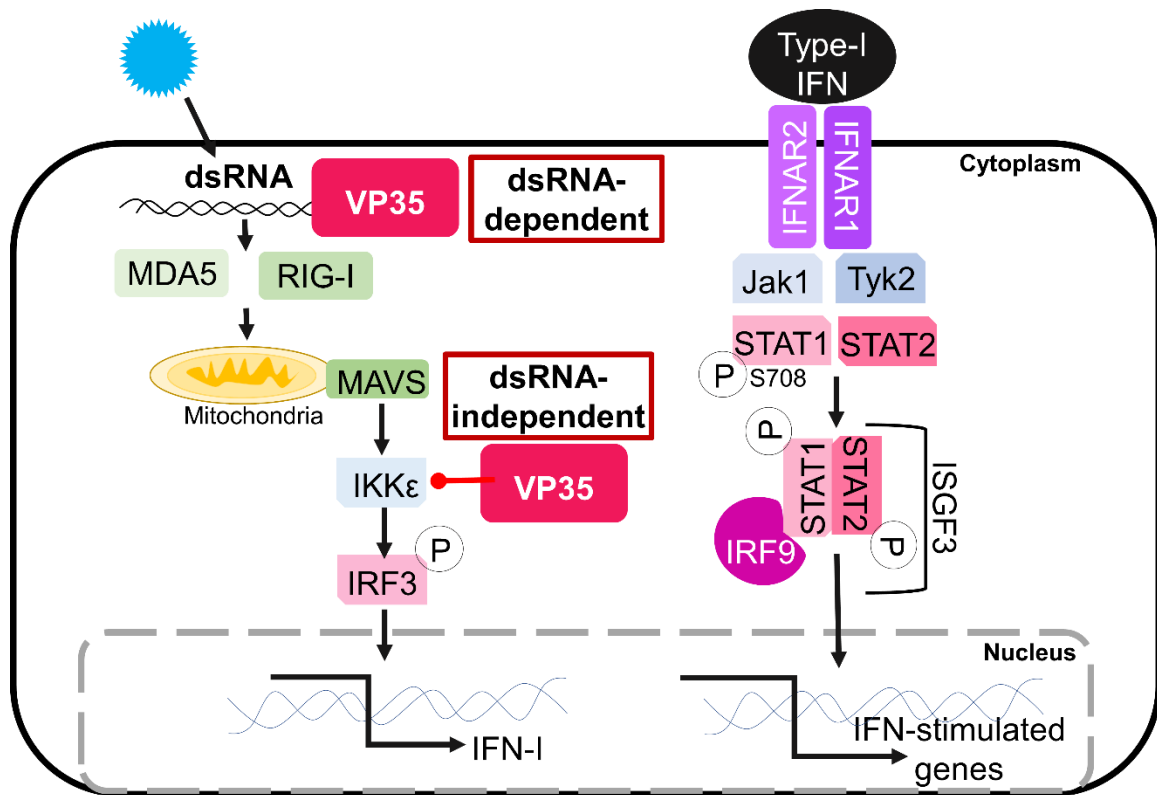


Figure 1.2 VP35 antagonism of type-I interferon induction

During Ebola virus infection, double-stranded (ds) RNA intermediates are produced and can act as a stimulus for the host cytoplasmic RNA receptors RIG-I and MDA5. Without VP35 present, the foreign RNA would activate the RIG-I-like receptors and activate MAVS leading to the activation kinases TBK1 and IKK ϵ . The kinases then phosphorylate transcription factors IRF3 and/or IRF7 which translocate to the nucleus to stimulate the expression of type I interferon (IFN). IFN will then signal through the type I IFN receptor (IFNAR1/2) to stimulate the formation of active STAT1/STAT2 heterodimers which interact with IRF9 to form the ISGF3 complex to trigger the expression of interferon-stimulated genes. VP35 inhibits the IFN-I induction pathway through dsRNA-dependent (direct binding to RNA to prevent recognition by RLRs) and -independent (blocking the IRF3 kinases) mechanisms. (Figure created by Sarah van Tol)

HYPOTHESIS & SPECIFIC AIMS

The unique role for TRIM6 in the context of EBOV infection prompted us to examine the role of VP35/K309 ubiquitination in-depth. The VP35/K309-TRIM6 study also raised related areas of study including ubiquitination at other K residues, non-covalent interaction with Ub, and the potential for redundancy among TRIM family members in ubiquitinating VP35. A VP35/K309A mutant receives less covalent Ub than wild-type VP35⁷⁹, but the other Ub-modified K(s) have not been identified. We also observed that VP35 interacts with non-covalent Ub⁷⁹, but the functional relevance is unknown. Further, Ub immunoprecipitated with VP35 in the absence of TRIM6⁷⁹ supporting that covalent Ub modification by another E3 ligase and/or interaction with unanchored Ub may regulate VP35. The overall goal of this dissertation was to understand the mechanism of TRIM6-mediated VP35/K309 ubiquitination and to investigate the functions of VP35's other Ub interactions.

The primary hypothesis that this thesis examines is: *ubiquitination of VP35/K309 is advantageous for Ebolavirus replication through enhancement of its polymerase co-factor activity.* To investigate our hypothesis, we utilized two VP35/309 mutants, encoding either a glycine (K309G) or an arginine (K309R) to dissect the functional contributions of Ub and a basic residue at VP35/309. This hypothesis was addressed through three specific aims:

Aim 1: To validate the ubiquitination and IFN-I antagonism phenotypes of the VP35/K309 mutants. *We hypothesized that VP35/309 mutation to either arginine or glycine would prevent ubiquitination, but only the glycine mutant would be impaired in its*

IFN-I antagonism. VP35/K309R and -G ubiquitination and IFN-I antagonism were compared to wild-type VP35. (Chapter 3: Figure 3.1)

Aim 2: To characterize the replication kinetics of rEBOV-VP35/K309R and -G. *We hypothesized that both rEBOV-VP35/K309R and -G would be attenuated in IFN-I competent and -incompetent cells due to loss of ubiquitination, but the K309G mutant would be additionally attenuated in IFN-I competent cells due to impaired IFN-I antagonism.* We performed replication kinetics experiments with rEBOV-VP35/wild-type, K309R, and -G viruses in IFN-I competent, A549, and incompetent, VeroE6, cells. (Chapter 3: Figures 3.2-3.6)

Aim 3: To elucidate the function or functions of VP35 that ubiquitination influences. *We hypothesized that loss of VP35/K309 ubiquitination would impair polymerase co-factor functions.* The VP35/K309R and -G mutants were compared to wild-type to compare their capacity to fulfill VP35's functions including polymerase co-factor activity, interaction with viral proteins, and regulation of virus assembly. (Chapter 3: Figure 3.7-3.13)

Secondarily, we also hypothesized that: *TRIM6-independent VP35 ubiquitination also regulates VP35's functions.* Expanding our understanding of VP35 ubiquitination provides insight whether blocking VP35 ubiquitination could be harnessed as a therapeutic target. This hypothesis was addressed through three specific aims:

Aim 4: To identify VP35 lysine residues that receive covalent ubiquitin and examine their function. *We hypothesized that at least one VP35 lysine, aside from K309, is ubiquitinated.* We made VP35 lysine-to-arginine mutants to identify which residues are modified and examined the mutants' polymerase co-factor activity, interaction with key viral proteins, and IFN-I antagonism. (Chapter 4)

Aim 5: To examine the function of VP35-anchored ubiquitination on EBOV's polymerase activity. *We hypothesized that VP35's interaction with unanchored ubiquitin enhances VP35's polymerase co-factor activity.* We confirmed VP35's interaction with unanchored, non-covalent K63- polyUb, identified the region of VP35 that facilitates this interaction, and utilized an USP that targets unanchored Ub to evaluate the role of unanchored Ub on polymerase activity. (Chapter 5)

Aim 6: To investigate the potential redundancy among TRIM6 family members in VP35 ubiquitination. *We hypothesized that a TRIM6 relative could interact with and ubiquitinate VP35.* We screened TRIM6-related TRIMs and PRY-SPRY-containing TRIM25 for interaction with VP35. After identifying TRIM25-VP35 interaction, we evaluated TRIM25-mediated VP35 ubiquitination and EBOV replication kinetics in TRIM25 knockout cells. (Chapter 6)

Chapter 2: Methods for Studying Ebola virus VP35 Ubiquitination and its Effects on Replication

CELLS AND VIRUSES

VeroE6 cells (ATCC CRL-1586), wild-type (ATCC CCL-185) and *Trim6*^{-/-} knockout ⁷⁹ A549 cells, and wt, *Trim25*^{-/-154}, or *Trim6*^{-/-} murine embryonic fibroblasts (MEFs) or bone marrow-derived dendritic cells (BMDCs) were used for infection studies. 293T cells (ATCC CRL-3216) were used for transfection. Cells were maintained in 1X DMEM (VeroE6, A549, 293T, and MEFs) or 1X RPMI-1640 (BMDCs) with 10% FBS and incubated at 37°C, 5% CO₂. EBOV full-length clone expressing enhanced green fluorescent protein (eGFP) ¹⁶³ was kindly provided by Drs. Jonathan S. Towner and Stuart T. Nichol (CDC). The recombinant VP35 mutant viruses (K309R or K309G) were generated based on this clone as described ⁷⁷. Briefly, the pcDNA3 subclone containing ApaI-NruI fragment of the EBOV plasmid was subjected to mutagenesis using the Q5 site-directed mutagenesis kit (New England BioLabs). Primers used for introduction of mutations in VP35 gene are listed in Table 2.1. Next, ApaI-NruI fragment in pEBOV was replaced with its mutagenized copies from pcDNA3 subclones, resulting in EBOV-eGFP/VP35-K309R and EBOV-eGFP/VP35-K309G constructs. The recombinant viruses were recovered upon transfection of 293T cells and amplified by a single passage in VeroE6 cells. The presence of introduced mutations in viral genome was confirmed by conventional Sanger sequencing. For infection in wt and *Trim25*^{-/-} MEFs, we used a mouse-adapted Ebola virus (Ebola virus M. musculus/COD/1976/MayingaCDC-808012) ¹⁶⁴.

All manipulations with infectious EBOV were performed in the Robert E. Shope and Galveston National Laboratory Biological Safety Level 4 facilities at UTMB.

GENERATION OF *TRIM6*^{-/-} MICE

To generate *Trim6*^{-/-} mice using CRISPR, plasmid pSpCas9(BB)-2A-GFP¹⁶⁵ (gift from Feng Zhang, Addgene 48138) expressing Cas9 and sgRNA targeting exon 2 of *Trim6* (Table 2.2) was injected into the pronuclei of C57BL/6J fertilized eggs at the UTMB Transgenic Mouse Core Facility. sgRNA was designed using the following link: <http://crispr.mit.edu:8079/>. We used PCR (primers listed in Table 2.2), Guide-it Mutation Detection Kit (Clontech/Takara Bio, San Jose, CA), T7E1 assay, and Sanger sequencing to screen founders. Subsequently, we validated mutant 8bp deletion allele sequence by amplifying an exon 2 region from founder genomic DNA, subcloning the amplicons, and sequencing the amplicons. The founder line was backcrossed to C57BL/6J twice before heterozygous intercrossing. Mice were genotyped at Transnetyx (Cordova, TN).

MEFs were prepared from E14.5-15.5 embryos from wt and *Trim6*^{-/-} mice and genotyped using previously described methods¹⁶⁶. BMDCs were prepared as described¹⁶⁷. Briefly, bone marrow cells collected from wt or *Trim6*^{-/-} mouse femurs were incubated with 20 ng/mL GM-CSF (Biolegend) for 6 days. On the sixth day, CD11b⁺ CD11c⁺ cells were sorted at 98% purity (BD FACSAria Fusion – UTMB Flow Cytometry and Cell Sorting Core Lab).

Animal breeding, CRISPR-Cas9 knockout line generation, and mouse-derived primary cells preparation was performed in accordance with the approved UTMB IACUC protocols.

VIRUS INFECTIONS AND PLAQUE ASSAYS

Cells were plated in 10% FBS DMEM 16 hours prior to infection. The virus inoculum was prepared in 2% FBS DMEM. A portion of the inoculate was saved for back

titration. At the time of infection, the medium was removed and 100 uL of the inoculum was added. The cells were incubated with the inoculum for 1 hour at 37°C, 5% CO₂ and rocked every 15 minutes. The cells were washed three times with 1X DPBS (Corning) to remove the inoculum and fresh 2% FBS DMEM was added. At the indicated time points, supernatants, protein, and RNA were collected for titration, immunoblot, and qPCR respectively. An Olympus (IX73) microscope was used to take fluorescence and bright field images.

Viral titers were determined by plaque assay on Vero (CCL-81) or VeroE6 (CRL-1586) cells as previously described ⁷⁹.

PLASMIDS

All plasmids used in the experiments are listed in Table 2.3. A brief description of plasmid construction methods used to generate new plasmids is provided here. The K309G and K309R mutations were cloned into both the untagged and FLAG-tagged VP35 plasmids using primers (Table 2.4) containing the appropriate point mutation and restriction enzymes sequences. The different N- and C-terminal VP35 K-to-R mutants were made with the primers listed in Table 2.1 and cloned into the untagged pCAGGS for full-length (FL) and N-terminus constructs or FLAG-pCAGGS for FLAG-VP35-FL,N-, or C-terminus constructs. To make the VP35 K-all-R mutant, we used a multistep approach to generate a VP35 construct with all sixteen lysine residues mutated to arginine (Table 2.4). In the first step, we introduced the K6, 119, 126, and 141-to-R mutations. Then we introduced the K63,67-to-R mutations into the K6,119,126,141R construct using a two-step PCR. We then made a separate construct that introduced the K184R and K282R mutations, and this PCR product was cloned into the K6-141R mutant using the AgeI and

XhoI restriction sites. The K248R and K252R mutations were inserted into the K6-141, 184,282R construct using a two-step PCR using the K309R construct as a template with the reverse primer encoding K319, 334, 339R mutations and the K6R forward primer. Finally, we mutated K216- and 222-to-R in the mutant VP35 construct using a two-step PCR. The VP35/K309R and -G constructs were amplified with primers (Table 2.4) containing KpnI and NotI restriction sites and sub-cloned using the corresponding restriction enzymes into the His-Strep pQE TriSystem vector 1 (QIAGEN). A catalytically inactive His-isopeptidase T (IsoT) plasmid was constructed using the primers listed in Table 2.4. Using HA-TRIM6 wt or C15A pCAGGS plasmids as a template, we PCR amplified these constructs with primers containing restriction sites SgfI and MluI to sub-clone the products into pCMV6-FLAG-Myc vector (Table 2.4). The PCR reactions were conducted using the AccuPrime *Taq* DNA Polymerase, high fidelity kit (Invitrogen). The mutant plasmids sequences were confirmed using Sanger sequencing (UTMB Molecular Genomics).

TRANSFECTIONS AND IMMUNOPRECIPITATIONS

293Ts were plated in 6-well plates (400,000 cells/well) in 10% FBS DMEM for 16 hours, followed by transfection using *TransIT-LT1* (Mirus) following the manufacturer's recommendations. A549 wt or T6-KO cells were plated in 6-well plates (400,000 cells/well) in 10% FBS DMEM for 16 hours followed by transfection using Lipofectamine 3000 (Thermo Scientific) and the media was changed 5-6 hours after transfection. Twenty-eight hours after transfection, 293T or A549 cells were lysed in RIPA buffer with complete protease inhibitor (Roche), n-ethylmaleimide (NEM), and iodoacetamide (IA) (RIPA complete). Lysates were cleared at 25,200 g for 20 minutes at 4°C, and 10% of the clarified

lysate was added to 2X Laemmli sample buffer (BioRad) with 5% beta-mercaptoethanol (β -ME) and boiled at 95°C for 10 minutes to generate whole cell extracts (WCE). The remaining clarified lysate was mixed with 7.5 uL of anti-HA-Agarose beads (Sigma) or anti-FLAG-Agarose beads (Sigma) and incubated at 4°C overnight on a rotating platform. For co-immunoprecipitation (IP) from infected cells, VeroE6 cells infected at an MOI of 0.01 PFU/cell were lysed in RIPA complete at 144 hpi. The clarified lysates were incubated with 1 ug of anti-mouse-IgG (BD Biosciences) or -VP35 (Kerafast) antibody and protein A beads (Cytiva) overnight. The beads were washed seven times with RIPA buffer with IA and NEM before boiling in 2X Laemmli buffer (HA and FLAG co-IP) or 65 uL RIPA complete with 25 uL 4X NuPAGE LDS Sample buffer (Thermo Scientific) and 10 uL 10X NuPAGE Sample Reducing Reagent (Thermo Scientific) (VP35/IgG co-IP).

PROTEIN PURIFICATION

To collect purified HA- or FLAG-tagged proteins, we transfected 293T cells and IP with anti-HA or -FLAG beads as described above prior to peptide elution. After the seven washes in 1X TBS-T, beads were washed once in peptide elution buffer (10 mM TRIS pH 7.4 and 150 mM NaCl in nuclease free water (NF H₂O)) without peptide. The protein was then eluted in 15 μ L of peptide elution buffer with HA- (1 mg/mL) or FLAG- (300 μ g/mL) peptide three times. The peptide purified protein was aliquoted and stored at -80°C until use.

***IN VITRO* UBIQUITIN BINDING ASSAY**

To evaluate VP35's interaction with free ubiquitin, we transfected 293T cells with FLAG-VP35, HA-NP, or empty vector for 30 hours and lysed cells in RIPA complete. Following

IP with anti-FLAG beads, cells were washed seven times with RIPA with IA and NEM then once with NT2. Following the NT2 wash, 200uL of fresh NT2 was added to the beads along with 500ng of recombinant mono-Ub, K48-polyUb (2-7 ubiquitin molecules), or K63-polyUb (2-7 ubiquitin molecules) (Boston Biochem). To check the input levels of Ub for each sample, 20uL was added to laemmli before incubation. After incubation at 4°C on a rotating platform overnight, the beads were washed seven times in NT2 before peptide elution. We then added 15uL of 4X laemmli with β ME to the 45 μ l of eluted protein and boiled at 95°C for 10 minutes. Samples from WCE, Ub inputs, and eluted samples were immunoblotted as described below.

IFN β LUCIFERASE PROMOTER ASSAY

293T cells were plated in a 96-well plate (20,000 cells/well) in 10% FBS DMEM for 16 hours prior to transfection. For the IKK ϵ -induction experiment, cells were co-transfected with 20 ng renilla (to normalize transfection efficiency), 50 ng IFN β -firefly luciferase promoter, 2 ng FLAG-IKK ϵ , and 5, 25, or 50 ng of empty vector or VP35-wt/K309R/K309G plasmids. Twenty-four hours after transfection, the cells were lysed and luciferase signal was measured using the Dual-Luciferase Reporter Assay System (Promega) with a Cytation 5 reader (Biotek). For the dsRNA-induction experiment, after 24 hours of plasmid transfection, high molecular weight (HMW) poly(I:C) (3.125 ug/mL) was transfected with Lipofectamine 2000 (Invitrogen). The cells were lysed at 16 hours after poly(I:C) transfection to measure luciferase. For both experiments, 30% of lysates were collected and boiled in 4X Laemmli sample buffer (Bio-Rad).

BIOTIN POLY(I:C) BINDING

Biotin-labeled HMW poly(I:C), 500 ng, (InvivoGen) was allowed to bind streptavidin-agarose beads (Sigma) in NT2 buffer overnight at 4°C on a rocking platform and washed seven times in NT2 buffer to remove any unbound biotin-poly(I:C). FLAG-peptide purified FLAG-VP35 was incubated with the biotin-poly(I:C) coated beads in 200 uL NT2 buffer for 4 hours at 4°C on a rocking platform. After seven washes in NT2 buffer, the beads were boiled at 95°C in 2X Laemmli sample buffer for 10 minutes.

MINIGENOME ASSAY

The monocistronic minigenome construct ⁶, previously modified by replacement of the chloramphenicol gene with the firefly luciferase gene ¹⁶⁸, was kindly provided by Dr. Elke Mühlberger (BU). The plasmids pCEZ-NP, pCEZ-VP35, pCEZ-VP30, pCEZ-L, and pC-T7 ¹⁶⁹ were kindly provided by Dr. Yoshihiro Kawaoka (UW). 293T cells were plated (50,000 cells/well) onto 24-well plates in 10% FBS 1X DMEM for 16 hours, and co-transfected with the following plasmids: EBOV minigenome (125 ng), pCEZ-VP30 (31.25 ng), pCEZ-NP (62.5 ng), pCEZ-L (500 ng), pC-T7 polymerase (125 ng), 25 or 100 ng of empty vector (pCAGGS) or pCAGGS-VP35 (wt, K309R, or K309G), and REN-Luc/pRL-TK plasmid (20 ng; Promega) expressing *Renilla* luciferase used as an internal control to normalize transfection efficiency. Fifty hours after transfection, the cells were lysed to measure luciferase signal as described above. A portion of the lysate was boiled at 95°C for 10 minutes in 4X Laemmli buffer to evaluate protein expression via immunoblot.

IFN β ELISA

Supernatants from EBOV-infected A549 cells (MOI = 2.5 PFU/cell) were collected at 48 hpi to measure IFN β using the VeriKine human IFN- β enzyme-linked immunosorbent assay (ELISA) kit (PBL Assay Science) according to the manufacturer's instructions. The limit of detection for the assay is 50 pg/ml.

WESTERN BLOTS

Protein samples were run on 4-15% or 7.5% Mini-PROTEAN- or Criterion-TGX Precast Gels (Bio-Rad). The proteins were then transferred onto methanol-activated Immun-Blot PVDF membrane (Bio-Rad), and the membrane was blocked in 5% Carnation powdered skim milk (Nestle) in 1X TBS-T (blocking buffer) for 1 hour. Primary antibodies were prepared in 2% bovine serum albumin 1X TBS-T with 0.02% sodium azide to the appropriate dilution: anti-FLAG (Sigma) 1:2000, anti-HA (Sigma) 1:2000, anti-His (Sigma) 1:2000, anti-VP35 (6C5 Kerafast) 1:1000, anti-NP (provided by Dr. Basler) 1:1000, anti-VP30 (provided by Dr. Basler) 1:1000, anti-VP24 (Sino Biological) 1:1000, anti-VP40 (GeneTex) 1:1000, phosphorylated IRF3 S386 (Cell Signaling) 1:1000, total IRF3 (Immuno-Biological) 1:1000, phosphorylated TBK1 S172 (Epitomics) 1:1000, total TBK1 (Novus Biologicals) 1:1000, phosphorylated STAT1 Y701 (Cell Signaling) 1:1000, total STAT1 (BD Biosciences) 1:1000, anti-ubiquitin (Enzo) 1:1000, anti-TRIM6 (Sigma) 1:1000, anti-TRIM25/ERP (BD Biosciences), anti-tubulin (Sigma) 1:2000, and anti-actin (Abcam) 1:2000. The next day, the blot was washed in 1X TBS-T prior to incubation with HRP-conjugated goat-anti-rabbit (GE Healthcare) or goat-anti-mouse (GE health care) for 1 hour. The blot was then washed and developed using Pierce ECL Western Blotting Substrate (Thermo Fisher) or SuperSignal West Femto Maximum Sensitivity Substrate

(Thermo Scientific). For blot quantifications, the area under the curve (AUC) was measured for each band of interest using ImageJ¹⁷⁰.

RNA EXTRACTIONS AND QUANTITATIVE PCR

Cells were lysed in Trizol (Thermo Fisher) or Tri-reagent (Zymo Research) and processed using the Direct-zol RNA kit (Zymo Research). For the standard qPCR reactions, cDNA was synthesized using the High-Capacity cDNA Reverse Transcription Kit (Applied Biosystems) following the manufacturer's instructions. The qPCR master mixes were prepared with *iTaq* Universal SYBR Green (Bio-Rad). The qPCR reactions were carried out using a CFX384 instrument (Bio-Rad). The relative mRNA expression levels were analyzed using CFX Manager software (Bio-Rad). The change in the threshold cycle (Δ CT) was calculated, with the 18S gene (human cells) or beta-actin (mouse cells) serving as the reference mRNA for normalization. The primers used to assess gene expression are listed in Table 2.5.

For the strand-specific PCR, 200 ng (MEF) or 500 ng (A549 and VeroE6) of RNA was used for first-strand cDNA synthesis using the RevertAid First Strand cDNA Synthesis kit (Thermo Scientific). Three different first-strand reactions were performed with a vRNA, cRNA, or mRNA tagged primer (Table 2.6). Prior to use in the qPCR reaction, the samples were diluted 1:5 in NF H₂O. To make the standards for quantification, minigenome plasmid DNA (vRNA and cRNA) or cDNA made from VeroE6 cells infected with EBOV (mRNAs) were cloned using the AccuPrime *Taq* DNA polymerase, high-fidelity kit (primers are listed in Table 2.6). The forward (vRNA and mRNAs) or reverse (cRNA) primers included the T7 polymerase site. After running the PCR product on a 0.7% agarose 1X TAE gel at 90 V for 1 hour, the DNA was extracted and purified using the QIAquick

Gel Extraction Kit (QIAGEN) and used as a template for in vitro transcription with the MEGAscript T7 Transcription Kit (Invitrogen). The RNA from the in vitro transcription was purified with the Direct-zol RNA kit with the on-column DNA digestion and quantified. In order to calculate the copy number with a standard curve, 1:10 dilutions ranging from 10^{10} - 10^4 of in vitro transcript cDNA was used in qPCR reactions (Table 2.6). To enumerate the copy number of each viral RNA species in the infected samples, the threshold cycle was plugged into the corresponding standard curve equation. To ensure the total RNA was similar between samples, standard qPCR for 18S and/or EBOV was run on cDNA generated with the high-capacity cDNA kit as described above. Limit of detection and specificity assays were also run to validate the assay (Figure 2.1).

VIRUS PURIFICATION

Supernatants from a T75 flasks of VeroE6 cells infected at an MOI of 0.01 PFU/cell were collected at 144 hpi for sucrose-gradient purification. The 15 mL of supernatant was first clarified to remove cellular debris at 1000 g for 10 minutes before loading onto a 25% sucrose cushion. The virus was then pelleted using SW32 rotors spun at ~82,000 g for 2 hours in a Beckman-Coulter L90K ultracentrifuge. The pelleted virus was resuspended in 1X STE buffer (10 mM Tris, 1 mM EDTA, 0.1 M NaCl) and loaded onto a 20-60% sucrose gradient and spun at ~153,000 g for 1.5 hours in a SW41 rotor. The virus band was collected, diluted in 1X STE buffer, and pelleted again in SW32 rotors at ~82,000 g for 1 hour. The pellet was resuspended in 500 uL of 1X STE buffer. All spins were conducted at 4°C. Aliquots of the purified virus were used for RNA or protein isolation and titration.

ATPASE ASSAY

Peptide purified FLAG-VP35 was incubated in ATPase buffer (20 mM Tris-HCl pH 8.0, 1.5 mM MgCl₂, and 1.5 mM DTT in NF H₂O) with or without ATP (2.5 mM final concentration) at 37°C for 30 minutes. Free phosphate was measured using the BIOMOL Green (Enzo) reagent for phosphate detection and read with the Cytation5 (620 nm). A standard curve was prepared with the provided phosphate standard according to the manufacturer's instructions.

STATISTICS

All analyses were performed in Graphpad Prism (Version 7.04). Heat maps were also generated with Graphpad Prism. Statistical tests, measures of statistical significance, and replication information are specified in the respective figure legends. Repeated measures two-way ANOVA with Bonferroni's post-test was applied for two factor comparisons (kinetics experiments), one-way ANOVA with Tukey's post-test was used for comparing three or more groups, and a student's t-test for comparing two groups.

Primer Name	Sequence
VP35 K309R F	AGCTTGCCAGCGGAGCTTGCGTC
VP35 K309G F	AGCTTGCCAGGGCAGCTTGCGTC
VP35 R	CGGGGAATGTCACCTCGA

Table 2.1 Oligonucleotides for introducing VP35/K309 mutations into pcDNA3

Primer sequences to generate mutations in the pcDNA3 sub-clone used to introduce the VP35/K309 mutations into the infectious clone that encodes rEBOV-eGFP.

Primer Name	Sequence
sgRNA <i>Trim6</i> exon 2	TGATAGGAGGTCCGGCACAC
<i>Trim6</i> F	GCTGGGAAGGTAGGAGACGA
<i>Trim6</i> R	GAGATCGTTCACAAAGCCAG

Table 2.2 sgRNA and screening primers for *Trim6*^{-/-} mice

sgRNA sequences used to generate *Trim6*^{-/-} mice and primer sequences used to screen for knockout mice. Sequences are listed 5' to 3'.

Plasmid Name	Vector	Source
Untagged VP35 wild-type	pCAGGS	⁶⁷
Untagged VP35/K309R	pCAGGS	Sarah van Tol (UTMB)
Untagged VP35/K309G	pCAGGS	Sarah van Tol (UTMB)
Untagged VP35/K6R	pCAGGS	Sarah van Tol (UTMB)
Untagged VP35/K6.67R	pCAGGS	Sarah van Tol (UTMB)
Untagged VP35/K119.126.141R	pCAGGS	Sarah van Tol (UTMB)
Untagged VP35/K119R	pCAGGS	Sarah van Tol (UTMB)
Untagged VP35/K126R	pCAGGS	Sarah van Tol (UTMB)
Untagged VP35/K141R	pCAGGS	Sarah van Tol (UTMB)
Untagged VP35/K119.126R	pCAGGS	Sarah van Tol (UTMB)
Untagged VP35/K119.141R	pCAGGS	Sarah van Tol (UTMB)
Untagged VP35/K126.141R	pCAGGS	Sarah van Tol (UTMB)
Untagged VP35/K184.216R	pCAGGS	Sarah van Tol (UTMB)
Untagged VP35/K6-216R	pCAGGS	Sarah van Tol (UTMB)
Untagged VP35/K-all-R	pCAGGS	Sarah van Tol (UTMB)
FLAG-VP35 wild-type	pCAGGS	⁶⁷
FLAG-VP35/K309R	pCAGGS	Sarah van Tol (UTMB)
FLAG-VP35/K309G	pCAGGS	Sarah van Tol (UTMB)
FLAG-VP35/R225E	pCAGGS	Sarah van Tol (UTMB)
FLAG-VP35/R225K	pCAGGS	Sarah van Tol (UTMB)
FLAG-VP35/ wild-type N-terminus	pCAGGS	From Chris Basler (Mount Sinai)
FLAG-VP35/K309R N-terminus	pCAGGS	Sarah van Tol (UTMB)
FLAG-VP35/K309G N-terminus	pCAGGS	Sarah van Tol (UTMB)
FLAG-VP35/K6R N-terminus	pCAGGS	Sarah van Tol (UTMB)
FLAG-VP35/K63,67R N-terminus	pCAGGS	Sarah van Tol (UTMB)
FLAG-VP35/K119.126.141R N-terminus	pCAGGS	Sarah van Tol (UTMB)
FLAG-VP35/K184.216R N-terminus	pCAGGS	Sarah van Tol (UTMB)
FLAG-VP35/K-all-R N-terminus	pCAGGS	Sarah van Tol (UTMB)
FLAG-VP35/wild-type C-terminus	pCAGGS	²²
FLAG-VP35/K309R C-terminus	pCAGGS	Sarah van Tol (UTMB)
FLAG-VP35/K-all-R C-terminus	pCAGGS	Sarah van Tol (UTMB)
His-VP35 wild-type	pQE-1	Sarah van Tol (UTMB)
His-VP35/K309R	pQE-1	Sarah van Tol (UTMB)
His-VP35/K309G	pQE-1	Sarah van Tol (UTMB)
VP35 wild-type subclone	pcDNA3	⁷⁷
VP35/K309R subclone	pcDNA3	Bukreyev lab (UTMB)
VP35/K309G subclone	pcDNA3	Bukreyev lab (UTMB)
EBOV-eGFP/VP35/WT	Full length clone	¹⁶³
EBOV-eGFP/VP35/K309R	Full length clone	Bukreyev lab (UTMB)
EBOV-eGFP/VP35/K309G	Full length clone	Bukreyev lab (UTMB)
HA-L ₁₋₅₀₅	pCAGGS	²²
HA-NP	pCAGGS	²²
HA-Ub	pRK5	Addgene (Cat #18712)
HA-Ub K-all-R	pRK5	Garcis-Sastre lab (Mount Sinai)

HA-Ub ΔGG	pCAGGS	From Gijs Versteeg (Garcis-Sastre lab, Mount Sinai)
HA-TRIM6 wild-type	pCAGGS	89
HA-TRIM6 C15A	pCAGGS	89
FLAG-TRIM6 wild-type	pCMV6	Sarah van Tol (UTMB)
FLAG-TRIM6 C15A	pCMV6	Sarah van Tol (UTMB)
FLAG-IKKε wild-type	pCAGGS	89
FLAG-IKKε K38A	pCAGGS	89
FLAG-OTU wild-type	pCAGGS	89
FLAG-OTU 2A	pCAGGS	89
EBOV L	pCEZ	169
EBOV NP	pCEZ	169
EBOV VP30	pCEZ	169
EBOV minigenome-firefly luciferase	p3E5EF.luc	168
T7 polymerase	pCEZ	169
Renilla luciferase	REN-Luc/pRL-TK	Promega (Cat # E2241)
IFNβ firefly luciferase promoter	pIFNβ fLuc	109
His-IsoT wild-type	pcDNA-4C	89
His-IsoT C335A	pcDNA-4C	Sarah van Tol (UTMB)
HA-TRIM25	pCAGGS	109
HA-TRIM5α	pLPCX	109
HA-TRIM21	pCAGGS	109
HA-TRIM22	pcDNA3.1(+)	109
HA-TRIM34	pLNCX2	109
RFP-TRIM25	pCAGGS	From Adolfo Garcia-Sastre Lab (Mount Sinai)
GST Empty	pEBG	From Michaela Gack (Cleveland Clinic)
GST-TRIM25-RING	pEBG	From Michaela Gack (Cleveland Clinic)
GST-TRIM25-BB	pEBG	From Michaela Gack (Cleveland Clinic)
GST-TRIM25-CC	pEBG	From Michaela Gack (Cleveland Clinic)
GST-TRIM25-SPRY	pEBG	From Michaela Gack (Cleveland Clinic)

Table 2.3 List of plasmids used

List of plasmids used in all experiments. For each construct the name, vector, and source are listed.

Primer Name	Sequence
pCAGGS VP35 NheI R	TATAATGCTAGCTCAAATTTTGAGTCCAAGTGTTTTACC ATCT
pCAGGS VP35 K309R XhoI F	ATTTCTCGAGGTGACATTCCCCGAGCTTGCCAGAGAAGC TTGCGTCCAGTCCCA
pCAGGS VP35 K309G XhoI R	ATTATACTCGAGGTGACATTCCCCGAGCTTGCCAGGGA AGCTTGCCTCCAGT
pQE-VP35 KpnI F	ATTATAGGTACCATGACAACACTAGAACAAAGGGCA
pQE-VP35 NotI R	TATAATGCGGCCGCAATTTTGAGTCCAAGTGTTTTACCA
VP35 N-C Overlap K216,222R F	CTAACTGAGGAAAATTTTGGGAGACCTGACATTTTCGGC AAGGGATTTGAGAAACATTATG
VP35 N-C Overlap K216,222R R	CATAATGTTTCTCAAATCCCTTGCCGAAATGTCAGGTCT CCCAAATTTTCCTCAGTTAG
VP35 K63,67 F	GCATCCCAAATGCAACAAACGAAGCCAAACCCGAAGAC GCGCAACAGTCAAACCCAAAC
VP35 K63,67 R	GTTTGGGTTTGACTGTTGCGCGTCTTCGGGTTTGGCTTC GTTTGTTCATTTGGGATGC
VP35 K319, 334,339R NheI R	AAGCTAGCTCAAATTCTGAGTCCAAGTGTTCTACCATCT TGAAGCTGAAAAACACATACCCAACCTCGATCAATCCT GGGCGATG
VP35 K119.126.141R AgeI R	AATAACCGGTTGTCATCACCAGAAGATCATATCTTGCAA CCATCTCAGCACAAACCCTGTTC AATGAGGAGATTGTTCTTGCCATATCATAAACTGGCCTT AGACCATT
VP35 K119R AgeI R	ATAATTACCGGTTGTCATCACCAGAAGATCATATTTTGC AACCATCTCAGCACAAACCCTGTTCAATGAGGAGATTG TTTTTGCCATATCATAAACTGGCCTTAGACCATT
VP35 K126R AgeI R	ATAATTACCGGTTGTCATCACCAGAAGATCATATTTTGC AACCATCTCAGCACAAACCCTGTTCAATGAGGAGATTG TTCTTGCCATATCATAAACTGGCTTTAGACCATT
VP35 K141R Age I R	ATAATTACCGGTTGTCATCACCAGAAGATCATATCTTGC AACCATCTCAGCACAAACCCTGTTCAATGAGGAGATTG TTTTTGCCATATCATAAACTGGCTTTAGACCATT
VP35 K119.126R AgeI R	ATAATTACCGGTTGTCATCACCAGAAGATCATATTTTGC AACCATCTCAGCACAAACCCTGTTCAATGAGGAGATTG TTCTTGCCATATCATAAACTGGCCTTAGACCATT
VP35 K119.141R AgeI R	ATAATTACCGGTTGTCATCACCAGAAGATCATATCTTGC AACCATCTCAGCACAAACCCTGTTCAATGAGGAGATTG TTTTTGCCATATCATAAACTGGCCTTAGACCATT
VP35 K126.141R AgeI R	ATAATTACCGGTTGTCATCACCAGAAGATCATATCTTGC AACCATCTCAGCACAAACCCTGTTCAATGAGGAGATTG TTCTTGCCATATCATAAACTGGCTTTAGACCATT

VP35 K6R NotI F	TATTGCGGCCGCAATGACAACCTAGAACAAAGGGGCAGGG GCCATACTGCGG
VP35 K282R XhoI R	TATTCTCGAGAGCGGATGTGGATGACAGGTGGAGCAGC ATCTTGGAAGATTGGAACCTCTTCTTGTAATTTGAATTAG GGCACA
VP35 K222,248,252R F	GCAAGGGATTTGAGAAACATTATGTATGATCACTTGCCT GGTTTTGGAACCTGCTTCCACCAATTAGTACAAGTGATT TGTAGATTGGGAAGAGATAGC
VP35 K222,248,252R R	GCTATCTCTTCCCAATCTACAAATCACTTGTACTAATTG GTGGAAAGCAGTTCCAAAACCAGGCAAGTGATCATACA TAATGTTTCTCAAATCCCTTGC
VP35 K184R AgeI-F	ACCGGTCGGGCAACAGCAACCGCTGCGGCAACTGAGGC TTATTGGGCCGAACATGGTCAACCACCCTGGACCATC ACTTTATGAAGAAAGTGCGATTCGGGGTAGGATTGA
TRIM6 F pCMV SgfI	ATTATAGCGATCGCCATGACTTCACCAGTACTGGTGGA
TRIM6 R pCMV Mlu	TATAATACGCGTAGAGCTTGGACGACGCAGGGTCAT
IsoT BstEII F	ATTATAGGTGACCAGTGCAGTGGAGGCCCTACT
IsoT AfeI R	TATAATAGCGCTTCAAGGCCTGGTCCCGGGAGA
IsoT C335A F	ATCCGGAACCTGGGTAACAGCGCCTACCTCAACTCTGTG GTCCAGGT
IsoT C335A R	ACCTGGACCACAGAGTTGAGGTAGGCGCTGTTACCCAG GTTCCGGAT

Table 2.4 Oligonucleotides to generate mutants

List of primers used to generate mutant plasmids. The name indicates the target, whether the primer is forward (F) or reverse, the mutation encoded if applicable, and the restriction site when applicable. The primer is listed 5' to 3'.

Primer Name	Sequence
EBOV F	TTTTCAATCCTCAACCGTAAGGC
EBOV R	CAGTCCGGTCCCAGAATGTG
Human Ifn-b F	TCTGGCACAAACAGGTAGTAGGC
Human Ifn-b R	GAGAAGCACAAACAGGAGAGCAA
Human ISG54 F	ATGTGCAACCCTACTGGCCTAT
Human ISG54 R	TGAGAGTCGGCCCAGTGATA
Human Mx1 F	GGCTGTTTACCAGACTCCGACA
Human Mx1 R	CACAAAGCCTGGCAGCTCTCTA
Human ISG15 F	TCCTGGTGAGGAATAACAAGGG
Human ISG15 R	GTCAGCCAGAACAGGTCGTC
Human Ddx58 F	GGCATGTTACACAGCTGACG
Human Ddx58 R	TGCAATATCCTCCACCACAA
18S F	GTAACCCGTTGAACCCATT
18S R	CCATCCAATCGGTAGTAGCG
Mouse Ifn-b F	CAGTCCAAGAAAGGACGAAC
Mouse Ifn-b R	GGCAGTGTAACCTTTCTGCAT
Mouse ISG54 F	CTGAGAGGGGAGTGGACTCTG
Mouse ISG54 R	GCACCTGCTTCATCCAAAGAT
Mouse ISG15 F	GCAAGCAGCCAGAAGCAGACTCC
Mouse ISG15 R	CGGACACCAGGAAATCGTTACCCC
Mouse Actin F	CGGTTCCGATGCCCTGAGGCTCTT
Mouse Actin R	CGTCACACTTCATGATGGAATTGA

Table 2.5 Oligonucleotides for standard quantitative PCR

List of primers used for quantitative PCR. The gene name indicates the species and target gene. Sequences are listed 5' to 3'.

Category	Name	Sequence
In vitro Transcription	vRNA F	CATAGTATCCTGATACTTGCAAAGGT
	vRNA T7 R	ggatcctaatacactcactatagggTGGACACACAAAAAGAAGAAATAGA
	cRNA T7 F	ggatcctaatacactcactatagggCATAGTATCCTGATACTTGCAAAGGT
	cRNA R	TGGACACACAAAAAGAAGAAATAGA
	mRNA R	TTTTTTTTTTTTTTTTTATAAT
	L mRNA T7 F	ggatcctaatacactcactatagggCTCCCGCAAGACGAGCAA CAAGATCAGGACCACACT
	NP mRNA T7 F	GGATCCTAATACGACTCACTATAGGG GATGAAGGATGAGCCTGTAG
	VP35 mRNA T7 F	GGATCCTAATACGACTCACTATAGGG TCCGCTCTCGAGGTGACA
	VP40 mRNA T7 F	GGATCCTAATACGACTCACTATAGGG TCACCATGGTAATCACACA
	VP24 mRNA T7 F	GGATCCTAATACGACTCACTATAGGG ATGAGTCCACACTGAAAG
First-strand cDNA synthesis	FS vRNA	GGCCGTCATGGTGGCGAATagctttaacgaaaggctctgggctc
	FS cRNA	GCTAGCTTCAGCTAGGCATCacacaagattaaggctatcaccg
	FS mRNA	CCAGATCGTTCGAGTCGTTTTTTTTTTTTTTTTTCTT AAT
Strand-specific qPCR	vRNA tag F	GGCCGTCATGGTGGCGAAT
	vRNA R	acacaagattaaggctatcaccg
	cRNA F	agctttaacgaaaggctctgggctc
	cRNA tag R	GCTAGCTTCAGCTAGGCATC
	mRNA tag R	CCAGATCGTTCGAGTCGT
	L mRNA F	ATTGCAATTGTGAAGAACGTTTC
	NP mRNA F	GATGAAGGATGAGCCTGTAG
	NP mRNA R	CCATGGTGGATATTCCTC
	VP35 mRNA F	TCCGCTCTCGAGGTGACA
	VP35 mRNA R	CAACCTCGATCAATCTTG
	VP40 mRNA F	TCACCATGGTAATCACACA
	VP40 mRNA R	TTCTCAATCACAGCTGGAA
	VP24 mRNA F	ATGAGTCCACACTGAAAG
	VP24 mRNA R	GATAGCAAGAGAGCTATT

Table 2.6 Oligonucleotides to assess synthesis of Ebola virus RNA species

List of primers used for to generate *in vitro* transcripts, synthesize genomic RNA (vRNA), complementary RNA (cRNA), or messenger RNA (mRNA) from RNA samples, and strand-specific qPCR primers. The gene name indicates the target RNA species or viral gene. Sequences are listed 5' to 3'.

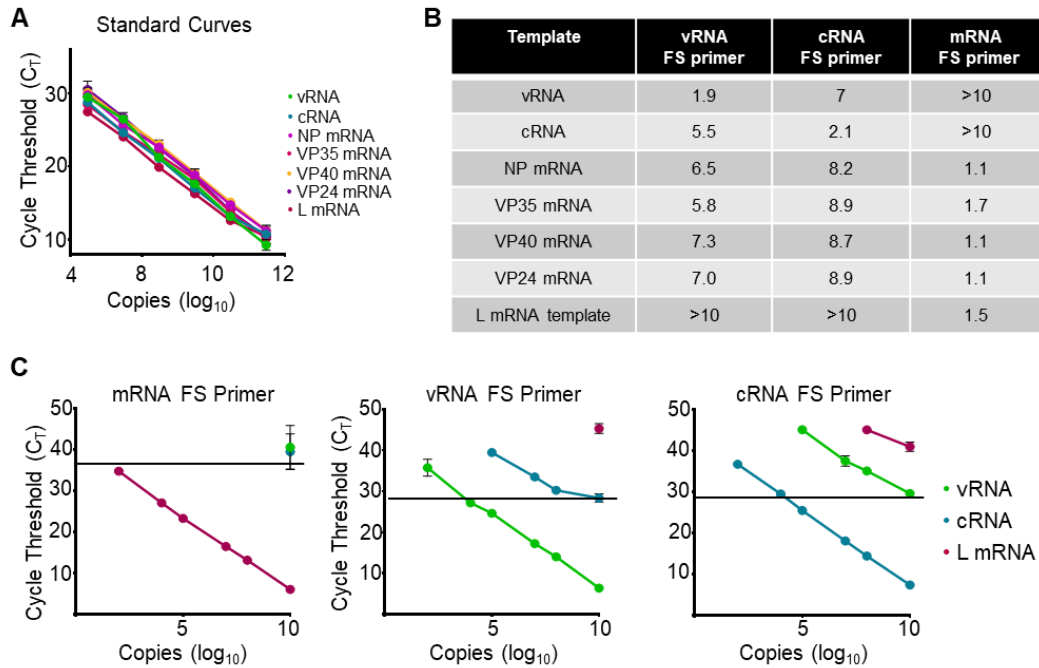


Figure 2.1 Validation of Ebola virus strand-specific quantitative PCR

(A) Representative standard curves for each viral RNA species tested, genomic RNA (vRNA), anti-genomic RNA (cRNA), and NP, VP35, VP40, VP24, and L transcripts (mRNA) run along with each strand-specific qPCR run. (B) Table of the limit of detection (\log_{10} copies) for each first-strand cDNA primer-in vitro transcript pair. (C) Graphical representation of how cycle threshold cut off values were determined for each first-strand primer/qPCR pair. (Figure reproduced with permission from van Tol et al., 2022)

Chapter 3: Ubiquitination of VP35 at Lysine 309 Regulates Viral Transcription and Assembly

A BASIC RESIDUE AND LACK OF UBIQUITINATION AT VP35/309 IS REQUIRED FOR EFFICIENT IFN-I ANTAGONISM

To investigate the role(s) of VP35 K309 ubiquitination, we generated two mutants. A lysine-to-arginine (K-to-R) mutant (K309R), intended to ablate Ub conjugation without disrupting dsRNA binding and dsRNA-dependent IFN-I antagonism, and a K-to- glycine (G) mutant (K309G), anticipated to lose both ubiquitination and IFN-I antagonism (Figure 3.1A). The substitution for a G, a small non-polar amino acid, is expected to disrupt the basic charge without disturbing the dsRNA-binding domain's structure, as has been observed for other central basic patch mutants, R312A and K339A ¹⁷¹. The combined use of these mutants is intended to disentangle the importance of ubiquitination from a basic residue at position 309.

We first used purified FLAG-tagged VP35 (FLAG-VP35) to test the mutants' capacity to bind dsRNA. As predicted, the wild-type (wt) and K309R VP35 proteins were equivalent in their ability to bind dsRNA after a biotin-poly(I:C) pull-down (Figure 3.1B). In contrast, VP35-K309G binding to dsRNA was significantly decreased (approx. 50%, Figure 3.1B). This same degree of attenuation has previously been observed with a VP35 K309A mutant ⁶⁵.

We then confirmed that these mutations reduce the levels of ubiquitinated VP35. In a co-immunoprecipitation assay (co-IP), after pulling down HA-tagged ubiquitin (HA-Ub) from 293T cells co-expressing VP35, the band corresponding to Ub-conjugated wt VP35 was not detected for the K309R and -G mutants (Figure 3.1C). When we pulled down

VP35 from infected VeroE6 cells we observed a decrease in Ub immunoprecipitated with VP35 (Figure 3.1D), confirming that VP35/309 is ubiquitinated during infection and either K-to-R or -G mutation ablates this modification.

We then proceeded to evaluate the impact of the K309 mutations on IFN-I antagonism. In line with the impaired dsRNA-binding, a low dose of VP35-K309G showed significantly less IFN antagonism as compared to wt VP35 and VP35/K309R upon stimulation with poly(I:C) in a IFN β -promoter luciferase assay (Figure 3.1E). Other basic residues in the IFN-inhibitory domain (IID) of VP35 that are also involved in dsRNA binding^{65,171} likely contribute to the VP35/K309G's antagonism at higher doses (Figure 3.1E).

VP35 also has the capacity to antagonize IFN-I induction through dsRNA binding-independent inhibition of the kinases TBK1 and IKK ϵ ^{68,72}, but the mechanism remains elusive. Unexpectedly, VP35/K309G was also modestly impaired in the antagonism of IKK ϵ -induced IFN β -luciferase promoter activity (Figure 3.1F). The VP35/K309R inhibited IFN β induction significantly more than wt VP35 at the highest dose (Figure 3.1F), suggesting that ubiquitination on K309 may reduce the ability of VP35 to antagonize IFN production. As previously reported⁷², VP35 wt binds to the IKK ϵ kinase mutant (K38A) (Figure 3.1G). The reduced ability of VP35/K309G to interact with IKK ϵ in a co-IP assay can explain the reduced antagonism in the luciferase assay, but IKK ϵ -binding for the K309R mutant was not consistently affected (Figure 3.1G).

Overall, these results suggest that a substitution of either K-to-R or -G prevents ubiquitination at position 309, but only the loss of a basic residue disrupts dsRNA binding

and IFN-I antagonism. In addition, lack of ubiquitination on K309 may also increase the ability of VP35 to antagonize IKK ϵ -induced IFN production.

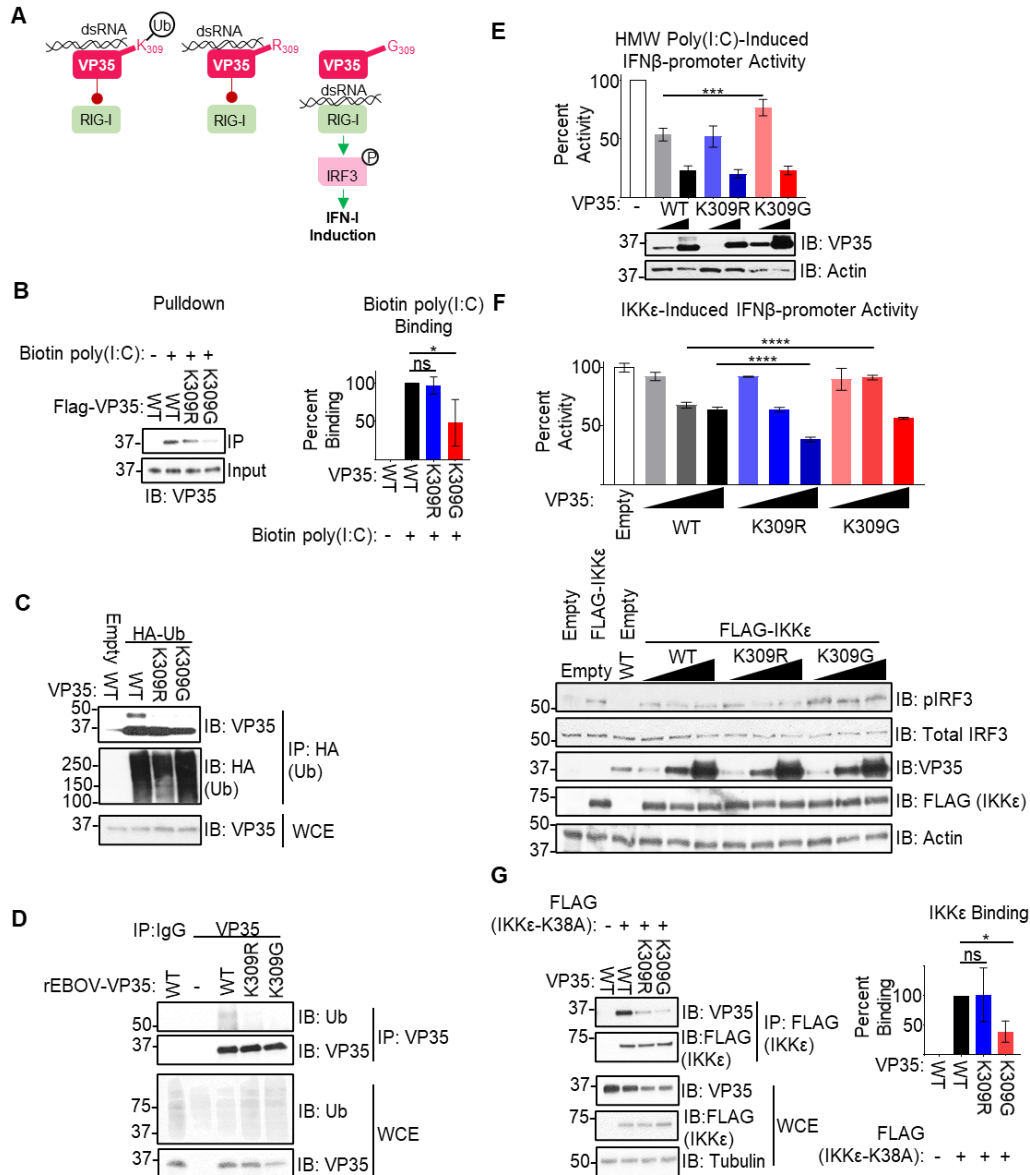


Figure 3.1 A basic residue and lack of ubiquitination at VP35/309 is required for most efficient IFN-I antagonism

(A) VP35 K309 is located in the IFN-inhibitory domain and is involved in binding double-stranded RNA (dsRNA) to prevent the activation of the host's cytoplasmic RNA sensor RIG-I and is ubiquitinated (white circle with 'Ub') at this position. Mutation of K309 to an arginine (R) is predicted to prevent ubiquitination at this site without disrupting dsRNA binding due to the conservation of a basic residue. The glycine (G) mutant is predicted to lose both ubiquitination and dsRNA binding, allowing enhanced activation of RIG-I, IRF3 phosphorylation (white circle with 'P'), and downstream IFN-I induction. (B) Peptide purified FLAG-VP35 WT and mutants were mixed with 500 ng biotin-poly(I:C), followed by biotin pull-down. The quantification (ImageJ) represents data from three independent experiments. The percent binding was calculated as follows: the ratio of VP35 bound to poly(I:C) (IP) to the VP35 input levels for each VP35 construct was divided by the wt VP35 ratio. (C) Whole cell extracts (WCE) from 293T cells co-expressing HA-Ub and

untagged VP35 (wt, K309R, or K309G) were used for immunoprecipitation (IP) with anti-HA beads. The presented western blot is representative of three independent experiments. (D) Lysates (WCE) from mock or rEBOV-VP35/wt, -K309R, or -K309G infected VeroE6 cells were used for IP with IgG (control) or anti-VP35 antibody, followed by immunoblot. The presented western blot is representative of two independent blots. (E) 293T cells were transfected with IFN β luciferase reporter and Renilla luciferase plasmid and transfected 24 hours later with 3.125 ug/mL high molecular weight (HMW) poly(I:C). The ratio of firefly luciferase (IFN β promoter activity) to renilla luciferase (transfection efficiency normalization) luminance was measured for each VP35 construct in the presence and absence of poly(I:C) stimulation. The percent activity relative to empty vector is presented. The quantification is from three independent experiments conducted in biological triplicate, and the IB is representative of the corresponding lysates. (F) As in E, but 2 ng IKK ϵ was transfected along with the luciferase plasmids. The ratio of firefly luciferase (IFN β promoter activity) to renilla luciferase (transfection efficiency normalization) luminance was measured for each VP35 construct in the presence and absence of IKK ϵ over-expression. The percent activity relative to empty vector is presented. The quantification is from two independent experiments conducted in biological triplicate, and the IB is representative of the corresponding lysates. (G) Untagged VP35 constructs were incubated with FLAG-IKK ϵ K38A, and lysates were immunoprecipitated with anti-FLAG-beads. The quantification (ImageJ) represents three independent experiments. The binding ratio ((IP: VP35/FLAG-IKK ϵ K38A)/(WCE: (VP35/FLAG-IKK ϵ K38A)/Tubulin)) for each VP35 construct was divided by wt VP35's ratio to determine percent binding. Analysis was done using a one-way ANOVA with Tukey's post-test for comparison between groups. P-value: * <0.05 , *** <0.001 , **** <0.0001 . (Figure reproduced with permission from van Tol et al., 2022)

IMPAIRMENT OF TRIM6-MEDIATED VP35/K309 UBIQUITINATION ATTENUATES EBOV REPLICATION

To assess how the loss of ubiquitination at VP35/K309 affects EBOV replication, we generated recombinant EBOV (rEBOV, expressing eGFP) mutant viruses bearing the K309G or -R mutations. Since we have shown that ubiquitination on K309 promotes VP35 activity as the co-factor of the viral polymerase ⁷⁹, we expected both mutants to be attenuated due to loss of ubiquitination and that the K309G mutant would be more severely affected due to loss of full IFN antagonism activity.

IFN-competent A549 cells were infected with the recombinant viruses at a multiplicity of infection (MOI) of 0.01 plaque-forming units (PFU) per cell to evaluate multiple cycles of replication. As predicted, both of the rEBOV-VP35/K309 mutants were significantly attenuated compared to the wt virus, but the K309G showed the stronger attenuation (Figure 3.2A). This was also reflected in quantification of viral RNA expression (Figure 3.2B) and viral replication monitored by fluorescence microscopy (Figure 3.2C). Similarly, both mutant viruses were also attenuated when infecting A549 cells in a single-cycle replication kinetics experiment (MOI = 2.5 PFU/cell) (Figure 3.2D-G). The EBOV RNA levels (Figure 3.2E), and the GFP signal (Figure 3.2F) also largely reflect these differences in titer. Attenuation of the rEBOV-VP35/K309 mutants is also observed in IFN-I competent primary MEFs (Figure 3.2 H-J). Overall, at the time point corresponding to the peak titer for wt virus, the K309R mutant was attenuated 0.8 or 0.5 log₁₀ and the K309G mutant was attenuated 3.1 or 2.7 log₁₀ when inoculated at an MOI of 0.01 or 2.5 PFU/cell, respectively (Figure 3.2K).

We next sought to confirm that additional attenuation of rEBOV-VP35/K309G is attributable to its impaired IFN-I antagonism. The induction of IFN β transcription (qPCR,

Figure 3.3A and 3.3B) and secreted IFN β (ELISA, Figure 3.3C) was higher in K309G-infected cells and lower in K309R-infected cells as compared to wt-infected cells. Induction of the IFN-stimulated genes (ISG) ISG54, Mx1, ISG15, and Ddx58 (the gene that encodes for RIG-I), showed similar dynamics to IFN β expression with the K309G highest and the K309R lowest (Figure 3.3D and 3.3E). Similar patterns in IFN β and ISG transcription were also observed during infection in primary MEFs (Figure 3.3F). Consistent with the qRT-PCR and ELISA data, activated TBK1 (pTBK1 S172), IRF3 (pIRF3 S396), and STAT1 (pSTAT1 Y701) were detected at higher levels at 24 hpi in K309G infected cells than wt-infected cells (Figure 3.3G). The K309R infected cells were depressed in TBK1, IRF3, and STAT1 activation and lagged in the induction of total STAT1 (an ISG) compared to wt-infected cells (Figure 3.3G).

To test the dependency of the attenuation on TRIM6, we infected wt or TRIM6 knockout cells⁷⁹ (T6-KO) with wt or mutant viruses. The wt virus was attenuated in the T6-KO A549 cells at low (0.01) (Figure 3.4 A-C) and high (2.5) MOI (Figure 3.4 D-F), but the K309 mutants were not additionally attenuated at peak titers. Similar results were observed during infection of primary bone marrow-derived dendritic cells (BMDCs) from newly generated *Trim6*^{-/-} mice (Figure 3.5A and 3.5B). Early during infection, before virus could be detected in supernatants, we measured EBOV genome copy number and observed significantly less viral RNA for the wt virus in T6-KO cells but not the K309 mutants (Figure 3.5A). We then measured viral titer later during infection in supernatants from wt or *Trim6*^{-/-} BMDCs infected with either the wt or K309R virus. Consistent with the results described above, the wt virus replicated significantly less in *Trim6*^{-/-} cells as compared to wt BMDCs, whereas the K309R virus replicated to comparable levels in wt and *Trim6*^{-/-}

BMDCs (Figure 3.5B). This further supports a role for TRIM6 and an intact K309 residue in efficient EBOV replication.

To evaluate whether any IFN-independent factors contributed to the difference in viral load between the K309R and -G mutants, we assessed infection kinetics in IFN-incompetent cells. We expected that during infection of VeroE6, cells incapable of IFN-I production, the replication of both mutants would be attenuated compared to wt but the difference between the mutant viruses observed in IFN-competent cells would be diminished. As predicted, both mutant viruses were attenuated compared to wt, however, the K309G mutant was more attenuated than the K309R mutant in both multi-cycle (Figure 3.6A and 3.6B) and single cycle (Figure 3.6C and 3.6D) kinetics experiments. The degree of attenuation of the K309R mutant in VeroE6 cells (0.8 and 0.5 log₁₀) at the time point corresponding to the peak titer for wt virus was equivalent to that observed in the A549 cells (Figure 3.2K and 3.6E). In contrast, the K309G mutant is less severely attenuated in VeroE6 cells (1.8 and 1.2 log₁₀) than in A549 cells (3.1 and 2.7 log₁₀) (Figure 3.2K and 3.6E), indicating that the attenuation of the K309G mutant virus is attributable, partially, to the reduced IFN antagonism function.

Overall, the replication kinetics experiments in the IFN-I incompetent and competent cells support that TRIM6-mediated ubiquitination of VP35/K309 promotes viral replication. The results of these experiments are also consistent with our experiments showing IFN antagonism is compromised for the K309G but bolstered for the K309R mutant. The unexpected additional attenuation of the K309G mutant in IFN-I incompetent cells suggests that a basic residue at this position is important for an additional function.

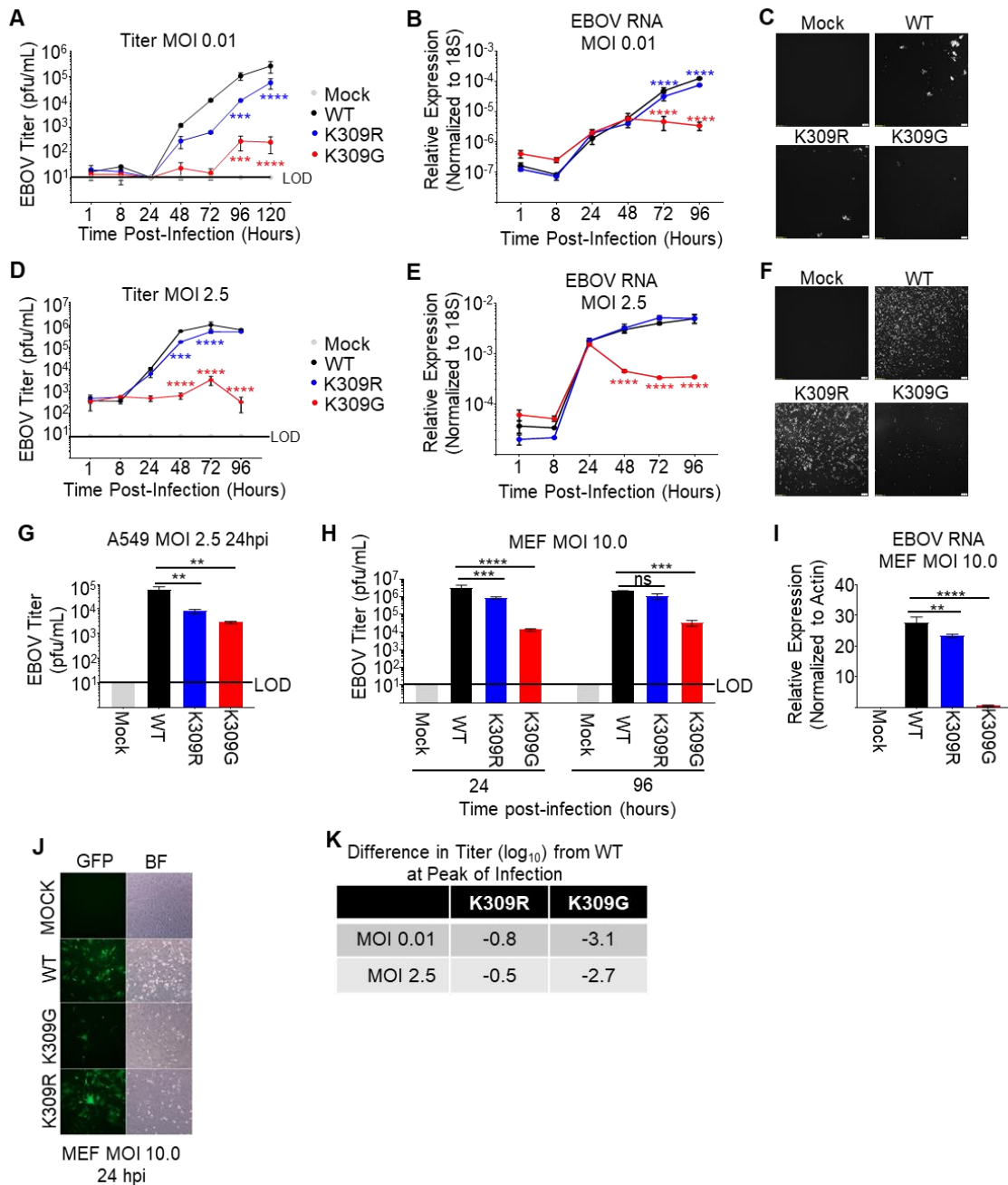


Figure 3.2 The replication of rEBOV-VP35/K309R and -G mutants is attenuated in IFN-competent cells

A549 cells (A-G) or murine embryonic fibroblasts (MEFs) (H-J) were mock infected (grey) or infected in triplicate wells with rEBOV-eGFP-VP35/wt (black), -K309R (blue), or -K309G (red) at an MOI of 0.01 (A-C) or 2.5 PFU/cell (D-G). At different time points, supernatants were collected for virus titration (A, D, G, H). The limit of detection (LOD) for the titrations (10 PFU/mL) is indicated (black line). Cells were lysed in TRIzol to isolate RNA and qPCR was performed for EBOV RNA (B, D, I). Cycle threshold values for EBOV RNA were normalized to 18S (A549) or actin (MEF) cycle threshold values. The

fluorescence microscopy images (GFP) are representative of the three images taken (C, F, J). The difference in titer (\log_{10}) between the mutant and wt viruses at the time point corresponding to the wt peak titer is summarized (K). The titration (A, D, G, H), qRT-PCR (B, E, I) were done in biological triplicate and are representative of two independent experiments. The data analysis was done using a two-way ANOVA (A, B, D, H) or one-way ANOVA (G, I) with Bonferroni's or Tukey's post-test for comparison between groups, respectively. P-value: * <0.05 , ** <0.01 , *** <0.001 , **** <0.0001 . For two-way ANOVA with Bonferroni's post-test statistical analysis, the non-significant differences ($P > 0.05$) are not indicated on the graph to prevent cluttering. Red and blue stars represent K309G and K309R comparison to wt, respectively. (Figure reproduced with permission from van Tol et al., 2022)

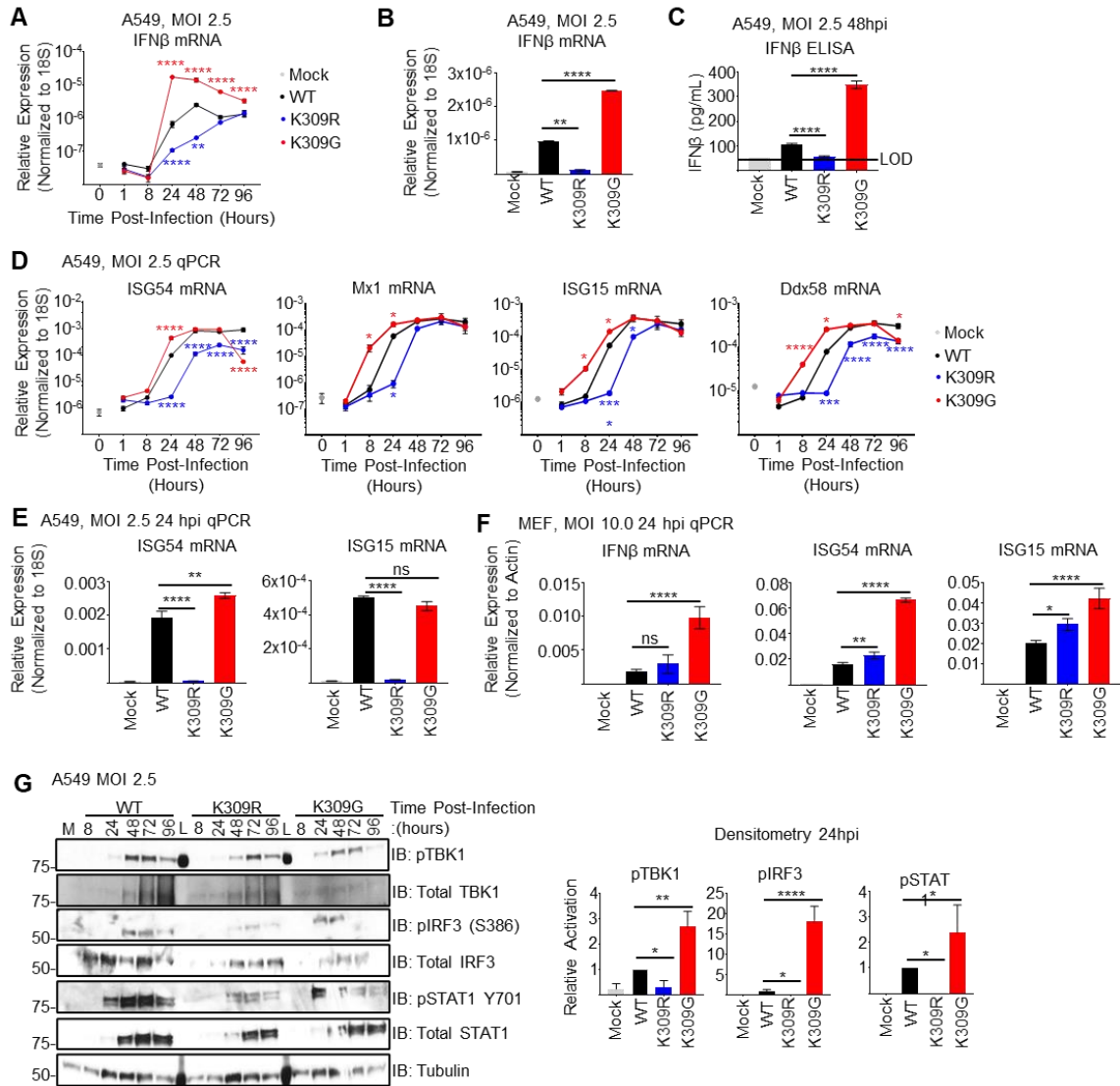


Figure 3.3 The rEBOV-VP35/K309G mutant is impaired in IFN-I antagonism during infection

A549 cells (A-E, G) or murine embryonic fibroblasts (MEFs) (F) were mock infected (grey) or infected in triplicate wells with rEBOV-eGFP-VP35/wt (black), -K309R (blue), or -K309G (red) at an MOI of 0.01 (A-C) or 2.5 PFU/cell (D-G). Cells were lysed in either TRIzol for RNA analysis (A, B, D-F) and relative expression of IFN β mRNA (A, B, F) or ISG mRNAs (D, E, F) was determined by normalizing the cycle threshold values for genes of interest to 18S (A549) or actin (MEF) cycle threshold values. Supernatants from infected A549 cells were collected in biological triplicate at 48 hours post-infection (hpi) to measure IFN β by ELISA (limit of detection (LOD) 50 pg/mL) (C). Cells were lysed in Laemmli buffer for immunoblot analysis (G). The area under the curve (AUC) for each protein was calculated using ImageJ to determine the relative activation of the interferon pathway regulators TBK1, IRF3, and STAT1 (phosphorylated protein/(respective total protein/tubulin)) was normalized to the activation levels in wt-infected cells. The western blots are representative of two independent experiments run in triplicate. The data analysis

was done using a two-way ANOVA (A, D) or one-way ANOVA (B, C, E-G) with Bonferroni's or Tukey's post-test for comparison between groups, respectively. P-value: * <0.05 , ** < 0.01 , *** <0.001 , **** <0.0001 . For two-way ANOVA with Bonferroni's post-test statistical analysis, the non-significant differences ($P > 0.05$) are not indicated on the graph to prevent cluttering. Red and blue stars represent K309G and K309R comparison to wt, respectively. (Figure reproduced with permission from van Tol et al., 2022)

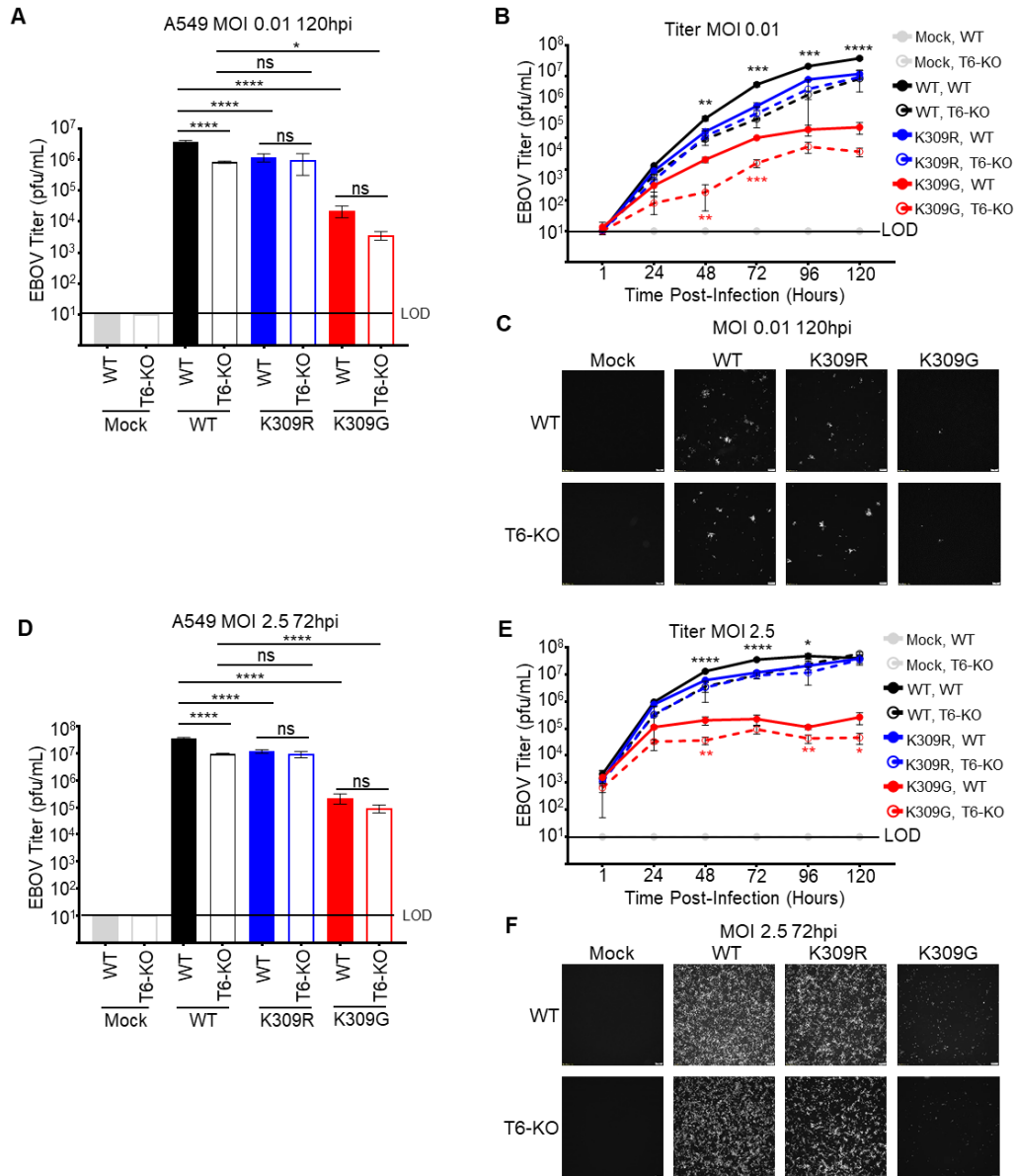


Figure 3.4 TRIM6-mediated VP35/K309 ubiquitination is required for efficient replication

Wild-type (WT) or TRIM6 knockout (T6-KO) A549 cells were infected with rEBOV-eGFP/VP35-wt, -K309R, or -K309G at a multiplicity of infection (MOI) of 0.01 PFU/cell (A-C) or 2.5 PFU/cell (D-F). The time points corresponding to the peak titer for wt virus, 120 hours post-infection (hpi) for MOI 0.01 (A) and 72 hpi for MOI 2.5 (B) are graphed separately to demonstrate the differences more clearly. The limit of detection (LOD), 10 PFU/mL, is indicated. Fluorescence images representative of three independent wells corresponding to an MOI of 0.01 PFU/cell (C) or 2.5 PFU/cell (E). The data analysis was done using a one-way ANOVA with Tukey's post-test (A and D) or two-way ANOVA with Bonferroni's post-test (B and E). P-value: * <0.05 , ** <0.01 , **** <0.0001 , and ns, not significant ($p > 0.05$). (Figure reproduced with permission from van Tol et al., 2022)

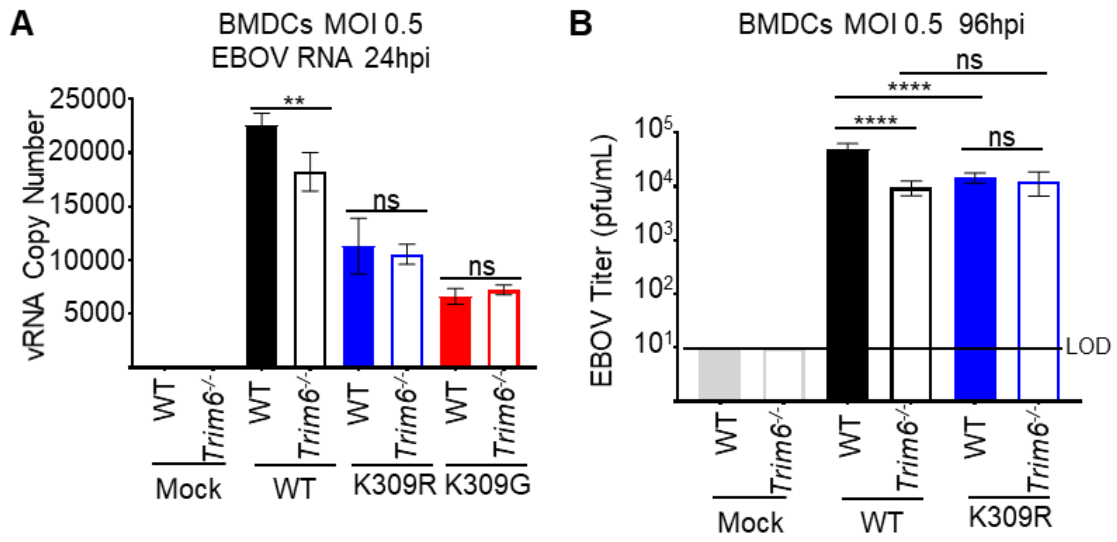


Figure 3.5 Attenuation of the rEBOV-VP35/K309R mutant is TRIM6-dependent in primary dendritic cells

Cell-sorted CD11b⁺CD11c⁺ bone marrow-derived dendritic cells (BMDCs) from WT or *Trim6*^{-/-} mice were infected with rEBOV-eGFP/VP35-wt, -K309R, or -K309G. (A) At 24 hours, RNA was collected for strand-specific qPCR for viral genomic RNA (vRNA). (B) Titer from WT or *Trim6*^{-/-} BMDCs infected with rEBOV-eGFP/VP35-wt or -K309R at an MOI of 0.5 PFU/cell for 96 hours. Samples for both strand-specific qPCR and titration were collected in biological triplicate. The data analysis was done using two-way ANOVA with Bonferroni's post-test (A and B). P-value: **<0.01, ****<0.0001, and ns, not significant (p> 0.05). (Figure reproduced with permission from van Tol et al., 2022)

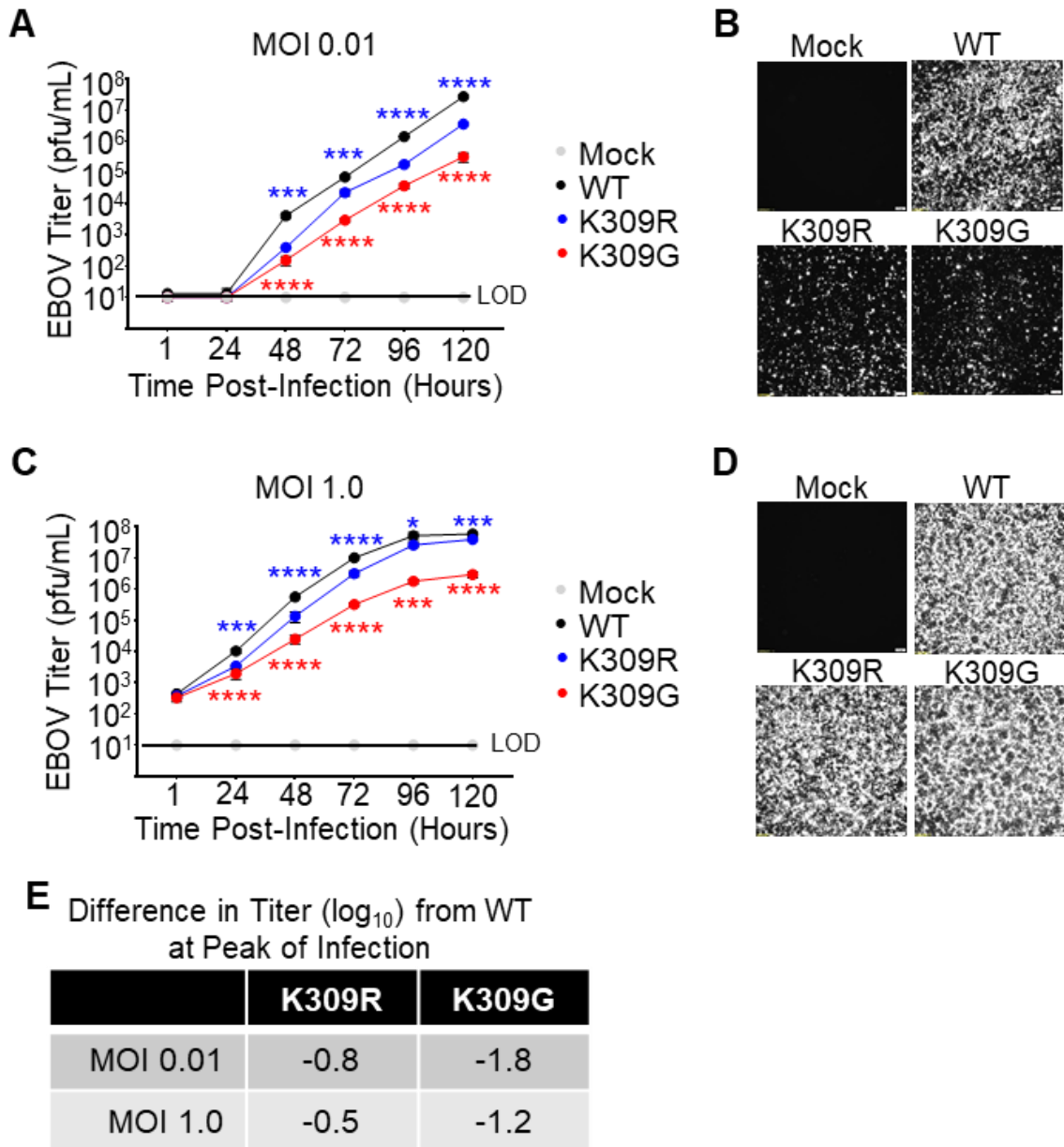


Figure 3.6 The replication of rEBOV-VP35/K309R and -G mutants is attenuated in IFN-incompetent cells

VeroE6 cells were mock infected (grey) or infected with rEBOV-eGFP-VP35/wt (black), -K309R (blue), or -K309G (red) viruses at an MOI of 0.01 (A-B) or 1.0 PFU/cell (C-D). The fluorescence microscopy images (GFP) are representative of the three images taken (B and D). The limit of detection (LOD), 10 PFU/mL, is indicated (A and C). (E) The difference in titer (\log_{10}) between the mutant and wt viruses at the time point corresponding to the wt peak titer is summarized. The titrations were collected in biological triplicate (A, C). The data analysis was done using a two-way ANOVA (A and B) with Bonferroni's post-test for comparison between groups. P-value: * <0.05 , *** <0.001 , **** <0.0001 . Red and blue stars represent K309G and K309R comparison to wt, respectively. Non-

significant differences, P-value >0.05 , are not indicated to prevent cluttering on the image.
(Figure reproduced with permission from van Tol et al., 2022)

UBIQUITINATION OF VP35/K309 ENHANCES VIRAL TRANSCRIPTASE ACTIVITY

Due to the observed attenuation of the rEBOV-VP35/K309R and -G mutant viruses in the IFN-I incompetent cells (Figure 3.6) and our previous finding that EBOV replication is impaired in TRIM6-KO cells ⁷⁹, we hypothesized that ubiquitination of VP35's K309 is important for VP35's polymerase co-factor activity. To test this, we used a monocistronic firefly luciferase expressing minigenome system ^{6,168} co-transfected with wt or mutant VP35 plasmid. Both the VP35/K309R and -G mutants possessed equivalent polymerase co-factor activities at the lower dose (25 ng) (Figure 3.7A), used to mimic polymerase activity early during infection when the NP:VP35 ratio is higher. However, the mutants' activity was decreased approximately 50% compared to wt VP35 when using a higher dose (100 ng) (Figure 3.7A). This result supports that ubiquitination of VP35 at K309 promotes polymerase co-factor activity.

We then sought to examine the molecular mechanism by which ubiquitination of VP35 affects the viral polymerase's function. Since the luciferase readout for this minigenome system cannot differentiate between the products of viral replication and transcription, we used a strand-specific qPCR to quantify the different viral RNA species during infection ^{8,172}. The strand-specific strategy's use of tagged primers enables the specific transcription of viral vRNA, cRNA, or mRNAs during the reverse transcription step of cDNA synthesis (Figure 3.7B). We measured the specific viral RNA species at 48 hr in infected A549 cells, because the total viral RNA of wt and mutant viruses is similar at this time point (Figure 3.7B), allowing comparison of specific viral RNA species without bias from the viral attenuation observed at later time points. The strand-specific analysis showed that both K309 mutants had decreased levels of L mRNA (70%), and only minimal

effects were observed in the vRNA and cRNA compared to wt virus (Figure 3.7C), suggesting that ubiquitination on VP35/K309 promotes efficient viral transcription.

To account for the potential effects of IFN in the attenuation of the mutant viruses and low levels of viral RNA present in the tested A549 samples, we evaluated the strand-specific RNA production in VeroE6 cells (MOI = 1.0 PFU/cell). We also measured the NP, VP35, VP30, and VP24 mRNAs in addition to L mRNA to assess whether changes in mRNA production differ along the transcriptional gradient (Figure 3.7B). Since the viral polymerase can only initiate transcription at the 3' end of the genome and re-initiates at the next transcription start site without falling off, a 3'-to-5' transcription gradient is generated with NP and L being the most and least abundant transcripts, respectively⁸⁻¹⁰. At 24 hpi, the copy number for vRNA and cRNA of the rEBOV-VP35/K309 mutants do not differ from the wt virus (Figure 3.7D). For EBOV genes NP, VP35 and VP24 the mRNA copy number was significantly lower for K309R as compared to wt, but not for K309G (Figure 3.7D). The copy numbers for VP40 and L transcripts were significantly lower for both mutants as compared to wt (Figure 3.7D). When looking at the ratios of copies for each RNA species relative to wt, the K309R mutant is more strongly affected than the K309G mutant and the 5' most gene, L, is the most strongly affected for both mutants (Figure 3.7E). Later in infection (72 hpi), the production of vRNA, cRNA, and all mRNAs, except NP, was lower for the K309 mutant viruses than wt (Figures 3.7F and 3.7G). For both time points, the severity of the transcriptional impairment was more pronounced for the genes on the 5' end of the genome (L > VP24, VP40, VP35 > NP) (Figures 3.7D-G). With standard qPCR, which does not differentiate the viral RNA species, viral RNA did not differ among the viruses at 24 hpi but was significantly lower for both mutants as compared

to wt at 72 hpi (Figure 3.7H). The increasing defect along the transcriptional gradient suggests that ubiquitination at K309 improves the polymerase's transcriptase function or stability when functioning as a transcriptase.

Since we previously reported that TRIM6 is responsible for ubiquitination on K309⁷⁹, and TRIM6 affects viral replication in a K309-dependent manner (Figures 3.4 and 3.5), we assessed the synthesis of the different viral RNA species in T6-KO cells. As observed in the VeroE6 cells with the K309 mutants, the levels of vRNA, cRNA, and NP mRNA did not differ between the wt and T6-KO cells (Figure 3.8A). The significant decrease in other viral mRNAs in the T6-KO cells followed a similar pattern to the VP35/309 mutant viruses with the degree of impairment increasing along the transcriptional gradient (L > VP24, VP40 > VP35) (Figure 3.8B). Similar results were observed in primary MEFs from *Trim6*^{-/-} mice infected with wt virus (Figures 3.8C and 3.8D).

We then evaluated whether the defect in viral transcription correlated with viral protein production. In wt and K309R-infected A549 cells, NP, VP35, and VP24 were similarly expressed, but VP40 and VP30 levels were substantially lower in K309R-infected cells (Figure 3.9A). No viral protein was detectable in K309G-infected A549 cells (Figure 3.9A). In VeroE6, as observed with the viral transcripts in the strand-specific qPCR, the viral protein expression was attenuated for both mutants with an increasing defect along the 3'-to-5' gradient, with the exception of VP24 which was affected less than VP40 (VP30 > VP40 > VP35, VP24 > NP) (Figure 3.9B). Interestingly, VP30 protein production was attenuated more strongly for the K309R mutant than for the K309G mutant (Figure 3.9B). Since the viral transcription factor is expressed measurably less by the mutants, VP30's

reduced presence could perpetuate the effects of a lack of VP35 ubiquitination across multiple cycles of replication.

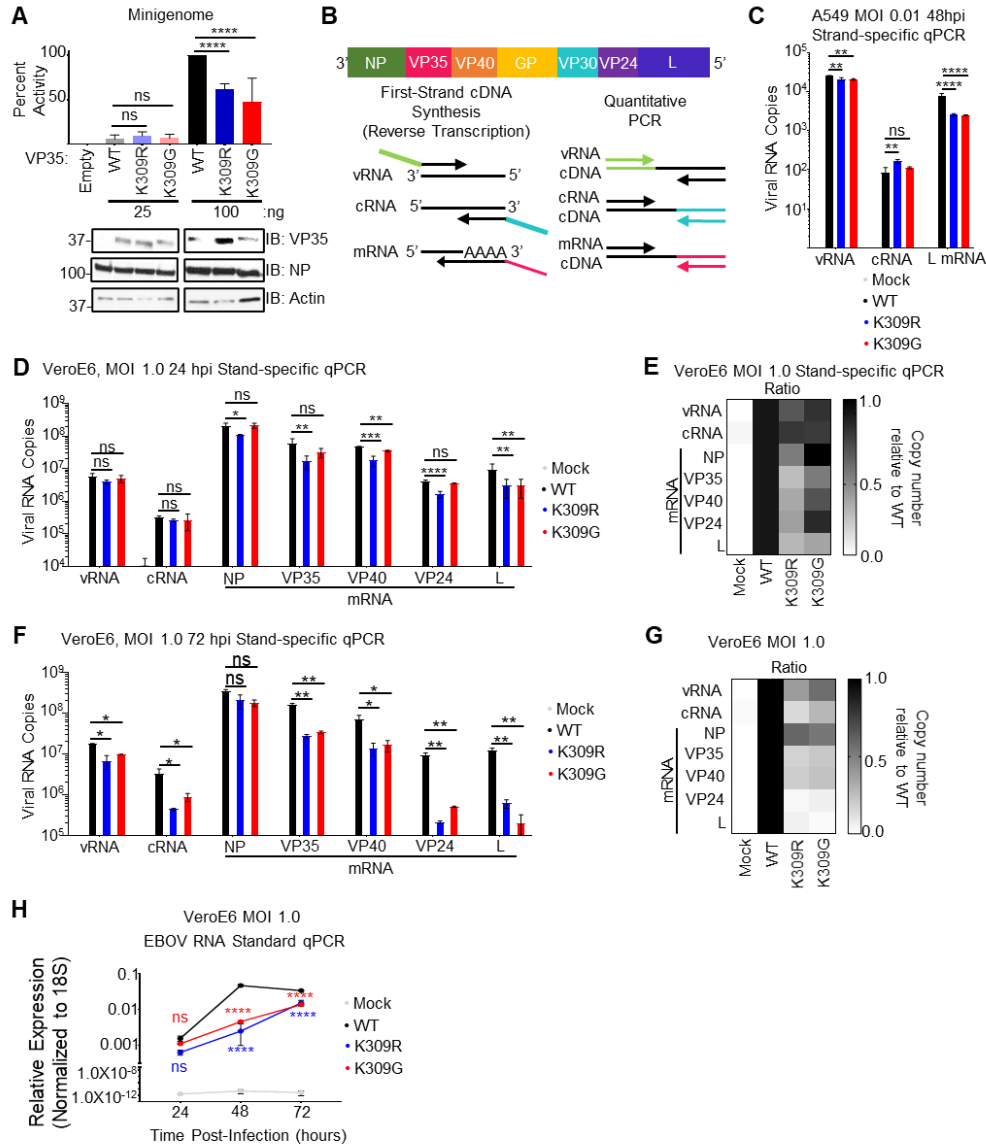


Figure 3.7 Ubiquitination of VP35/309 enhances viral transcriptase function

(A) Minigenome components (renilla, VP30, NP, L, T7 polymerase, and EBOV minigenome luciferase plasmid) were co-expressed with 25 or 100 ng of empty vector (pCAGGS) or VP35/wt, -K309R, or K309G in 293T cells. At 50 hours post-transfection, the cells were lysed to measure luciferase and evaluate protein expression. Quantification is from two independent experiments conducted in biological triplicate. (B) Graphical representation of the EBOV genome and the strand-specific qPCR approach. (C) A549 cells were infected with rEBOV-eGFP-VP35/wt (black), -K309R (blue), or -K309G (red) viruses at an MOI of 0.01 PFU/cell for 48 hours and RNA was collected for strand-specific qRT-PCR (triplicates). (D) VeroE6 cells were mock (grey) treated or infected with rEBOV-eGFP-VP35/wt, -K309R, or -K309G viruses at an MOI of 1.0 PFU/cell for 24 hours and RNA was collected for strand-specific qRT-PCR (three biological replicates from two independent experiments with qRT-PCR run in triplicate). (E) Heat map representing the

ratio of copy number relative to wt for each viral RNA species corresponding to the data presented in panel D. (F) VeroE6 cells were infected with rEBOV-eGFP-VP35/wt (black), -K309R (blue), or -K309G (red) at an MOI of 1.0 PFU/cell for 72 hours and RNA was collected for strand-specific qRT-PCR (two biological replicates run in triplicate). (G) Heat map representing the ratio of copy number relative to wt for each viral RNA species corresponding to the data presented in panel F. (H) Standard qPCR for viral RNA of VeroE6 cells at 24, 48, and 72 hpi (corresponding to the Figure 3.6.C in biological triplicate). The EBOV RNA cycle threshold was normalized to the 18S cycle threshold value. The data analysis was done using a one-way ANOVA with Tukey's post-test (A, C, D, F) or a two-way ANOVA with Bonferonni's post-test (H) for comparison between groups. P-value: * <0.05 , ** <0.01 , *** <0.001 , **** <0.0001 ; ns, not significant ($p>0.05$). (Figure reproduced with permission from van Tol et al., 2022)

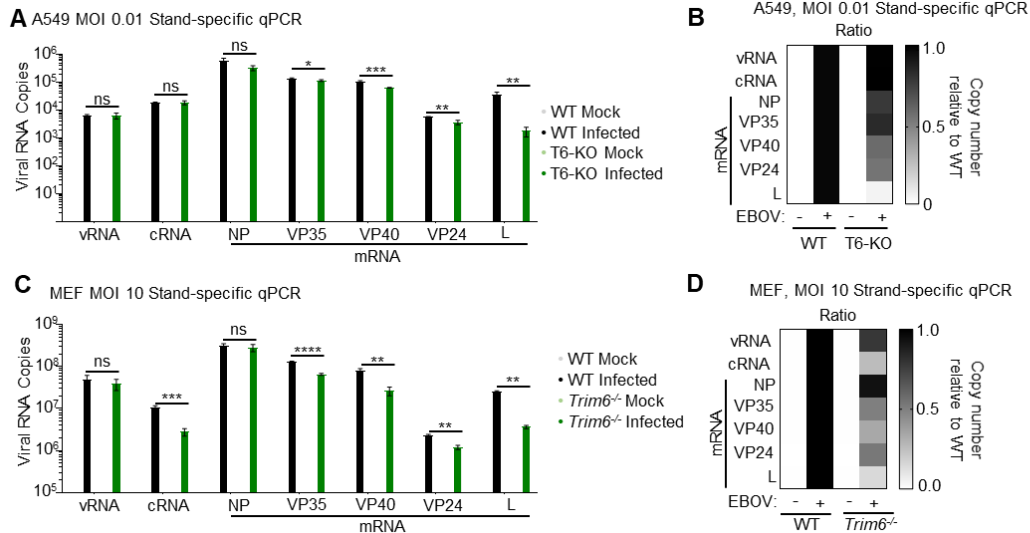


Figure 3.8 TRIM6 regulates viral transcriptase function

(A) WT (black) or TRIM6-knockout (T6-KO) (green) A549 cells were infected with rEBOV-eGFP-VP35/wt at an MOI of 2.5 PFU/cell for 24 hours and RNA was collected for strand-specific qRT-PCR (triplicates). (B) Heat map representing the ratio of copy number relative to wt for each viral RNA species corresponding to the data presented in panel A. (D) WT (black) or Trim6^{-/-} (green) murine embryonic fibroblasts (MEFs) were infected with rEBOV-eGFP-VP35/wt at an MOI of 10.0 PFU/cell for 96 hours and RNA was collected for strand-specific qRT-PCR (triplicates). (E) Heat map representing the ratio of copy number relative to wt for each viral RNA species corresponding to the data presented in panel D. The data analysis was done using a student's t-test (A and C). P-value: * <0.05, **<0.01, ***<0.001, ****<0.0001; ns, not significant (p>0.05). (Figure reproduced with permission from van Tol et al., 2022)

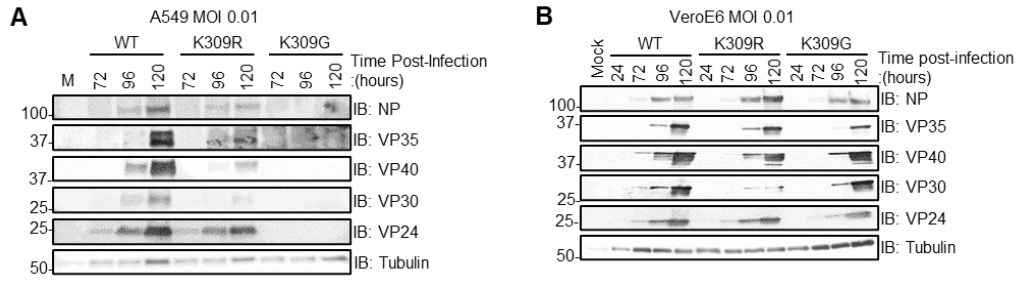


Figure 3.9 Viral protein synthesis is dysregulated in the absence of VP35/K309 ubiquitination

Protein lysates from A549 (A) or VeroE6 cells (B) infected with rEBOV-eGFP-VP35/wt, -K309R, or -K309G at an MOI of 0.01 PFU/cell, or mock-infected, were analyzed for the time-course expression of viral proteins. (Figure reproduced with permission from van Tol et al., 2022)

MUTATION OF VP35/309 DYSREGULATES VP35'S INTERACTION WITH EBOV PROTEINS BUT NOT BINDING WITH TRIM6 OR ITSELF

Due to the observed defect in polymerase co-factor activity for both VP35/309 mutants (Figure 3.7A), and because TRIM6 is able to facilitate ubiquitination of VP35⁷⁹, we evaluated the capacity of the VP35 mutants to interact with TRIM6 and viral proteins critical for polymerase function. Co-IP experiments showed that wt and the VP35/309 mutants interact with similar efficiencies with HA-TRIM6 (Figure 3.10A). The similar binding of the mutants indicates that neither ubiquitination nor a basic residue at VP35/309 are required to interact with TRIM6.

Since oligomerization regulates multiple VP35 functions^{21,27,33,171}, we also assessed whether mutation of K309 impacts self-interaction. We co-expressed His-tagged VP35 with the corresponding FLAG-tagged VP35 construct, and the Co-IP experiment showed no obvious defect in self-interaction (Figure 3.10B).

To test for the interaction of VP35 with L, we used an HA-tagged N-terminal construct of L (HA-L₁₋₅₀₅²²). The N-terminus of L is sufficient to interact with VP35²⁰. Pulldown of HA-L₁₋₅₀₅, following co-transfection with VP35, showed impaired interaction with the VP35/309 mutants compared to wt (Figure 3.10C). The L-VP35 interaction was disrupted to a similar degree between the K309R and -G mutants implying that ubiquitination, rather than a basic residue, is needed for high-affinity binding. TRIM6 is required for this L-VP35 interaction because ectopic expression of wt VP35 and HA-L₁₋₅₀₅ resulted in significantly less VP35 binding to L in T6-KO as compared to wt A549 cells (Figure 3.10D). We also observe endogenous TRIM6 being pulled down with HA-L₁₋₅₀₅, suggesting that VP35, L and TRIM6 may form complex (Figure 3.10D). To further test the dependence of TRIM6-mediated VP35 ubiquitination, we co-transfected T6-KO A549

cells with wt VP35 and HA-L₁₋₅₀₅ in the presence of wt or a catalytic TRIM6 mutant (C15A) that is unable to ligate ubiquitin onto its targets^{79,89}. We observed that reconstitution with the wt, but not the C15A mutant, enhanced (10-fold) VP35's interaction with L (Figure 3.10E).

Interactions between VP35 and NP are required for coupling viral replication with NP encapsidation of the nascent vRNA or cRNA, chaperoning free NP (NP^o) to prevent pre-mature NP-RNA interaction, and assembling the nucleocapsids²²⁻²⁴. Further, VP35 has two distinct NP-interacting regions, one in the N-terminus^{23,24} and the other in the C-terminus²². Due to the complexity of NP-VP35 interactions, we tested how ablation of K309 ubiquitination affects their binding in a cell-free environment. To test binding *in vitro*, lysates from FLAG-VP35 (wt, K309R, or K309G) or empty vector transfected cells were added to FLAG-beads and washed prior to the addition of purified HA-NP. Interestingly, HA-NP bound the FLAG-VP35/K309R mutant approximately 2.5-fold more efficiently than wt FLAG-VP35, but the FLAG-VP35/K309G-HA-NP interaction did not differ from wt VP35 (Figure 3.11A), suggesting that lack of ubiquitination on VP35/309 while retaining the basic residue increases interaction with NP. To test the dependence of TRIM6 on this phenotype, we co-transfected wt VP35 and HA-NP in wt and T6-KO cells. As expected, the amount of VP35 bound to NP is higher (6-fold) in T6-KO cells (Figure 3.11B).

To test the importance of ubiquitination of VP35/309 more directly, and to rule out any minor effects due to structural changes of the K-to-R mutation, we used the ovarian tumor deubiquitinase (OTU) of Crimean-Congo hemorrhagic fever virus¹⁷³ which removes endogenous Ub from modified proteins and has been used previously to

demonstrate functions of ubiquitinated proteins^{55,89,110,174}. We used the OTU to remove endogenous Ub from VP35 wt prior to incubation with HA-NP-coated beads *in vitro* (Figure 3.11C). As expected, we observed more Ub associated with wt- than K309R VP35 immunoprecipitated with an anti-VP35 antibody, and the wt OTU was able to remove all the ubiquitin associated with VP35 (Figures 3.11D and 3.11E). VP35 was co-expressed with wt FLAG-OTU or a catalytically impaired mutant (FLAG-OTU-2A). The OTU activity was inactivated upon lysis with the deubiquitinase inhibitor N-ethylamine (NEM), and the lysates were mixed with HA-beads containing HA-NP purified from separate lysates. Consistent with the *in vitro* NP-VP35 interaction experiment, VP35 K309R binding to HA-NP was stronger (5-fold) than wt VP35 in the absence of OTU (Figures 3.11D and 3.11F). Co-expression with OTU-wt increased (5-fold) the amount of VP35 wt that bound HA-NP to a similar level as the untreated K309R mutant (Figures 3.11D and 3.11F). In contrast, co-expression with the catalytically inactive OTU-2A mutant had only minimal effects on VP35 wt's binding to HA-NP (Figures 3.11D and 3.11F), confirming that the lack of ubiquitin on VP35/K309 facilitates interaction with NP. The OTU co-expression did not impact the K309R mutant's interaction with NP (Figures 3.11D and 3.11F), suggesting that VP35/K309 ubiquitination is responsible for impeding full interaction with NP. Further, we did not observe a significant increase in the binding of a K-all-R VP35 mutant, which has all sixteen of its lysine residues mutated to arginine to completely prevent Ub conjugation onto VP35, to NP compared to K309R VP35 supporting that ubiquitination on K309 is responsible for impeding NP binding (Figures 3.11D and 3.11F).

We also evaluated VP35's interaction with viral proteins during infection in VeroE6 cells. The K309G, but not the K309R, mutant was impaired in its interaction with NP, VP30, and VP40 compared to wt VP35 (Figure 3.12). Both VP35/309 ubiquitination and a basic residue are important for interaction with VP24, as lack of ubiquitin increased (K309R) and loss of a basic residue (K309G) decreased this interaction (Figure 3.12). The differential interaction between VP35 and viral proteins associated with mature nucleocapsid formation and budding, VP24 and VP40, may contribute to the excess attenuation of K309G mutant when infecting IFN-I incompetent cells (Figures 3.6A and 3.6C).

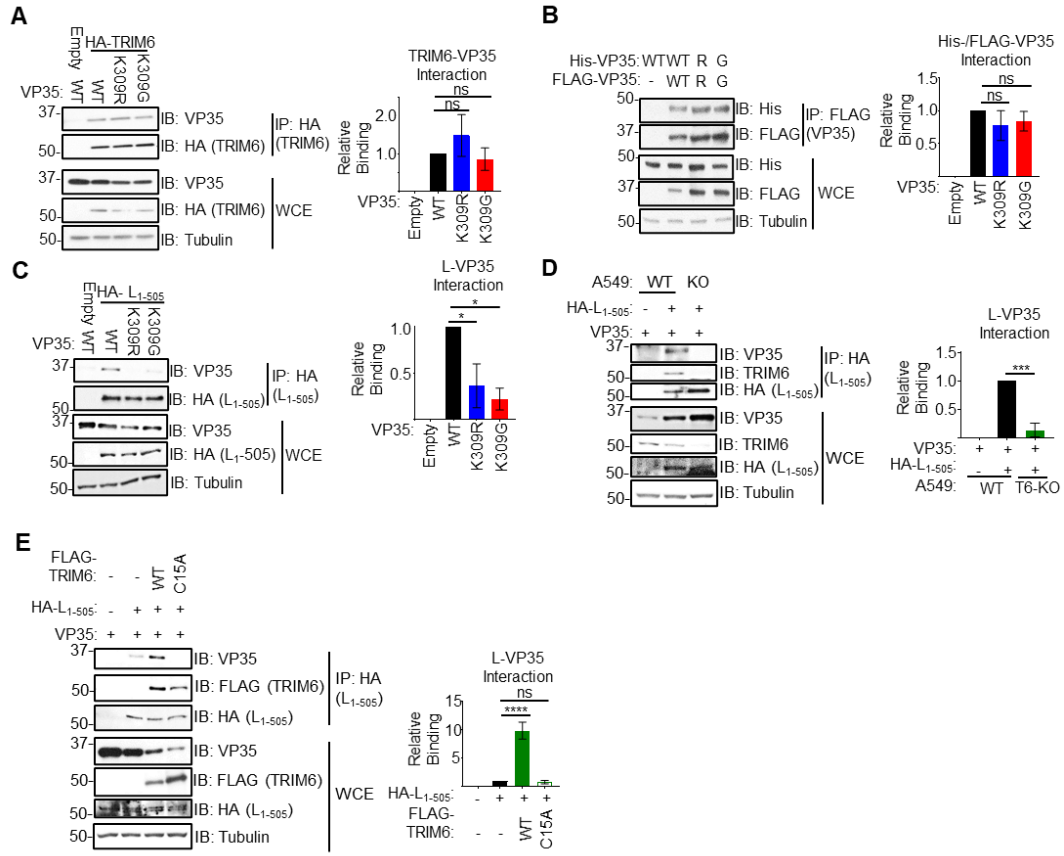


Figure 3.10 Mutation of VP35 at K309 dysregulates VP35's interaction with the EBOV polymerase but not TRIM6 or itself

(A) Lysates (WCE) and HA-immunoprecipitation (IP) from 293T cells co-transfected with untagged VP35 (wt, K309R, or K309G) with HA-TRIM6 or pCAGGS (empty vector). The quantification is based on immunoblot densitometry (area under the curve) determined using ImageJ from three independent experiments. The binding ratio ((IP: VP35/HA-TRIM6)/(WCE: (VP35/HA-TRIM6)/Tubulin)) for each VP35 construct was divided by wt VP35's ratio to determine relative binding. (B) 293T cells were co-transfected with His- or FLAG-tagged VP35 and FLAG IPs were performed. The quantification is based on AUC determined using ImageJ from three independent experiments. The binding ratio ((IP: His-VP35/FLAG-VP35)/(WCE: (His-VP35/FLAG-VP35)/Tubulin)) for each VP35 construct was divided by wt VP35's ratio to determine relative binding. (C) WCE and HA-IP from 293T cells co-transfected with untagged VP35 (wt, K309R, or K309G) with HA-L₁₋₅₀₅ or empty vector. Immunoblot quantification from two independent experiments. The binding ratio ((IP: VP35/HA-L₁₋₅₀₅)/(WCE: (VP35/HA-L₁₋₅₀₅)/Tubulin)) for each VP35 construct was divided by wt VP35's ratio to determine relative binding. (D) HA-L₁₋₅₀₅ and untagged wt VP35 were co-transfected into wt or TRIM6 knockout (T6-KO) A549 cells, and WCE were immunoprecipitated with anti-HA-tagged beads. The quantification is from data collected from three independent experiments. The binding ratio ((IP: VP35/HA-L₁₋₅₀₅)/(WCE: (VP35/HA-L₁₋₅₀₅)/Tubulin)) for lysates from wt and T6-KO cells was divided by the wt's ratio to determine relative binding. (E) HA-L₁₋₅₀₅ and untagged wt VP35 were co-transfected with FLAG-tagged TRIM6 wt or -C15A or empty vector into T6-KO A549

cells, and WCE were immunoprecipitated with anti-HA-tagged beads. The quantification is from data collected from two independent experiments. The binding ratio ((IP: VP35/HA-L₁₋₅₀₅)/(WCE: (VP35/HA-L₁₋₅₀₅)/Tubulin)) for lysates from T6-KO cells transfected with empty vector, HA-TRIM6-wt, or -C15A was divided by the ratio of empty vector transfected cells to determine relative binding. The data analysis was done using a one-way ANOVA with Tukey's post-test for comparison between groups (A-E). P-value: *<0.05, **<0.01, ***<0.001, ****<0.0001; ns, not significant (p>0.05). (Figure reproduced with permission from van Tol et al., 2022)

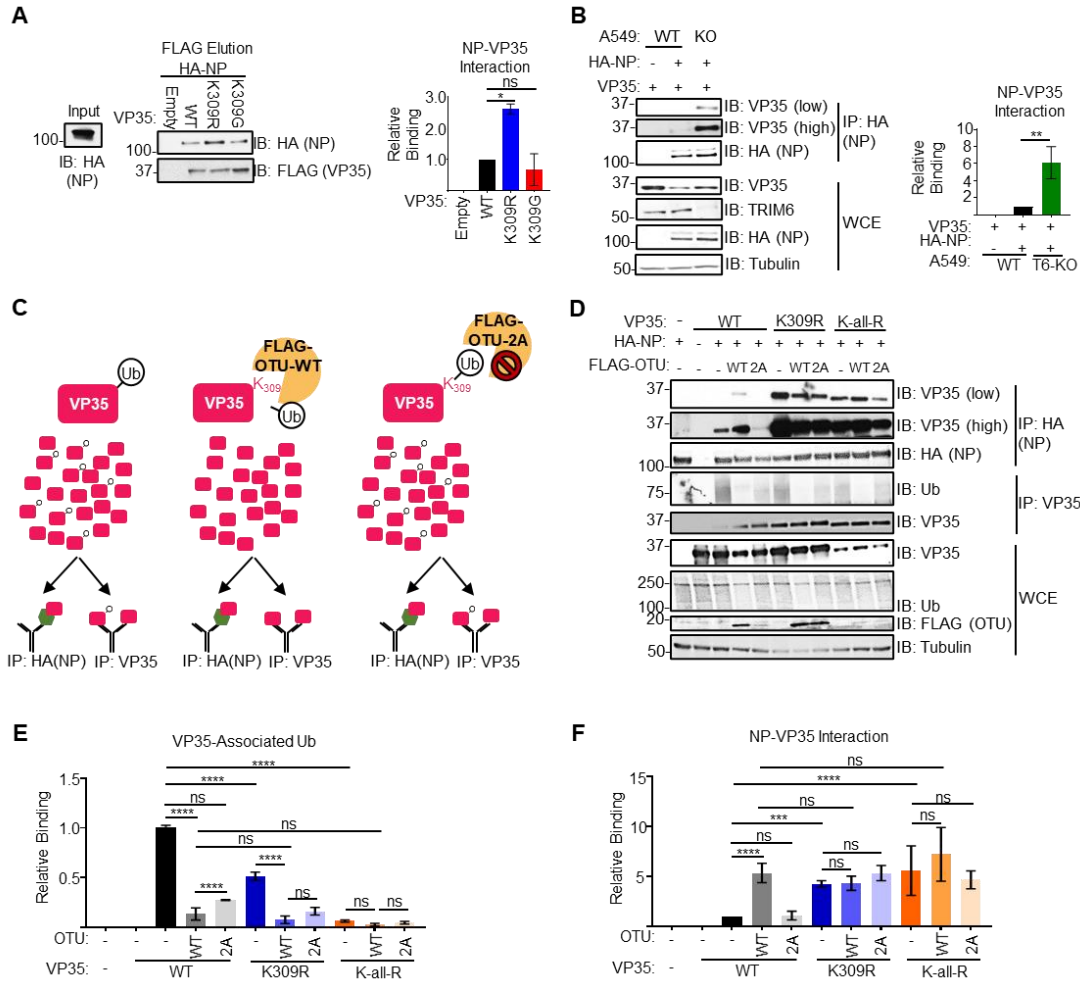


Figure 3.11 Ubiquitination of VP35 at K309 impedes interaction with EBOV nucleoprotein

(A) HA-NP (input) was added to beads bound with lysates from empty vector or FLAG-VP35 (wt, K309R, or K309G) transfected 293T cells, washed, and FLAG-eluted. Immunoblot quantification from two independent experiments. The binding ratio (HA-NP/FLAG-VP35) for each VP35 construct was divided by the ratio of wt VP35 to determine relative binding. (B) HA-NP and untagged wt VP35 were co-transfected into wt or T6-KO A549 cells and the WCE were immunoprecipitated with anti-HA beads. The blot quantifications are representative of two independent experiments. The binding ratio ((IP: VP35/HA-NP)/(WCE: (VP35/HA-NP)/Tubulin)) for lysates from wt and T6-KO cells was divided by the wt's ratio to determine relative binding. (C) Diagram depicting the experiment set-up for the deubiquitinase experiment. When wild-type VP35 (pink rectangle) is expressed, several ubiquitin molecules will be ubiquitinated (white circle with 'Ub') at lysine 309. When co-expressed with catalytically active, wt ovarian tumor (OTU) deubiquitinase, the covalently linked ubiquitin will be cleaved from VP35. The catalytically inactive mutant, OTU-2A, has two key cysteine residues mutated to alanine and is not able to cleave ubiquitin from substrates. Lysates cells co-expressing VP35 and FLAG-OTU were added onto beads coated with either HA-NP (antibody molecule with

green hexagon) or VP35-specific antibody (antibody with pink rectangle). (D) 293T cells were co-transfected with untagged VP35 (wt, K309R, or K-all-R) and empty vector or FLAG-OTU (wt or -2A). The WCE from VP35 FLAG-OTU co-transfected cells were incubated with the anti-HA (IP:HA), IgG-protein A, or anti-VP35-protein (IP: VP35) coated beads, bound with lysates from HA-NP or empty vector transfected cells to pulldown VP35 (IP:HA) or ubiquitin (IP: VP35). The western blot is representative of two independent experiments run in duplicate. (E) The area under the curve (AUC) for each protein from the western blots in panel D were calculated using ImageJ. The relative binding ratio (VP35 IP: (Ub/VP35)/WCE: (Ub/VP35)/tubulin) for VP35-associated ubiquitin was determined for each condition and divided by the ratio for wt VP35 without OTU treatment. (F) The area under the curve (AUC) for each protein from the western blots in panel D were calculated using ImageJ. The relative binding ratio (HA-NP IP: (VP35/HA-NP)/WCE: (VP35/tubulin) for VP35-NP binding was determined for each condition and divided by the ratio for wt VP35 without OTU treatment. The data analysis was done using a one-way ANOVA with Tukey's post-test (A and B) or two-way ANOVA with Bonferroni's post-test (E and F) for comparison between groups. P-value: * <0.05 , ** <0.01 , *** <0.001 , **** <0.0001 ; ns, not significant ($p>0.05$). (Figure reproduced with permission from van Tol et al., 2022)

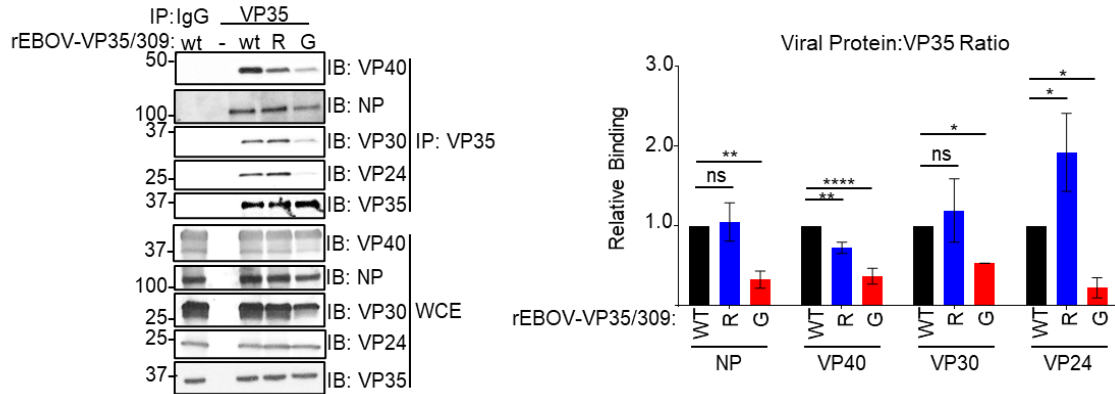


Figure 3.12 Lack of ubiquitination and a basic residue at VP35/309 dysregulates VP35's interaction with viral proteins

Lysates from mock or rEBOV-VP35/wt/-K309R or -K309G infected (MOI = 0.01 PFU/cell for 144 hours) VeroE6 cells were immunoprecipitated (IP) with IgG or anti-VP35 antibody with protein A beads in RIPA complete and used for western blot to assess interaction with viral proteins VP40, NP, VP24 and VP30. Lysates used for this experiment were also used for Figure 3.1C. The area under the curve (AUC) for each protein was calculated using ImageJ from western blots run in triplicate. The relative binding ratio (IP: (viral protein/VP35)/WCE: (viral protein/VP35)) was for all VP35 constructs and divided by wt VP35's ratio. The data analysis was done using a one-way ANOVA with Tukey's post-test for comparison between groups. P-value: * <0.05 , ** <0.01 , *** <0.001 , **** <0.0001 ; ns, not significant ($p>0.05$). (Figure reproduced with permission from van Tol et al., 2022)

LACK OF UBIQUITINATION AND A BASIC RESIDUE AT VP35/309 DYSREGULATES VIRUS ASSEMBLY

Due to the differences between the VP35/K309R and -G mutants in their production of infectious virus in IFN-I incompetent VeroE6 cells, despite similar levels of viral RNA, we hypothesized that both ubiquitination and retention of a basic residue at VP35/309 contribute to virus assembly. To evaluate the integrity of virus assembly, we collected samples from the supernatants and lysates of VeroE6 infected cells and the corresponding sucrose-gradient purified virus. When evaluating the relative amounts of viral proteins incorporated into the virion, the K309R and -G mutant virions contained similar amounts of NP, VP40, VP30, and VP24 relative to the amount of VP35 (Figure 3.13A). The K309G mutant trended toward lower VP35 incorporation relative to NP and VP24, but the difference was not significant (Figure 3.13A). This suggests that the K309 mutants have as similar viral protein composition to wt (Figure 3.13A) despite the dysregulated intracellular viral protein ratios (Figure 3.9). When we measured packaged viral vRNA copies in the sucrose purified virus, the K309R mutant packaged as much vRNA as wt but the K309G mutant packaged significantly less (Figure 3.13B). As a measure of genome packaging efficiency, we compared packaged and intracellular vRNA copies and observed a 2-fold increase for the K309R mutant and a 3-fold decrease for the K309G mutant (Figure 3.13C). We then evaluated the mutants' infectivity by comparing the titer (PFU/mL) to packaged vRNA and found that the infectivity was reduced for both the K309R (78%) and -G (92%) mutants (Figure 3.13D). Finally, we compared the overall efficiency of infectious virus production by calculating the ratio of infectious virus (PFU/mL) in supernatants and the intracellular vRNA copies for the corresponding cell lysates. We found 55% ($\sim 0.4 \log_{10}$) and 98% ($\sim 1.5 \log_{10}$) less infectious virus/intracellular genome copy for the K309R and -

G mutant viruses respectively (Figure 3.13E), which correlates with the differences observed in the kinetics experiments (Figure 3.6E). Overall, these results suggest that both ubiquitination and a basic residue at VP35/309 are important for coordinating the assembly of infectious virus. Despite the VP35/K309R mutant's increased packaging efficiency, the infectivity is impaired likely due to the premature packing of vRNA potentially associated with the increased VP24 binding. In contrast, the rEBOV-VP35/K309G mutant is impaired in both virus assembly and infectivity correlating with impaired VP35-VP24 and -VP40 interactions.

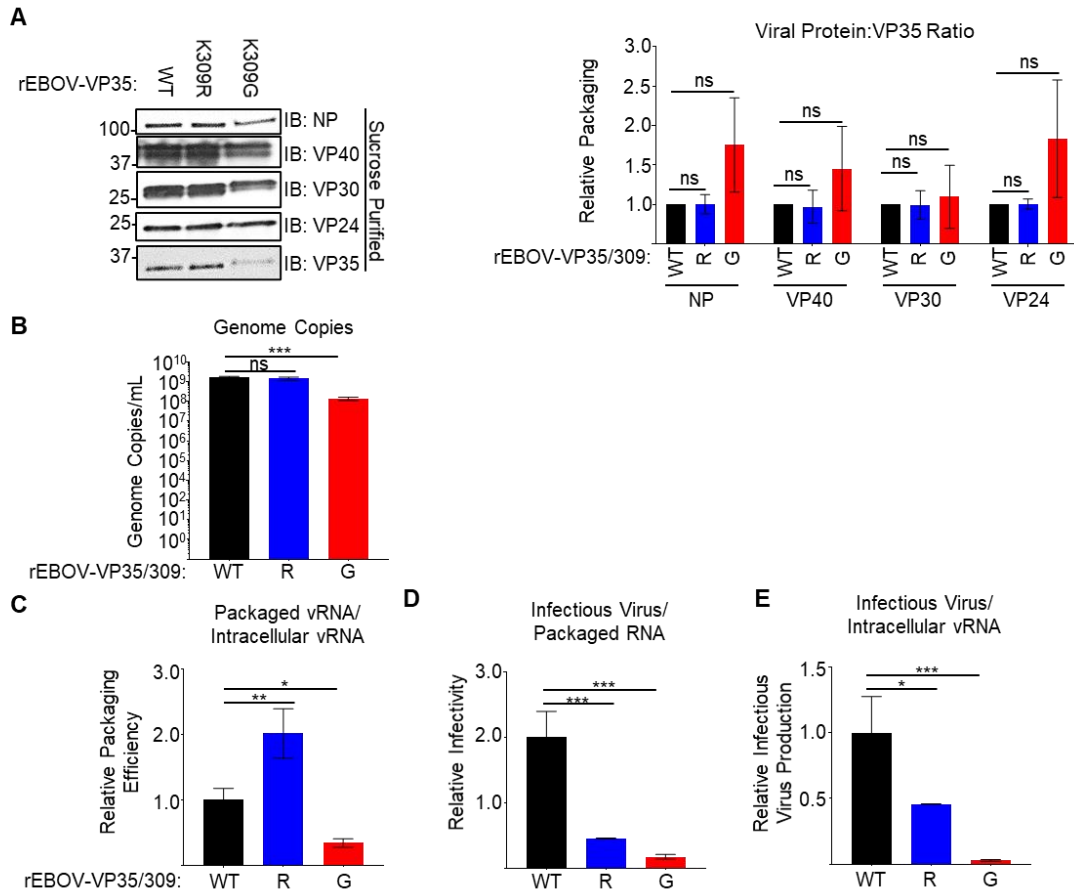


Figure 3.13 Lack of ubiquitination and a basic residue at VP35/309 dysregulates virus assembly

(A) Protein lysates (WCE) from VeroE6 cells infected cells (MOI = 0.01 PFU/cell, 144 hours) with rEBOV-eGFP-VP35/wt (WT), -K309R (R), or -K309G (G) and corresponding sucrose-gradient purified virus. The area under the curve (AUC) for each antibody were calculated using ImageJ from western blots run in triplicate. The packaging ratio (purified virus: (viral protein/VP35)/WCE (panel B): (viral protein/VP35)) was for all VP35 constructs and divided by wt VP35's ratio. (B) The number of viral genome copies was determined using strand-specific qPCR of sucrose-gradient-purified virus. (C) The ratio of packaged to intracellular RNA copies was determined using strand-specific qPCR for genomic RNA on lysates from cells and the purified virus, and the ratio was normalized to the value for wt virus. (D) The ratio of infectious virus to packaged genome copies was determined by titrating the sucrose-gradient purified virus (PFU/mL) and strand-specific PCR to calculate the vRNA copies in the corresponding sample, and the ratio was normalized to the value for the wt virus. (E) The ratio of infectious virus to intracellular genome copies was determined using the supernatant titer and intracellular genome copy number, and the ratio was normalized to the value for the wt virus. This experiment was performed in triplicate (B-E). The data analysis was done using a one-way ANOVA with Tukey's post-test for comparison between groups (A-E). P-value: * <0.05 , ** <0.01 , *** <0.001 , **** <0.0001 ; ns, not significant ($p>0.05$). (Figure reproduced with permission from van Tol et al., 2022)

Chapter 4: VP35's N-terminus can be Ubiquitinated and Mutation of the K119.126.141 Cluster Attenuates VP35's Polymerase Co-Factor

Activity

MULTIPLE LYSINE RESIDUES IN VP35'S N-TERMINUS ARE UBIQUITINATED

Since we have consistently observed Ub-conjugated forms of VP35 after VP35/309 mutation⁷⁹, we wanted to identify the other lysine residue that accept this post-translational modification. We used N-terminal (aa 1-221) and C-terminal (aa 222-340) constructs and K-to-R mutants for the 16 different lysine residues to aid in identifying the ubiquitin-modified sites (Figure 4.1A). Further, we were interested in understanding the role of VP35 ubiquitination at the other site(s).

We first wanted to determine whether the other covalent ubiquitination modification occurs on VP35's N- or C-terminal lysine residue(s). To test this, FLAG-VP35-wt full-length (FL), N-terminus, or C-terminus was co-expressed with HA-Ub-wt before immunoprecipitation with anti-HA beads. As expected, we observe Ub-conjugated, FL and C-terminus VP35 (Figure 4.1B). We also found Ub-conjugated forms for VP35's N-terminus (Figure 4.1B). To determine whether residues other than VP35/K309 are ubiquitinated on VP35's C-terminus, we expressed wt, K309R, or K-all-R (all eight C-terminus lysine residues mutated to R) with HA-Ub. The K309R mutation ablated most of the Ub-conjugated on VP35's C-terminus, but we cannot completely rule out that other C-terminal lysine residues may accept Ub. Repeating these experiments with a VP35 C-terminal construct alternatively tagged to eliminate extra lysine residues present in the FLAG epitope, such as His, will provide more conclusive results.

In an attempt to narrow down which lysine residues in VP35's N-terminus may receive conjugated ubiquitin, we sent FLAG-VP35-N-terminus immunoprecipitated from 293T cells for mass spectrometry analysis. Two VP35 peptides with diglycine modification, indicative of ubiquitination, were identified (Figure 4.1D). The predicted ubiquitinated residues corresponded to T35, K119, and K126 (Figure 4.1D). The mass spectrometry results also indicated that a K in the FLAG peptide also receives conjugated ubiquitin. Based on these results, we wanted to test whether the FLAG tag received conjugated Ub and determine how many K residues in the N-terminus are Ub-modified. We co-expressed either untagged- or FLAG-N-terminus -wt or K-all-R (all eight N-terminal lysine residues mutated to arginine) with HA-Ub-wt or -K-all-R. Consistent with the mass spectrometry results, the FLAG-VP35-N-K-all-R construct still had Ub-VP35 conjugates that were ablated when using the untagged-VP35-N-K-all-R (Figure 4.1E). Using the HA-Ub-K-all-R mutant, which can be covalently linked onto target proteins but cannot form Ub chains, we found that there are two Ub-conjugated VP35 bands for the untagged-VP35-N-wt (Figure 4.1E). Importantly, the HA-Ub-K-all-R-conjugated VP35 bands are absent for the untagged-VP35-N-K-all-R construct (Figure 4.1E). These results suggest that at least two N-terminal Ks are ubiquitinated.

In an attempt to validate the mass spectrometry results indicating that VP35/K119 and -126 receive conjugated Ub, we generated K-to-R mutants either singly or in groups in an untagged, full-length VP35 construct. Mutation of any N-terminal lysine residue (K6R, K63.67R, K119.126.141R, or K184.216R) decreased the number of HA-Ub-conjugated VP35 bands (Figure 4.1F). The FL VP35 construct with all of the N-terminal lysine residues mutated to arginine (K6-216R) still had HA-Ub-conjugated bands,

consistent with ubiquitination at VP35/K309 (Figure 4.1F). Since all of the N-terminal VP35 lysine residues seem capable of receiving Ub, we are unsure whether their Ub modification occurs non-specifically unlike the VP35/K309-Ub modification.

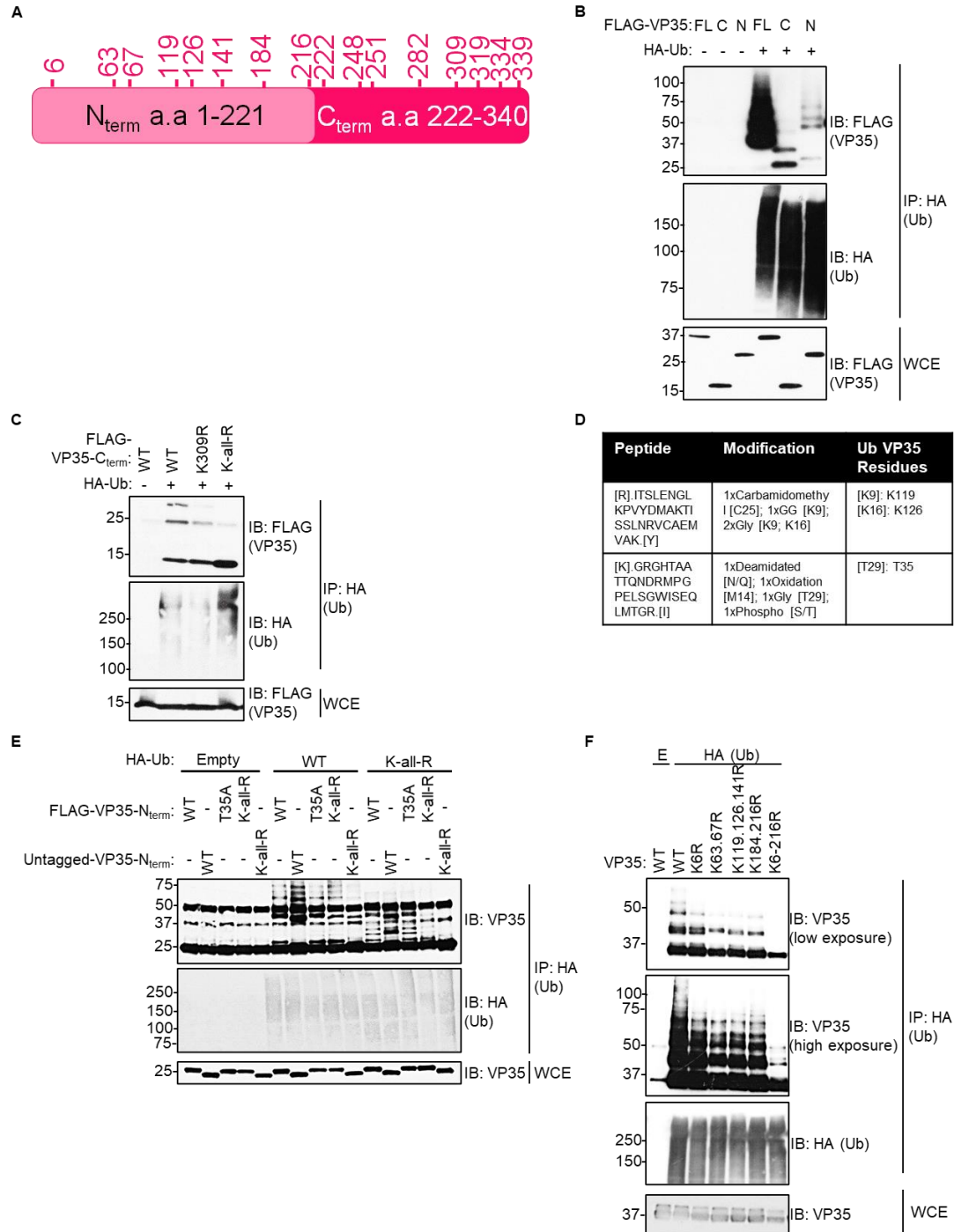


Figure 4.1 Multiple lysine residues in VP35's N-terminus are ubiquitinated

(A) Linear schematic of VP35's N (amino acids 1-221)- and C (a.a. 222-340)-termini with the position of the sixteen amino acids marked. (B) Lysates (WCE) from 293T cells co-expressing FLAG-VP35 full-length (FL), N- (N), or C (C)-terminus with HA-Ub were immunoprecipitated (IP) with anti-HA beads to evaluate the ubiquitin-conjugated forms of VP35. (C) WCE from 293T cells co-expressing FLAG-C- wild-type (WT), K309R, or K-all-R with HA-Ub were IP with anti-HA beads to evaluate the ubiquitin-conjugated forms

of VP35's C-terminus. (D) Summary of ubiquitinated VP35 peptides for FLAG-VP35-N. (E) WCE from 293T cells co-expressing untagged- or FLAG-VP35-N WT, T35A, or K-all-R with HA-Ub WT or K-all-R were IP with anti-HA beads to determine whether the FLAG tag could be ubiquitinated and how many VP35-N lysine residues are ubiquitinated. (F) WCE from 293T cells co-expressing FL untagged-VP35 WT, K6R, K63.67R, K119.126.141R, K184.216R, or K6-216R with HA-Ub WT were IP with anti-HA beads to determine which VP35-N lysine residues are ubiquitinated. (Figure made by Sarah van Tol)

MUTATION OF VP35'S LYSINE RESIDUES AT POSITIONS 119,126, AND 141 TO ARGININE IMPAIRS VP35'S POLYMERASE CO-FACTOR ACTIVITY

We found that several of the K residues can be ubiquitinated, and we were interested in whether any of the K-to-R mutations have functional consequences. First, we screened the mutants in a minigenome assay using the optimal VP35 dose (100 ng) to test their polymerase co-factor activity. There was no significant difference in polymerase co-factor function for the K6R or K63.67R mutants, but the K119.126.141R, K184.216R, and K6-216R mutants had significantly lower activity (Figure 4.2A). We repeated the experiment with just the K119.126.141R, K184.216R, and K6-216R constructs at a lower dose of VP35 (25 ng), and only the K119.126.141R and K6-216R mutants were attenuated (Figure 4.2B). Importantly, the magnitude of attenuation for the K119.126.141R and K6-216R mutants was similar suggesting that K119.126.141 group is functionally important. We titrated the levels of VP35 wt and K119.126.141R, and the mutant is impaired in its polymerase co-factor function at all doses (Figure 4.2C). To evaluate whether one specific residue in the K119.126.141 group drives the phenotype, we mutated these residues singly or in pairs alongside the K119.126.141R mutant. At a low dose of VP35 (25 ng), K119R and K119.126R mutants were not significantly impaired, but all other mutants lost activity (Figure 4.2D). When using the optimal VP35 dose (100 ng), all of the mutants were attenuated (Figure 4.2D). Interestingly, all the mutants containing the K141R substitution tended to be impaired more strongly (Figure 4.2D). Overall, these data suggest retention of a K for residues 119, 126, and 141 is important for polymerase co-factor function.

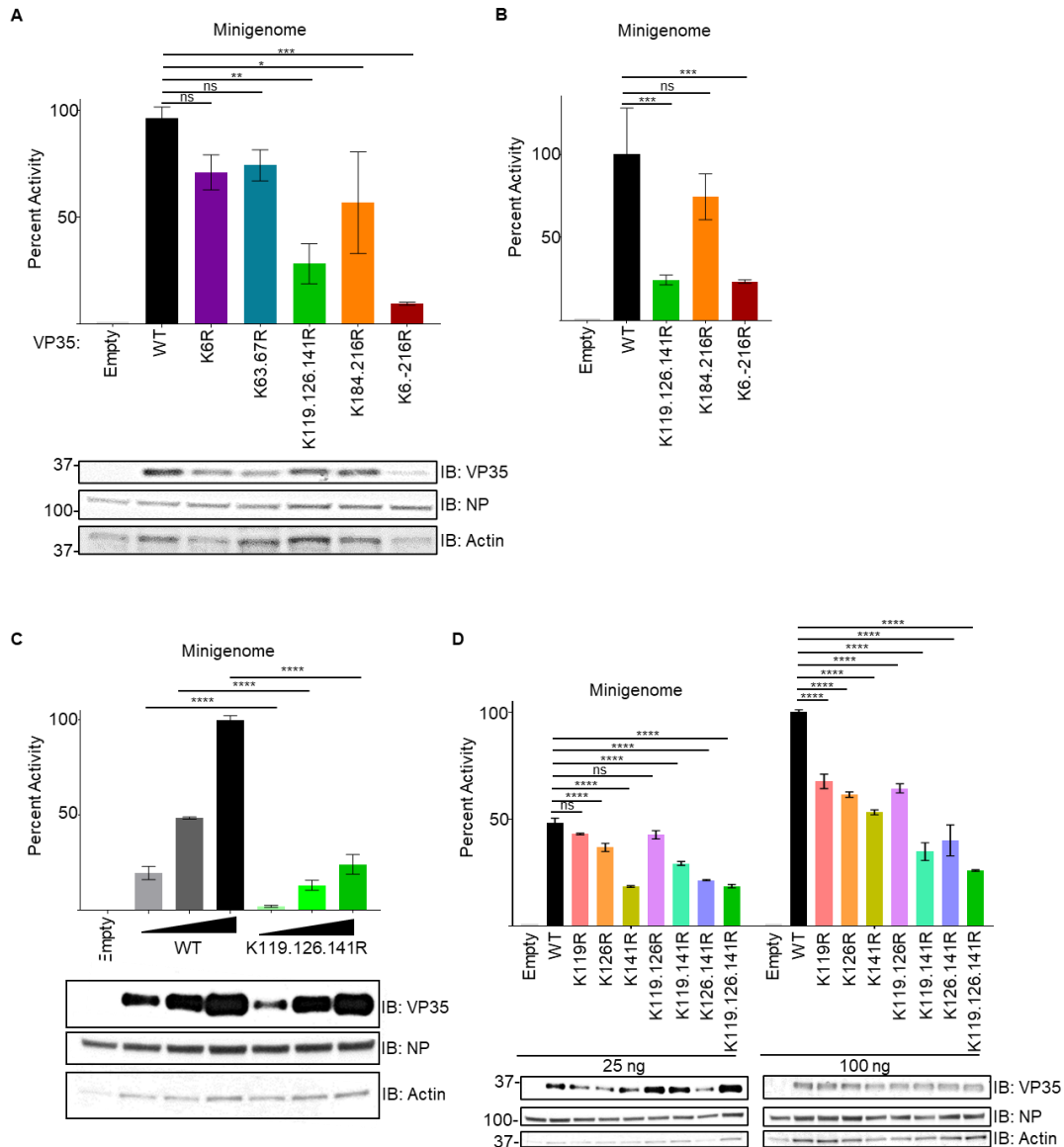


Figure 4.2 Mutation of VP35's lysine residues at positions 119, 126, and 141 to arginine impairs VP35's polymerase co-factor activity

(A) Minigenome components (renilla, VP30, NP, L, T7 polymerase, and EBOV minigenome luciferase plasmid) were co-expressed with 100 ng of empty vector (pCAGGS) or VP35/wt, K6R, K63.67R, K119.126.141R, K184.216R, or K6-216R in 293T cells. At 50 hours post-transfection, the cells were lysed to measure luciferase and evaluate protein expression. Quantification is from two independent experiments conducted in biological triplicate. Lysates from transfected cells were also lysed in Laemmli for subsequent immunoblotting to monitor protein expression. (B) Minigenome assay as in panel A with 25ng of pCAGGS, VP35/wt, K119.126.141R, K184.216R, or K6-216R. Quantification is from one experiment conducted in biological triplicate. (C) VP35/wt or K119.126.141R were co-expressed with minigenome components at three dose: 25, 50, and 100 ng. Quantification is from one experiment conducted in biological

triplicate. (D) VP35/wt, K119R, K126R, K141R, K119.126R, K119.141R, K126.141R, or K119.126.141R we co-expressed with minigenome components at two doses: 25 and 100 ng. Quantification is from one experiment conducted in biological triplicate. The data analysis was done using a one-way ANOVA with Tukey's post-test (A and B) or two-way ANOVA with Bonferroni's post-test (C and D) for comparison between groups. P-value: * <0.05 , ** <0.01 , *** <0.001 , **** <0.0001 ; ns, not significant ($p>0.05$). (Figure made by Sarah van Tol)

MUTATION OF VP35'S N-TERMINAL LYSINE RESIDUES TO ARGININE DOES NOT ALTER IFN-I INHIBITION, HOMO-OLIGOMERIZATION, OR INTERACTION WITH OTHER VIRAL PROTEINS

We wanted to investigate whether any of the N-terminal K-to-R mutations impacted VP35's other functions. None of the mutants were impaired in their antagonism of HMW poly(I:C)-induced (Figure 4.3A) or IKK ϵ -induced (Figure 4.3B) IFN β -promoter activity, as expected since the C-terminus contains the dsRNA binding domain. Importantly, all of the untagged full-length K-to-R mutants retained their ability to self-interact with a FLAG-VP35-N-terminal construct containing the corresponding K-to-R mutation(s) (Figure 4.3C). We also did not observe a consistent impairment in the mutants' interaction with the N-terminal construct of the EBOV polymerase (HA-L₁₋₅₀₅) (Figure 4.3D). No difference in the NP-VP35 interaction was detected for the K6R, K63.67R, or K184.216R mutants, but we did observe a slight increase in binding for the K119.126.141R mutant (Figure 4.3E). However, when we repeated the different K119.126.141 group mutants, we did not observe a change in VP35-NP interaction (Figure 4.3F).

Overall, these results suggest that mutation of the N-terminal lysine residues partially blocks Ub conjugation. The K119.126.141 group, particularly K141, is important for VP35's full polymerase co-factor function although mutation of these residues do not impede VP35's interactions known to be important for polymerase activity including binding with itself, the polymerase, or nucleoprotein. Further experiments are needed to link ubiquitination at these sites to the polymerase co-factor phenotype more directly. Alternatively, the K119.126.141 residues are located within the region of VP35 mapped to be required for VP35's ATPase- and helicase-like activities³⁶, and additional experiments are needed to evaluate this group's contribution to VP35's enzymatic activities.

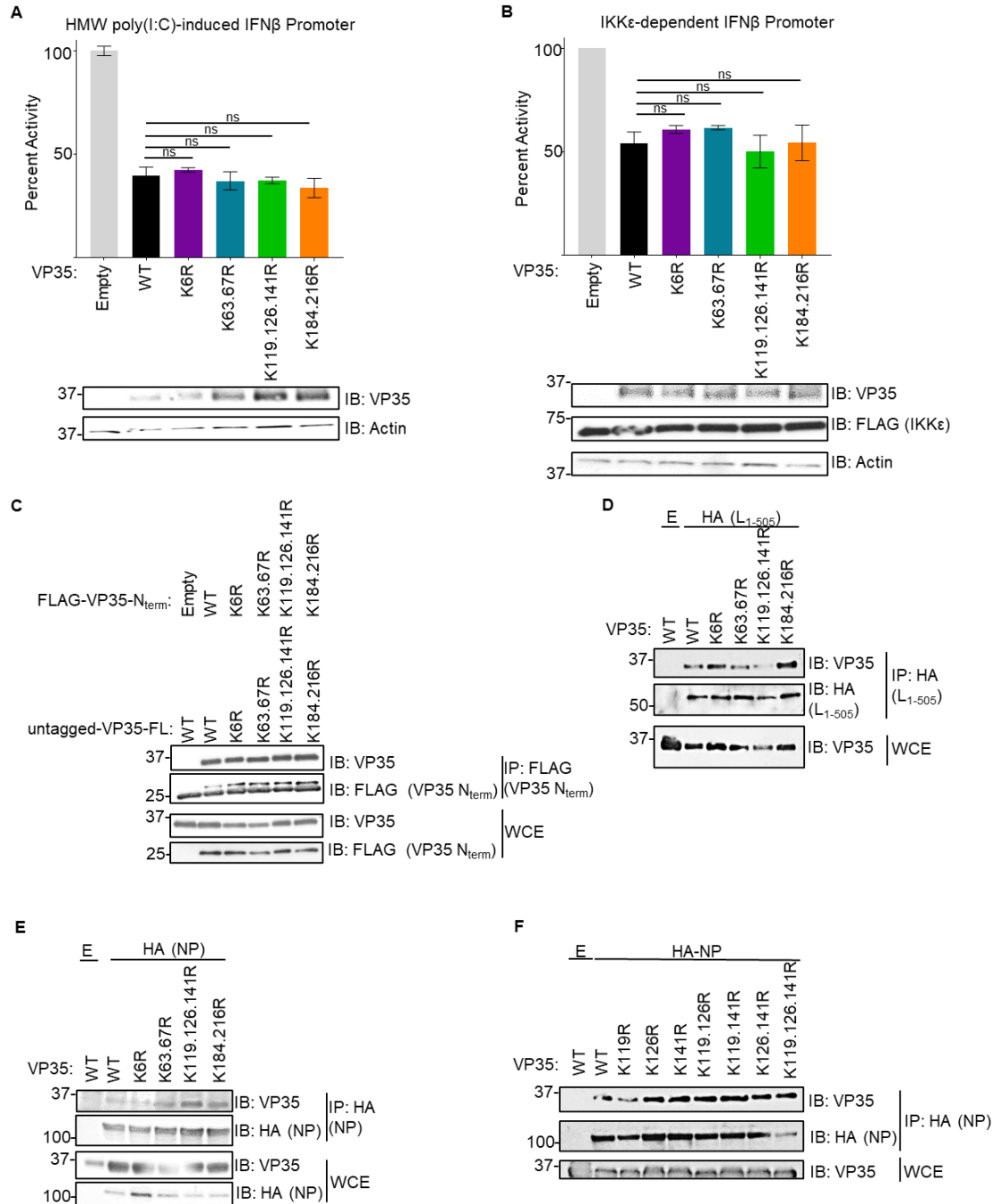


Figure 4.3 Mutation of VP35's N-terminal lysine residues to arginine does not alter IFN-I inhibition, homo-oligomerization, or interaction with other viral proteins

(A) 293T cells were transfected with IFN β luciferase reporter and Renilla luciferase plasmid and transfected 24 hours later with 3.125 μ g/mL high molecular weight (HMW) poly(I:C). The ratio of firefly luciferase (IFN β promoter activity) to renilla luciferase (transfection efficiency normalization) luminance was measured for each VP35 construct in the presence and absence of poly(I:C) stimulation. The percent activity relative to empty vector is presented. The quantification is from two independent experiments conducted in

biological triplicate, and the IB is representative of the corresponding lysates. (B) As in A, but 2 ng IKK ϵ was transfected along with the luciferase plasmids to stimulate the IFN β promoter. The ratio of firefly luciferase (IFN β promoter activity) to renilla luciferase (transfection efficiency normalization) luminance was measured for each VP35 construct in the presence and absence of IKK ϵ over-expression. The percent activity relative to empty vector is presented. The quantification is from two independent experiments conducted in biological triplicate, and the IB is representative of the corresponding lysates. (C) Lysates (WCE) from 293T cells co-expressing FLAG-VP35-N-terminus (N) wild-type (WT) or K-to-R mutants with the corresponding full-length (FL), untagged VP35 K-to-R mutants were immunoprecipitated (IP) with anti-FLAG beads to evaluate self-interaction. (D) WCE from 293T cells co-expressing FL, untagged VP35 K-to-R mutants with HA-L₁₋₅₀₅ were IP with anti-HA beads to evaluate binding with Ebola virus' polymerase. (E and F) WCE from 293T cells co-expressing FL, untagged VP35 K-to-R mutants with HA-NP were IP with anti-HA beads to evaluate binding with Ebola virus' nucleoprotein. The data analysis was done using a one-way ANOVA with Tukey's post-test for comparison between groups (A and B). P-value: ns, not significant ($p > 0.05$). (Figure made by Sarah van Tol)

Chapter 5: VP35 and NP's Interaction with Unanchored, K63-linked Polyubiquitin Enhances Polymerase Activity

VP35 INTERACTS WITH UNANCHORED UBIQUITIN

We observed that VP35 non-covalently interacts with ubiquitin ⁷⁹, but we did not study the VP35-ubiquitin binding mechanism or investigate its contribution toward Ebola virus replication. Here, we used a combination of co-expression, *in vitro*, and *in silico* binding studies with a minigenome assay to understand the interaction's biological relevance.

Our first question was whether VP35 interacts with free Ub. We used an Ub mutant with the C-terminal diglycine residues deleted (HA-Ub- Δ GG) to prevent Ub conjugation onto target proteins. Co-expression of FLAG-VP35-wt with HA-Ub-wt pulled down free VP35 and VP35-Ub conjugates as expected, but when co-expressed with HA-Ub- Δ GG only the free VP35 pulls down (Figure 5.1A). We still observed a slightly higher molecular weight band of VP35 being pulled down with the Δ GG mutant, but we suspect that this is a phosphorylated form of VP35 as it runs at a slightly lower molecular weight than mono-ubiquitinated VP35.

After observing that VP35 can bind to mono-ubiquitin, we wanted to evaluate whether treatment with an unanchored Ub-specific deubiquitinase could selectively prevent VP35's non-covalent Ub interaction. To investigate whether we could selectively block the non-covalent VP35-Ub interaction without impeding the covalent modification onto VP35's target lysine residues, we used two different deubiquitinases: OTU or isopeptidase T (IsoT) (Figure 5.1B). OTU cleaves both free and project-conjugated Ub molecules, but IsoT specifically binds to the C-terminal diglycine motif that is only present

on free, non-conjugated ubiquitin allowing targeted cleavage of unanchored ubiquitin chains (Figure 5.1B)¹⁷⁵. Co-expression of FLAG-VP35-N and HA-Ub-wt with GFP-OTU-wt prevents VP35's interaction with unanchored Ub and Ub conjugation onto VP35 (Figure 5.1C). OTU's catalytic activity is required, since co-expression with the mutant GFP-OTU-2A does not prevent Ub's covalent modification of VP35 or the non-covalent interaction (Figure 5.1C). In contrast, co-expression with His-IsoT specifically impaired the non-covalent interaction (Figure 5.1C). The disruption of the non-covalent VP35-ubiquitin binding increases as we increase the IsoT dose (Figure 5.1D). Importantly, treatment with a catalytically inactive mutant, His-IsoT-C335A¹⁷⁵, does not impede VP35's ability to bind Ub (Figure 5.1E). Overall, these data support that IsoT treatment can specifically impede VP35's interaction with unanchored Ub.

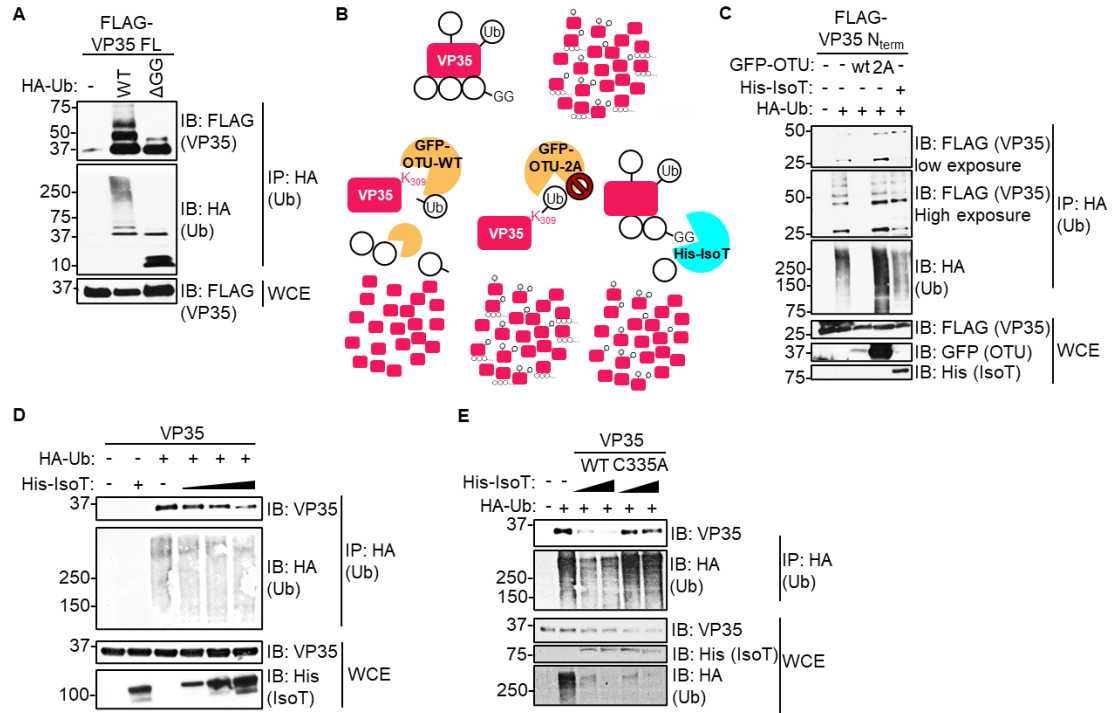


Figure 5.1 VP35 interacts with unanchored ubiquitin

(A) Lysates (WCE) from 293T cells co-expressing FLAG-VP35-full-length (FL) with the empty vector (pCAGGS), HA-Ub-wild-type (WT) or delta diglycine (Δ GG) were immunoprecipitated (IP) with anti-HA beads to evaluate interaction with free ubiquitin. (B) Schematic depicting VP35's (pink rectangle with 'VP35') covalent and non-covalent associations with ubiquitin (white circles). VP35 receives covalent ubiquitin onto at least two different lysine residues (Ub- with stick) and interacts with unanchored ubiquitin (depicted as three ubiquitin molecules linked with an available C-terminal diglycine). The ovarian tumor (OTU) deubiquitinase (yellow partial circle) cleaves both conjugated and non-conjugated ubiquitin, but the mutant OTU-2A lacks catalytic activity (red 'no' symbol). Isopeptidase T (IsoT) is an ubiquitin-specific peptidase that specifically binds the C-terminal diglycine of free ubiquitin and will breakdown only free ubiquitin chains. (C) WCE from 293T cells co-expressing FLAG-VP35-N-terminus with the empty vector (pCAGGS), GFP-OTU-WT or -2A, or IsoT and HA-Ub. The lysates were IP with anti-HA beads to evaluate interaction with free ubiquitin and the ubiquitin-conjugated forms of VP35. (D) WCE from 293T cells co-expressing untagged, full-length VP35 with the empty vector or increasing doses of IsoT in the presence or absence of HA-Ub. The lysates were IP with anti-HA beads to evaluate VP35's interaction with free ubiquitin. (E) WCE from 293T cells co-expressing untagged, full-length VP35 with the empty vector or IsoT WT or catalytic mutant C335A with or without HA-Ub. The lysates were IP with anti-HA beads to evaluate VP35's interaction with free ubiquitin. (Figure made by Sarah van Tol)

VP35'S C-TERMINUS AND NP INTERACT WITH K63-LINKED POLYUBIQUITIN

Since VP35 could interact with host proteins containing UBDs in experiments using HA-Ub-wt over-expression, we cannot show that VP35 directly interacts with free Ub using this experiment. To circumvent this limitation and identify the type of ubiquitin that VP35 interacts with, we developed an *in vitro* binding experiment that mixed recombinant Ub with VP35 (Figure 5.2A). We IP FLAG-VP35-wt from 293T cells with anti-FLAG coated bead, washed seven times, and incubated FLAG-VP35 coated beads with recombinant mono-Ub, K48-polyUb (2-7 Ub molecules), or K63-polyUb (2-7 Ub molecules) overnight before washing and eluting with FLAG-peptide (Figure 5.2A). We found that VP35 specifically interacts with K63-polyUb of at least 4 Ub molecules (Figure 5.2B).

We then wanted to test which VP35 domain facilitates interaction with the K63-polyUb. Using the same *in vitro* experimental set-up, we bound FLAG-VP35-wt FL, N-terminus, or C-terminus to beads before adding K63-polyUb. Both FLAG-VP35 FL and C-terminus efficiently pulled down ubiquitin, suggesting that the C-terminus facilitates this interaction (Figure 5.2C). To evaluate whether ubiquitin conjugation onto VP35/K309 influences interaction with unanchored ubiquitin, we immunoprecipitated FLAG-VP35-wt, K309R, -G and allowed K63-polyUb to bind. Neither a basic residue nor ubiquitination at VP35/309 influences this interaction as both the R and G mutants bound the recombinant Ub as well as wt (Figure 5.2D).

In order to predict the VP35 residues that interact with unanchored ubiquitin, the VP35-IID structure was modeled with mono-Ub for docking simulations (Dr. Rafael Najmanovich at University of Montreal). The residues predicted to be important for

interaction are VP35/R225:Ub/E18 and VP35/K222:Ub/E16 (Figure 5.2E). Interestingly, both of these basic residues are located within VP35's FBP²². First basic patch R and K residues have been shown to be important for NP binding and retention of a basic residue is essential for minigenome activity²², but the reason is unknown. We tested whether mutation of the predicted Ub-interacting R225 to glutamic acid (E) or K would disrupt interaction with K63-polyUb. Consistent with the model, mutation to a negative charge (R225E) partially disrupted VP35-Ub interaction (Figure 5.2F). In contrast, conservation of a basic residue (R225K) did not alter this interaction.

Since VP35's FBP is predicted to influence interaction with nucleoprotein and we observe a potential importance for this region in the interaction with unanchored ubiquitin, we investigated whether EBOV NP can interact with ubiquitin non-covalently. As with VP35, we find that NP specifically binds K63-polyUb chains that are at least 4 Ub molecules long (Figure 5.2G). This suggests that K63-polyUb chains may facilitate VP35-NP interaction that is important for polymerase function.

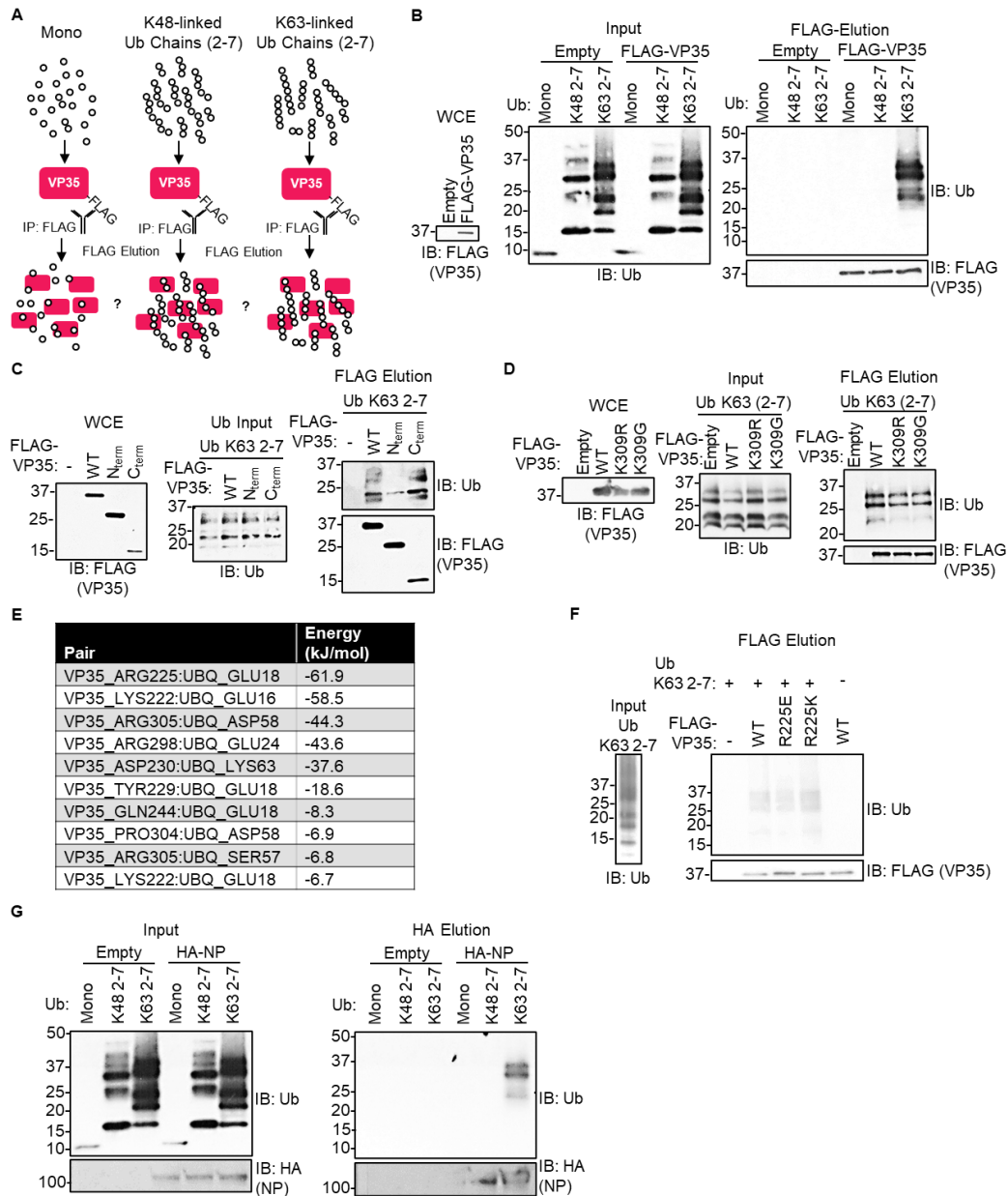


Figure 5.2 VP35's C-terminus and NP interact with K63-linked polyubiquitin

(A) Schematic demonstrating the experimental approach to evaluate VP35's (pink rectangle) interaction with recombinant mono-ubiquitin ('mono', single circles), K48-linked polyubiquitin chains of 2-7 molecules ('K48-linked Ub Chains (2-7)', staggered circles in groups), K63-linked polyubiquitin chains of 2-7 molecules ('K63-linked Ub Chains (2-7)', straight circles in groups). Recombinant ubiquitin was added onto anti-FLAG beads coated with semi-purified FLAG-VP35 prior to elution with FLAG peptide. (B) Immunoblots from the *in vitro* ubiquitin binding assay show the input FLAG-VP35 levels from transfected 293T cells lysates (WCE), the ubiquitin input for each sample, and the bound ubiquitin following FLAG peptide elution. (C) Immunoblots from the *in vitro*

ubiquitin binding assay as in panel B with FLAG-VP35 full-length (FL), N- (N), or C- (C) terminus incubated with K63-linked polyubiquitin chains. (D) Immunoblots from the in vitro ubiquitin binding assay as in panel B with full-length FLAG-VP35 wild-type (WT), K309R/ or -G incubated with K63-linked polyubiquitin chains. (E) Free energy values from *in silico* analysis predicting VP35-Ub interacting residues. (F) Immunoblots from the in vitro ubiquitin binding assay as in panel B with full-length FLAG-VP35 wild-type (WT), R225E/ or -K incubated with K63-linked polyubiquitin chains. (G) Immunoblots from the in vitro ubiquitin binding assay as in panel B with HA-NP and HA-peptide elution. (Figure made by Sarah van Tol)

CLEAVAGE OF UNANCHORED UBIQUITIN BLOCKS EBOLA VIRUS' POLYMERASE ACTIVITY

To test the functional relevance of unanchored ubiquitin, we co-expressed increasing amounts of His-IsoT with the EBOV minigenome components. We observed a dose-dependent attenuation of minigenome activity when His-IsoT was expressed (Figure 5.3A). Since high amounts of IsoT resulted in impaired VP35 and NP expression (Figure 5.3A), we elected to perform future experiments with 15 ng of His-IsoT. We observed that expression of His-IsoT-wt, but not the catalytic mutant (C335A), consistently impaired minigenome activity approximately 50% (Figure 5.3B). This supports that unanchored Ub is important for EBOV's polymerase function.

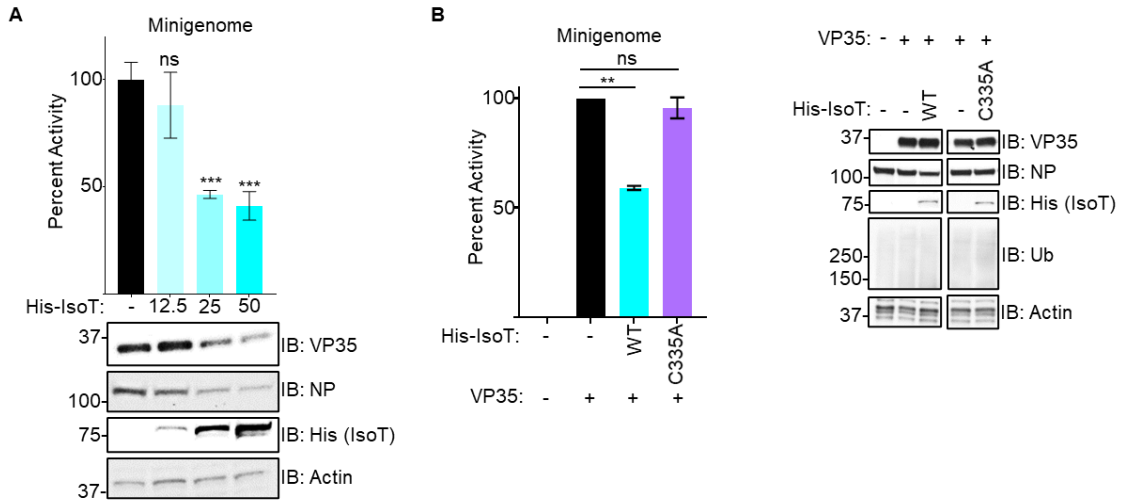


Figure 5.3 Cleavage of unanchored ubiquitin blocks Ebola virus' polymerase activity

(A) Minigenome components (renilla, VP30, NP, L, T7 polymerase, and EBOV minigenome luciferase plasmid) were co-expressed with 50 ng of VP35 with increasing amounts of isopeptidase T (IsoT) or pCAGGS (empty) in 293T cells. At 50 hours post-transfection, the cells were lysed to measure luciferase and evaluate protein expression. Quantification is from two independent experiments conducted in biological triplicate. Lysates from transfected cells were also lysed in Laemmli for subsequent immunoblotting to monitor protein expression. (B) Minigenome assay as in panel A with 15 ng of IsoT wild-type (WT) or catalytic mutant C335A. Quantification is from two independent experiments conducted in biological triplicate. Lysates from transfected cells were also lysed in Laemmli for subsequent immunoblotting to monitor protein expression. The data analysis was done using a one-way ANOVA with Tukey's post-test (A and B) for comparison between groups. P-value: **<0.01, ***<0.001; ns, not significant (p>0.05). (Figure made by Sarah van Tol)

FREE UBIQUITIN IS PACKAGES IN TO EBOLA VIRUS PARTICLES

IAV incorporates unanchored poly-ubiquitin into its virions to facilitate virus replication¹⁷⁶. Since we observed a proviral role for unanchored Ub in facilitating EBOV's polymerase activity and found that K63-polyUb interacts with VP35 and NP, we were curious whether EBOV also packages free, unanchored Ub into progeny virus. We used the sucrose-purified virus from Figure 3.13 to test for packaged Ub. The rEBOV-eGFP-VP35/wt, K09R, and -G viruses all incorporated at least mono-, di-, tri-, and tetra-Ub into their particles (Figure 5.4). Future experiments are needed to understand the functional relevance and mechanism of Ub incorporation into EBOV particles.

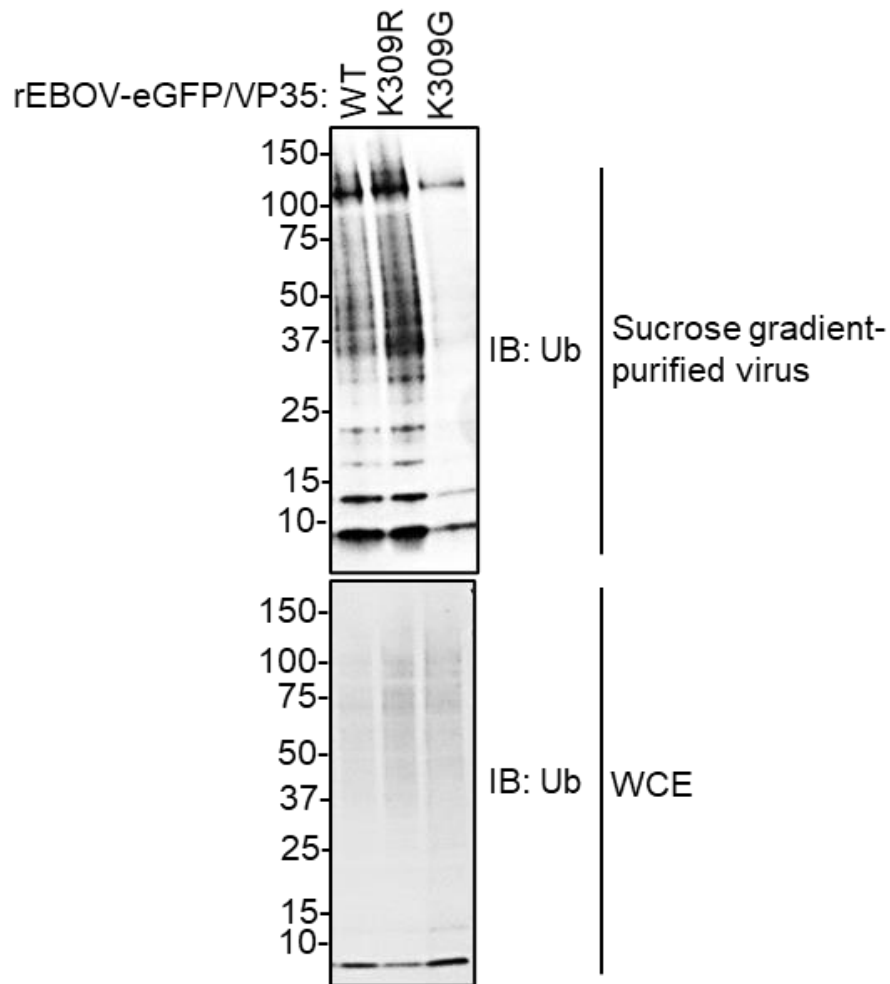


Figure 5.4 Free ubiquitin is packaged into Ebola virus particles

Protein lysates (WCE) from VeroE6 cells infected cells (MOI = 0.01 PFU/cell, 144 hours) with rEBOV-eGFP-VP35/wt (WT), -K309R (R), or -K309G (G) and corresponding sucrose-gradient purified virus. Immunoblots for ubiquitin are shown. The viral proteins for the corresponding samples are in Figure 3.13B. (Figure made by Sarah van Tol)

Chapter 6: TRIM25 is Proviral and can Ubiquitinate VP35

TRIM25 INTERACTS WITH VP35'S C-TERMINUS

TRIM6 is among a large sub-group of TRIMs that contain a SPRY domain. Since TRIM6 interacts with VP35 via its C-terminal SPRY domain⁷⁹, we were interested in investigating the potential for redundancy of VP35 ubiquitination via other TRIMs with a SPRY domain. Although we did not see an additional attenuation of the rEBOV-VP35/K309 mutant viruses in T6-KO compared to wt A549s, we cannot rule out that other TRIM family members may facilitate VP35 ubiquitination at K309 in cells with low or absent TRIM6 expression or ubiquitinate other VP35 lysine residues. Investigating the potential contribution of other TRIMs is important for the development of potential therapeutics that would target a TRIM6-VP35 interaction and understanding how TRIMs may influence EBOV infections *in vivo*.

For our first step in investigating TRIM family redundancy, we screened VP35 binding to TRIM6's closest family members (TRIM5 α , TRIM21, TRIM22, and TRIM34) and TRIM25. We found that only HA-TRIM25 and -TRIM6 bound to VP35 (Figure 6.1A). Of note, the HA-TRIM22 plasmid did not express well compared to the other TRIMs, and the lack of VP35-TRIM22 interaction needs to be validated. After finding that VP35 and TRIM25 interact, we tested which VP35 and TRIM25 domains interacted. We observed that TRIM25s SPRY domain efficiently binds to VP35, but the B-box can also be able to bind (Figure 6.1B). As with HA-TRIM6, HA-TRIM25 binds to FLAG-VP35 FL and C-terminus but not the N-terminus (Figure 6.1C). Interestingly, VP35 seemed to bind with HA-TRIM25 more strongly than HA-TRIM6 (Figures 6.1A and 6.1C).

Since TRIM25 interacts with VP35's C-terminus, we were interested whether the capacity for VP35/309 ubiquitination and/or the presence of a basic residue was important for interaction. The VP35/K309R mutant bound to TRIM25 as well as wt VP35, but the K309G mutant was impaired in this interaction (Figure 6.1D). Since the VP35/K309G mutant is additionally attenuated and uniquely impaired in interaction with TRIM25 but not TRIM6, further studies are needed to evaluate the functional relevance of VP35-TRIM25 interaction. We also examined TRIM25 interaction of our VP35 N-terminus K-to-R mutants. Both the K6R and K63.67R mutants appeared to lose some binding with TRIM25 (Figure 6.1E), but this experiment should be repeated to confirm the result. Importantly, the K119.126.141R retains the capacity to interact with TRIM25 (Figure 6.1E) despite being impaired in its polymerase co-factor function.

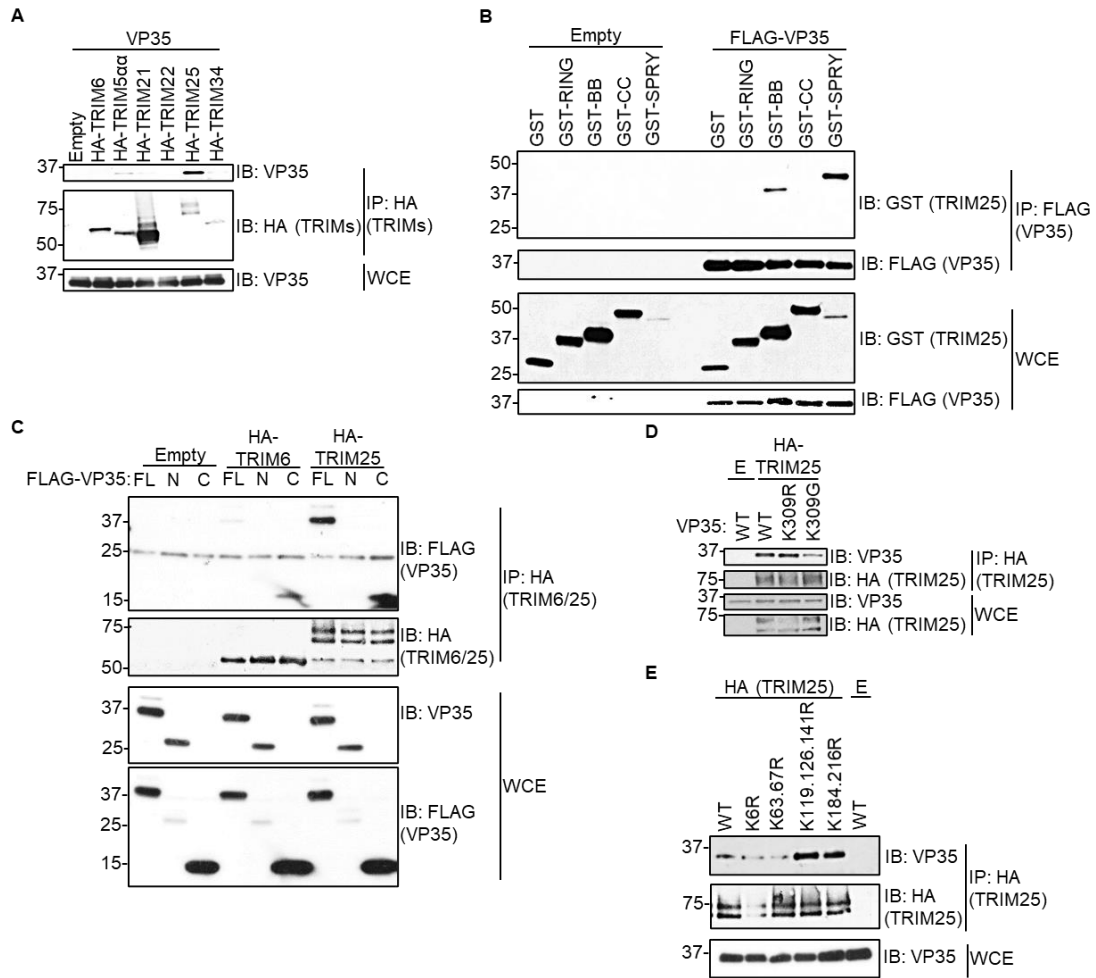


Figure 6.1 TRIM25 interacts with VP35's C-terminus

(A) Lysates (WCE) from 293T cells co-expressing full-length (FL), untagged VP35 with the pCAGGS vector (empty) or a HA-tagged TRIM (5 α , 6, 21, 22, 25, or 34) were immunoprecipitated (IP) with anti-HA beads to screen VP35's interaction with TRIMs related to TRIM6. (B) WCE from 293T cells co-expressing GST alone or GST-tagged TRIM25 domains with empty vector or FL FLAG-tagged VP35 were IP with anti-FLAG beads. (C) WCE from 293T cells co-expressing empty vector, HA-TRIM6, or HA-TRIM6 with FLAG-VP35-FL, N- (N), or C- (C) terminus were IP with anti-HA beads. (D) WCE from 293T cells co-expressing FL FLAG-VP35/ wild-type (WT), K309R, or -G with HA-TRIM25 were IP with anti-HA beads. (E) WCE from 293T cells co-expressing FL FLAG-VP35/ wild-type (WT), K6R, K63.67R, K119.126.141R, or K184.216R with HA-TRIM25 were IP with anti-HA beads. (Figure made by Sarah van Tol)

TRIM25 CAN FACILITATE VP35 UBIQUITINATION AND VP35'S NON-COVALENT INTERACTION WITH UBIQUITIN

We next wanted to interrogate whether TRIM25 can facilitate VP35 ubiquitination. When co-expressed with HA-Ub and RFP-TRIM25, we observe an enhancement in the Ub-conjugated forms of VP35 suggesting that TRIM25 can ubiquitinate VP35 (Figure 6.2A). To investigate whether TRIM25 could ubiquitinate lysine residues aside from VP35/K309, we co-expressed RFP-TRIM25 and HA-Ub with VP35 wt, K309R, or -G. We found an increase in the amount of free VP35 that co-IP with HA-Ub for all VP35 constructs and a clear increase in the number and intensity of Ub-conjugated VP35 bands for VP35 wt and K309R (Figure 6.2B). Of note, the TRIM25 and VP35 expression in the lysates of cells transfected with the VP35/K309R could explain the more subtle increase in ubiquitin-conjugated VP35 for this mutant. The increased ligation of Ub on to VP35/K309G, however, still supports that TRIM25 may be conjugating Ub onto the N-terminal lysine residues, and this warrants further investigation. Additionally, VP35's increased interaction with Ub in the presence of TRIM25 suggests the possibility that TRIM25 participates in the synthesis of K63-polyUb (Figure 6.2B).

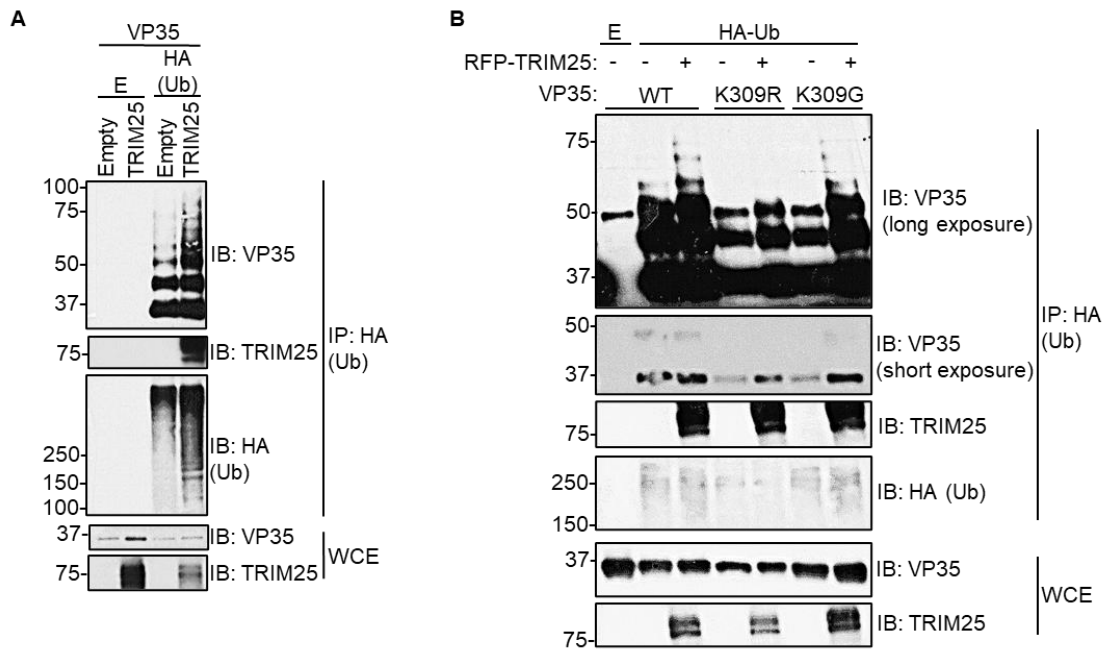


Figure 6.2 TRIM25 can facilitate VP35 ubiquitination and VP35's non-covalent interaction with ubiquitin

(A) Lysates (WCE) from 293T cells co-expressing full-length (FL), untagged VP35 with the pCAGGS vector (empty) or fed fluorescent protein (RFP)-tagged TRIM25 in the presence or absence of HA-Ub were immunoprecipitated (IP) with anti-HA beads to monitor VP35's ubiquitination. (B) WCE from 293T cells co-expressing FL, untagged VP35/ wild-type (WT), K309R, or -G with empty vector or RFP-TRIM25 in the presence or absence of HA-Ub were IP with anti-HA beads to monitor VP35's ubiquitination. The same VP35 immunoblot (IB) from IP samples are shown at short and long exposures. (Figure made by Sarah van Tol)

TRIM25 IS A PROVIRAL FACTOR FOR EBOLA VIRUS REPLICATION

To investigate the functional relevance of TRIM25 during EBOV infection, we infected wt or *Trim25*^{-/-} MEFs with either a rEBOV-eGFP or a mouse-adapted EBOV (ma-EBOV). At a low MOI 0.05, we observe ~3-4 log₁₀ attenuation in *Trim25*^{-/-} MEFs infected with rEBOV-eGFP and do not detect GFP through 96 hpi (Figure 6.3A). At an intermediate MOI, 0.5, the virus was attenuated ~3-3.5 log₁₀ in *Trim25*^{-/-} compared to wt MEFs at the later time points (Figure 6.3B). When infecting at a high MOI, 5.0 to simulate synchronized infection, the magnitude of attenuation was reduced to 1-2 log₁₀ and some GFP fluorescence signal could be detected in *Trim25*^{-/-} MEFs at 96hpi (Figure 6.3C). We observed similar attenuation in *Trim25*^{-/-} MEFs infected with ma-EBOV at all time points (Figures 6.3D-F). Of note, the magnitude of attenuation at 168 hpi was less striking for the ma-EBOV than the rEBOV-eGFP. TRIM25, like TRIM6, is generally considered an antiviral protein in association with its role as a positive regulator of IFN-I pathways, including during IAV infection^{142,159}. To ensure the *Trim25*^{-/-} MEFs were not generally defective in their support of virus replication, we infected wt and *Trim25*^{-/-} cells with IAV expressing GFP (GFP-IAV). Importantly, we did not observe a difference in fluorescence following GFP-IAV infection (Figure 6.3G), suggesting that proviral function of TRIM25 is EBOV-specific. In the future, it will be important to recover and sequence virus from *Trim25*^{-/-} cells to monitor for mutant viruses that may provide insight into the residues important for VP35's interaction with TRIM25. Repeating the replication kinetic experiments in human cells, such as TRIM25-KO A549s, is important to confirm that TRIM25's proviral phenotype is translatable to human infection.

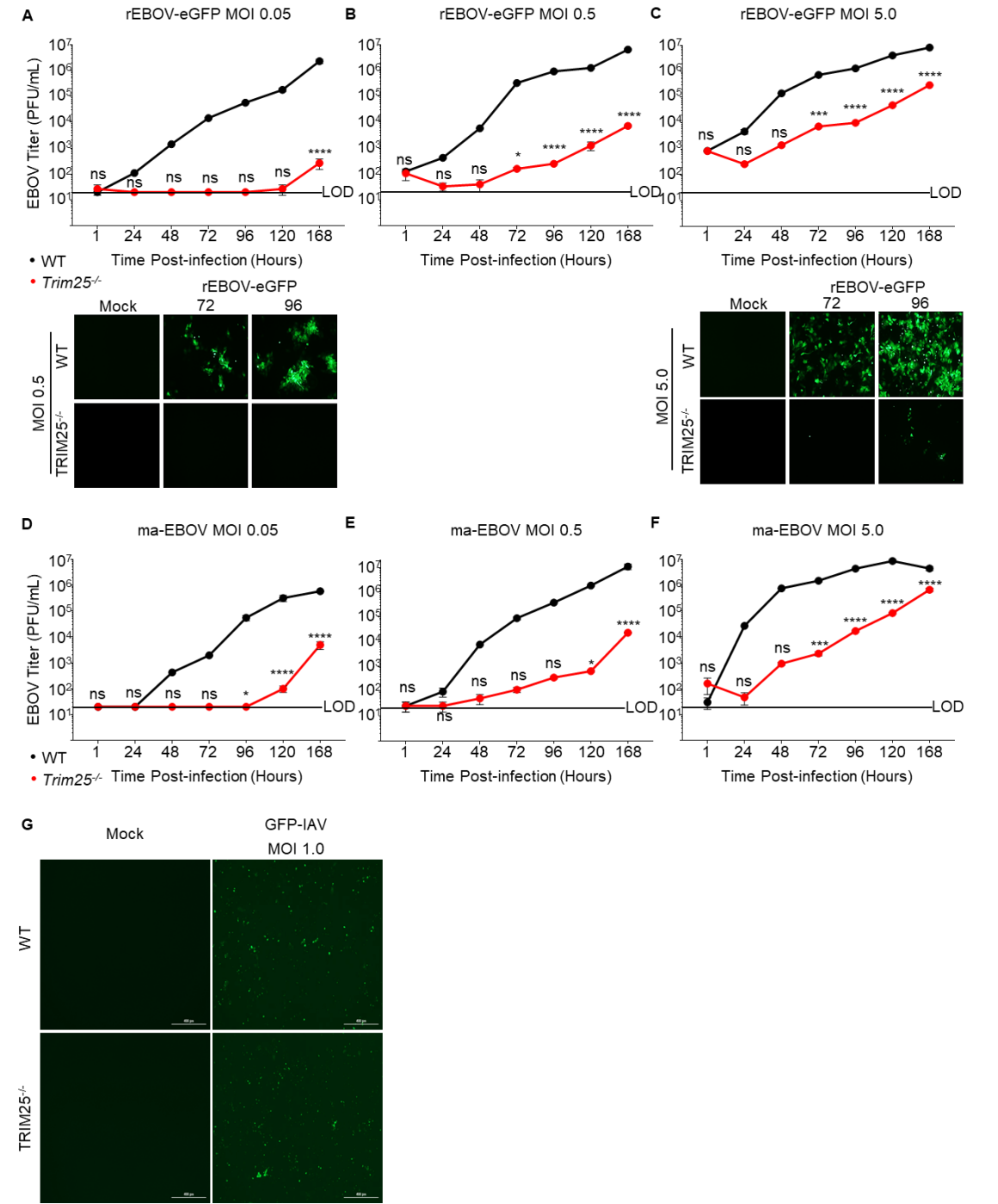


Figure 6.3 TRIM25 is a proviral factor for Ebola virus replication

(A-C) Wild-type (WT) (black) and *Trim25*^{-/-} (red) murine embryonic fibroblasts (MEFs) were infected with recombinant Ebola virus expressing green fluorescent protein (rEBOV-eGFP) at several multiplicities of infection (MOI): 0.05 (A), 0.5 (B), or 5.0 (C) plaque forming units (PFU) per cell. Supernatants from infected cells were titrated and the titers, PFU/mL, are shown. Presented data is from biological triplicates and are representative of

two independent experiments. The limit of detection (LOD) 20 PFU/mL is shown. Fluorescence micrographs during infection with MOI 0.05 (A) and 5.0 (C) show GFP signal at 72- and 96 hours post-infection. (D-F) WT and *Trim25*^{-/-} MEFs were infected with a mouse-adapted EBOV (ma-EBOV) at several MOIs: 0.05 (D), 0.5 (E), and 5.0 (F). Supernatants from infected cells were titrated and the titers, PFU/mL, are shown. Presented data is from biological triplicates and are representative of two independent experiments. (G) WT and *Trim25*^{-/-} MEFs were infected with a recombinant, GFP-expressing influenza virus (GFP-IAV) at MOI 1.0 for 48 hours. Representative GFP fluorescence images are presented. The data analysis was done using a two-way ANOVA with Bonferroni's post-test (A-F) for comparison between groups. P-value: *<0.05, ***<0.001, ****<0.0001; ns, not significant (p>0.05). (Figure made by Sarah van Tol)

Chapter 7: Discussion

Ebola virus VP35 fulfills many essential roles throughout the virus' life cycle. The main functions attributed to VP35 include IFN-I antagonism and polymerase co-factor activity. VP35-mediated coordination of nucleocapsid formation and genome incorporation into a virion has been noted^{12,37}, but these assembly functions are not well-characterized. Further, the molecular mechanisms that govern which activity VP35 engages in have not been elucidated. The results of our experiments support that VP35 ubiquitination and non-covalent interaction with Ub contribute toward organizing VP35's functions.

UBIQUITINATION OF EBOLA VIRUS VP35 AT LYSINE 309 REGULATES VIRAL TRANSCRIPTION AND ASSEMBLY

We used two different mutant recombinant viruses and VP35 expression plasmids to disassociate the importance of a basic residue from conjugated Ub at residue 309. After confirming that both mutations reduced Ub conjugation onto VP35, we evaluated the contribution of VP35/K309 ubiquitination in regulating VP35's dsRNA-dependent and -independent IFN antagonism activity. Based on the structure of VP35's IID and previous biochemical assays¹⁷¹, VP35/K309 enhances dsRNA binding but is not required as other residues within the CBP directly interacting with dsRNA. This is consistent with our observation that purified FLAG-VP35/K309G binding to biotin-poly(I:C) is decreased by 50% and only the low dose of the VP35 mutant was impaired in a poly(I:C)-induced IFN β promoter luciferase assay. Unexpectedly, we found that the K309G mutant was also deficient in IKK ϵ binding and preventing IKK ϵ -induced IFN β promoter activation (Figure 7.1A). The K309R mutant had enhanced dsRNA-independent IFN antagonism implying

that ubiquitination on K309 reduces IFN antagonism (Figure 7.1A). One potential explanation could be that ubiquitin conjugated onto VP35/K309 provides steric hindrance reducing interaction with other components of the IFN pathway. In the context of infection, the rEBOV-VP35/K309G mutant virus induced a more rapid and intense IFN-I induction than the wt virus. In contrast, IFN-I induction lags in K309R-infected cells. It is unclear whether the delay is secondary to differences in viral load or a result of VP35/K309R more efficiently antagonizing IFN-I.

Viral replication for both mutants is attenuated in IFN-I competent (A549, BMDCs, and MEFs) and -incompetent (VeroE6) cells, suggesting that preventing VP35/K309 ubiquitination impairs virus replication independent of VP35's role as an IFN-I antagonist. We previously found that TRIM6 facilitates VP35's polymerase co-factor activity using a minigenome assay ⁷⁹, and we expected that blocking VP35/K309 ubiquitination directly affects VP35's co-factor function and that the attenuation is dependent on TRIM6. We elected to use A549 cells for the replication assays since we had T6-KO cells available and had characterized EBOV replication thoroughly in these cells ⁷⁹, but we acknowledge that different cell types may differ in their dependence on VP35/K309 ubiquitination for efficient replication. Infection studies in T6-KO A549s, MEFs, and BMDCs demonstrate that the wt virus is attenuated when TRIM6 is absent, but the mutants' replication is not affected further. The consistent results across multiple cell types, including cells of mouse and human origin, supports that these findings are relevant. Importantly, neither mutation prevented VP35 from interacting with TRIM6. These results support that TRIM6-mediated Ub conjugation onto VP35/K309 affords EBOV a replication advantage.

To understand how K309 ubiquitination is advantageous for VP35's co-factor function, we measured the synthesis of different viral RNA species and evaluated VP35's interaction with the viral transcriptase. The strand-specific RNA qPCR results suggest that ubiquitination specifically benefits transcriptase but not replicase activity. Both mutants were similarly impaired in their interaction with the N-terminus of the viral polymerase (HA-L₁₋₅₀₅), but the K309R mutant's affinity for VP30 was not negatively impacted. The immunoprecipitation of endogenous TRIM6 with L and VP35 supports that these factors may interact during infection to promote the polymerase's transcriptase activity. The phenotypic relevance of the Ub-supported interaction with L appears to present as disproportionately lower transcription of 5' viral genes relative to NP transcripts, encoded by the 3' most gene, in the rEBOV-VP35/K309R/-G-infected cells or wt virus-infected TRIM6 knockout cells (Figure 7.1B). We speculate that ubiquitination may facilitate a L-VP35 interaction that favors transcriptase stability to prevent it from falling off and having to re-initiate. To our knowledge, the mechanisms regulating EBOV's transcriptase re-initiation efficiency or processivity along the genome have not yet been identified, and we provide the first evidence that ubiquitination of VP35 regulates viral transcriptase function. Alternatively, VP35 could aid the polymerase in overcoming secondary structures in the vRNA that are more abundant in the VP40, VP30, and L genes. Recently, VP35 has also been described to possess ATPase-like and helicase-like activities that are required for polymerase co-factor function³⁶. Although we found the VP35/K309 mutants retain ATPase activity (Figure 7.2) and recent studies suggest that residues in the N-terminus of VP35 (amino acids 137-170) are required for helicase activity³⁶, the potential role for ubiquitination in regulating VP35's helicase-like activity cannot be ruled out.

Although the structure for EBOV VP35 in complex with L has not been solved, the structures for two other non-segmented, negative sense RNA viruses (Human metapneumovirus (HMPV) and respiratory syncytial virus (RSV)), whose phosphoproteins (P; the functional equivalent to VP35 in other NNS RNA viruses¹⁷⁷) also form asymmetric tetramers, have been solved^{178,179}. In the HMPV and RSV polymerase structures, the four different monomers of P adopt distinct orientations that enable the different monomers to participate in unique functions simultaneously. For example, the HMPV P is positioned such that the coiled-coil is anchored to L but the N-terminal nucleoprotein (N) binding region (equivalent to VP35's NPBP) can bind monomeric N (N^o) at the exit tunnel to enable nascent vRNA or cRNA to be encapsidated¹⁷⁸. At the same time, P₂'s C-terminus is at the RNA entry tunnel to facilitate L's interaction with NP-RNA¹⁷⁸. EBOV VP35 can also form asymmetric tetramers²⁸, and it is feasible to hypothesize that VP35 may similarly be able to perform multiple functions when in complex with the L. The strand-specific RNA qPCR results suggest that ubiquitination specifically benefits polymerase transcriptase but not replicase activity. Further, since only the K309R mutant is differentially enhanced in the NP interaction and both the K309R and -G mutants appear equally impaired in their polymerase co-factor activity, we propose that ubiquitination would not alter VP35's recruitment of NP^o or NP-RNA to the exit or entry tunnels of the polymerase, respectively. Instead, we propose VP35/K309 ubiquitination induces a VP35-L interaction required for efficient transcription across the genome.

Removing the capacity for VP35/K309 ubiquitination results in an initiation-biased transcriptase that causes dysregulated intracellular proportions of viral proteins. The decrease in VP30 availability, particularly in the K309R-mutant infected cells, may

contribute to the transcriptional defect and feedback to amplify the defect in later rounds of replication. This is in line with our observation that the transcriptional defect is more pronounced and vRNA and cRNA synthesis is attenuated at 72 hpi for both mutants. Reducing the intracellular pool of VP40 may translate to impaired virus assembly which is consistent with the similar amount of total viral RNA and GFP signal despite lower production of infectious virus in mutant-infected VeroE6 cells. We were unable to correlate the L protein levels due to lack of antibody, but we anticipate that lower amounts of L protein would have compounding effects on viral replication and transcription following primary transcription.

Unexpectedly, we found that the viral load in supernatants collected from rEBOV-VP35/K309G infected cells was significantly lower than the K309R mutant in IFN-I deficient cells. The difference in titer, despite similar total viral RNA levels and transcriptional defects between the mutants, led us to hypothesize that a basic residue and the capacity for ubiquitin conjugation at VP35/K309 are important for virus assembly. We found that in contrast to the K309R mutant's increased interaction with VP24, the K309G-VP24 interaction is impaired. As recruitment of VP24 is important for nucleocapsid rigidification ¹¹, the difference in the mutants' interaction with VP24 could contribute to the difference in virus production. The incorporation of VP24 into the nucleocapsid has also been reported to switch off active replication and trigger the movement of full-length/mature nucleocapsids into VP40-GP membranes ¹³. As VP35/K309R interacts with VP24 more strongly than wt, the K309R mutant's lack of ubiquitination may recruit more VP24 to nucleocapsids prematurely turning off the viral polymerase activity prior to synthesizing the complete viral genome. The packaging of incomplete genomes into

virions would explain the decrease in virus infectivity despite the K309R mutant's increased packaging efficiency (Figure 7.1C). We also found that the VP35-VP24 interaction is impaired significantly in the K309G mutant which may prevent assembly of mature virions. NP dynamically transitions between the NP-RNA bound and unbound states and VP24 and VP40 interact with NP^{11,13,37,180}. We speculate that VP35 ubiquitination may prevent the adoption of a VP35-NP conformation that facilitates VP24 recruitment and subsequent nucleocapsid maturation. Alternatively, the ubiquitination status of VP35 could directly influence VP24's association with the nucleocapsid. Within the sucrose-purified virus, we found that the K309G mutant did not package an approximately 38 kDa form of VP24, which may be a ubiquitinated or SUMOylated form of VP24¹⁰², and the K309R mutant packages more of this modified VP24 (Figure 7.3). Further studies are needed to identify this form of VP24 and whether it can influence the virus' budding and/or infectivity.

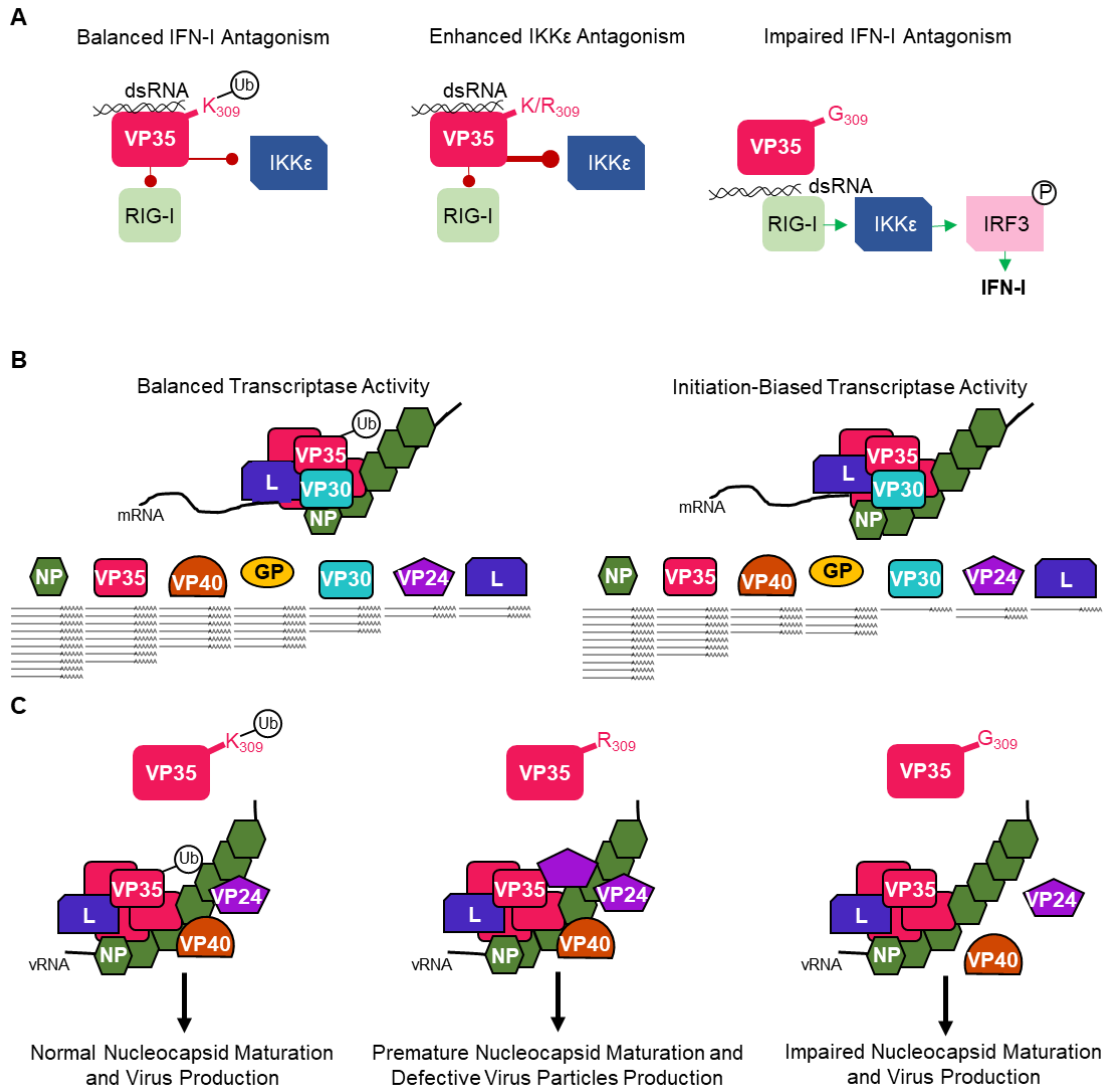


Figure 7.1 A basic residue and ubiquitination capacity of VP35/K309 coordinates VP35's functions

(A) Both ubiquitinated (white circle with Ub) and non-ubiquitinated (K/R₃₀₉) VP35 bind double-stranded RNA (dsRNA) to antagonize RIG-I. Loss of a basic residue (G₃₀₉) impairs dsRNA binding which allows RIG-I activation and downstream IRF3 phosphorylation (white circle with P) leading to type I interferon (IFN-I) induction. In the absence of ubiquitination, VP35 (K/R₃₀₉) impedes IKKε activation more efficiently. (B) In the context of the viral transcriptase, comprised of the viral polymerase (L), VP35, and the transcription factor (VP30), the capacity for VP35/K309 to be ubiquitinated enables balanced transcriptional activity. Under this balanced transcriptase function, a 3'-to-5' transcriptional gradient is generated and viral proteins are produced in an optimal ratio. When VP35/309 is unable to receive ubiquitination, the transcriptase is biased toward transcriptional initiation and the transcriptional gradient is dysregulated resulting in unbalanced intracellular viral protein ratios. (C) When VP35/309 has the capacity for ubiquitination, the recruitment of VP24 and VP40 is regulated and progeny virions are assembled normally. In the absence of ubiquitin and when a basic residue is present at

VP35/309, VP24 is more efficiently recruited to VP35 prematurely and some immature nucleocapsids are incorporated into progeny virions resulting in the defective viruses. When the basic residue is lost (K309G), interaction with VP24 and VP40 is impaired which reduces virus production. (Figure reproduced with permission from van Tol et al., 2022)

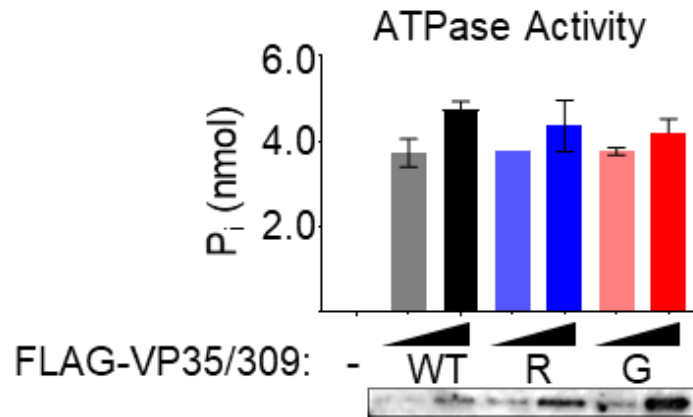


Figure 7.2 Mutation of VP35 at K309 does not alter VP35's ATPase activity

FLAG-purified VP35 (wt, K309R, or K309G) was used in an ATPase activity assay. The concentration of free phosphate (P_i) was determined using a standard curve with the BIOMOL Green phosphate standard. A fraction of the completed reaction was boiled in 4X Laemmli sample buffer to compare the amount of VP35 added. The assay was completed in biological triplicate. The data analysis was done using a one-way ANOVA with Tukey's post-test for comparison between groups. No significant differences were identified. (Figure reproduced with permission from van Tol et al., 2022)

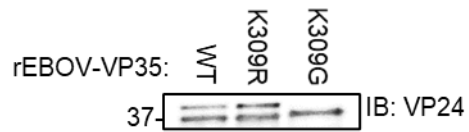


Figure 7.3 A modified form of VP24 is present in rEBOV-eGFP-VP35/wild-type and K309R but not K309G particles

VP24 immunoblot for sucrose gradient purified rEBOV-eGFP-VP35-wild-type (WT), K309R, or-G lysed in 4X NuPAGE with 10X NuPAGE reducing reagent. The band at 35 kDa is VP35 show through from a previous antibody. Blot of VP24 running at native length (~24kDa) is located in Figure 3.13A. (Figure made by Sarah van Tol)

VP35'S N-TERMINAL K119, 126, AND 141 CAN BE UBIQUITINATED AND FACILITATE VP35'S POLYMERASE CO-FACTOR ACTIVITY

Our initial TRIM6-VP35 study revealed that at least one other lysine residue can receive covalent ubiquitination, but we did not know which residue was modified or the functional significance. Here, we show that multiple residues in VP35's N-terminus can be modified by ubiquitin including K119, -126, and -141. Mass-spectrometry on IP FLAG-VP35-N-terminus found diglycine modification in K119 and -126, supporting that these two residues can be ubiquitin modified. The K119.126.141 cluster is located within the region of VP35 known to promote oligomerization and interaction with L (Figure 1.1C). Although our co-expression assays did not indicate an obvious defect in self-interaction or binding with L, we did observe a significant impairment in polymerase co-factor activity for K-to-R mutants in the K119.126.141 cluster using a minigenome assay. We also did not observe differences in the K-to-R mutants' interaction with NP. The VP35/K141R mutant was the least active of the K119.126.141 cluster mutants in polymerase co-factor activity. Interestingly, K141 is located within the 40 amino acid region mapped to VP35's helicase-like activity (Figure 1.1C) ³⁶. Although VP35 does not contain any conventional helicase motifs, like those found in flavivirus NS3 ¹⁸¹ or enterovirus 71 2CATPase ¹⁸², mutation of key K residues has been shown to abrogate the RNA helicase function through prevention of cation and ATP binding ^{144,183,184}. It is possible that K141 is important for mediating nucleotide binding to facilitate helicase activity and K119 and/or -126 ubiquitination regulate VP35's ability hydrolyze ATP or unwind RNA.

UNANCHORED UBIQUITIN REGULATES EBOV POLYMERASE ACTIVITY

We expanded our understanding of VP35's non-covalent interaction with K63-polyUb. VP35's C-terminus, likely residues within the FBP including R225, facilitate the interaction. Retention of basic residues within VP35's FBP is required for minigenome activity²². The basic residues are predicted to interact with NP-RNA in order to bridge the NP-encapsidated RNA template to the polymerase to allow virus replication and transcription²². Since we observed that the R225E mutant attenuates VP35's interaction with unanchored Ub, we investigated whether NP also interacts non-covalently with K63-polyUb. The observation that both VP35 and NP interact with K63-polyUb and over-expression of the unanchored Ub-specific USP IsoT impairs minigenome activity suggest that K63-polyUb is important for EBOV's polymerase. Unanchored K63-polyUb has been shown to provide a platform for signaling complex assembly^{49,55,185-187}, and an analogous scaffold could stabilize the interaction of EBOV's polymerase with template NP-RNA.

Additionally, we found that free Ub is incorporated into EBOV particles. The inclusion of mono-Ub as well as polyUb chains could impact EBOV infectivity as observed for IAV¹⁷⁶. IAV packages mono-, di-, tri-, and tetra-polyUb, and the host E3 ubiquitin ligase HDAC6 facilitates uncoating of the viral nucleocapsids through recruitment to aggresomes^{176,188}. Our sucrose gradient purified EBOV, including both rEBOV-eGFP-VP35/K309 mutants, efficiently packaged mono-Ub and short-chains of polyUb as seen with IAV. The incorporation of these molecules could aid in EBOV uncoating or, as VP35 and NP interact with K63-polyUb at least four Ub moieties long, could form a scaffold to aid in the initiation of viral transcription following entry. Future studies are needed to investigate the chain linkage of the packaged polyUb. It is also important to consider

whether Ub packing occurs stochastically while the virion is being assembled. Investigation of Ub packing into virions among filoviruses and across diverse virus genera would offer insight into the conservation of ubiquitin packaging and may allude to its importance.

TRIM25 IS PROVIRAL DURING EBOV INFECTION AND CAN UBIQUITINATE VP35

We observed that TRIM25, but not other TRIM6-related TRIMs, is able to interact with and ubiquitinate VP35. Interestingly, the TRIM25-VP35 interaction seemed to be stronger than TRIM6's. The EBOV attenuation was more dramatic in the *Trim25^{-/-}* (100-10,000 fold) than the *Trim6^{-/-}* (2-10 fold) MEFs. We also observed that TRIM25 can facilitate VP35 ubiquitination for both wt and K309 mutants as well as enhance VP35's non-covalent interaction with polyUb. Since we observed impaired TRIM25-VP35/K309G interaction, it is important to investigate whether this phenotype could be related to VP35/K309G's defective interactions with IKK ϵ or other viral proteins and contribute to this mutant's impaired virus replication. Follow-up studies are also needed to identify which VP35 K(s) that TRIM25 ubiquitinates.

TRIM25 may also contribute to the synthesis of the K63-polyUb observed to enhance EBOV's polymerase co-factor activity. TRIM25 has previously been shown to cooperate with the E2 Ube2D3 to synthesize unanchored K63-polyUb to activate the RIG-I-mediated IFN-I induction following dsRNA recognition ⁵⁵. Recently, both TRIM25 and Ube2D3 were identified as interactors with the EBOV polymerase ¹⁸⁹. Ube2D3 was among the 64 high-confidence interactors screened with siRNA to evaluate the effect of polymerase interactors during EBOV infection. An siRNA targeting Ube2D3 strongly attenuated EBOV replication suggesting a potential proviral role ¹⁸⁹. The connection between TRIM25 and Ube2D3 in the synthesis of K63-polyUb suggests that TRIM25 may facilitate K63-polyUb during EBOV infection to promote viral replication.

VP35 may have evolved to interact with TRIM25 to facilitate EBOV replication, and the ability to bind TRIM6 evolved in parallel as a consequence of their conserved PRY-

SPRY domains. Since rEBOV-eGFP-VP35/K309R was not additionally attenuated in TRIM6-KO A549 cells, we predict that TRIM25 ubiquitinates the N-terminal VP35 residues or synthesizes unanchored K63-polyUb to promote EBOV's polymerase activity (Figure 7.4). Studies with both TRIM6 and -25 knocked-out will offer insight as to whether these TRIMs play redundant or complementary roles in VP35 ubiquitination.

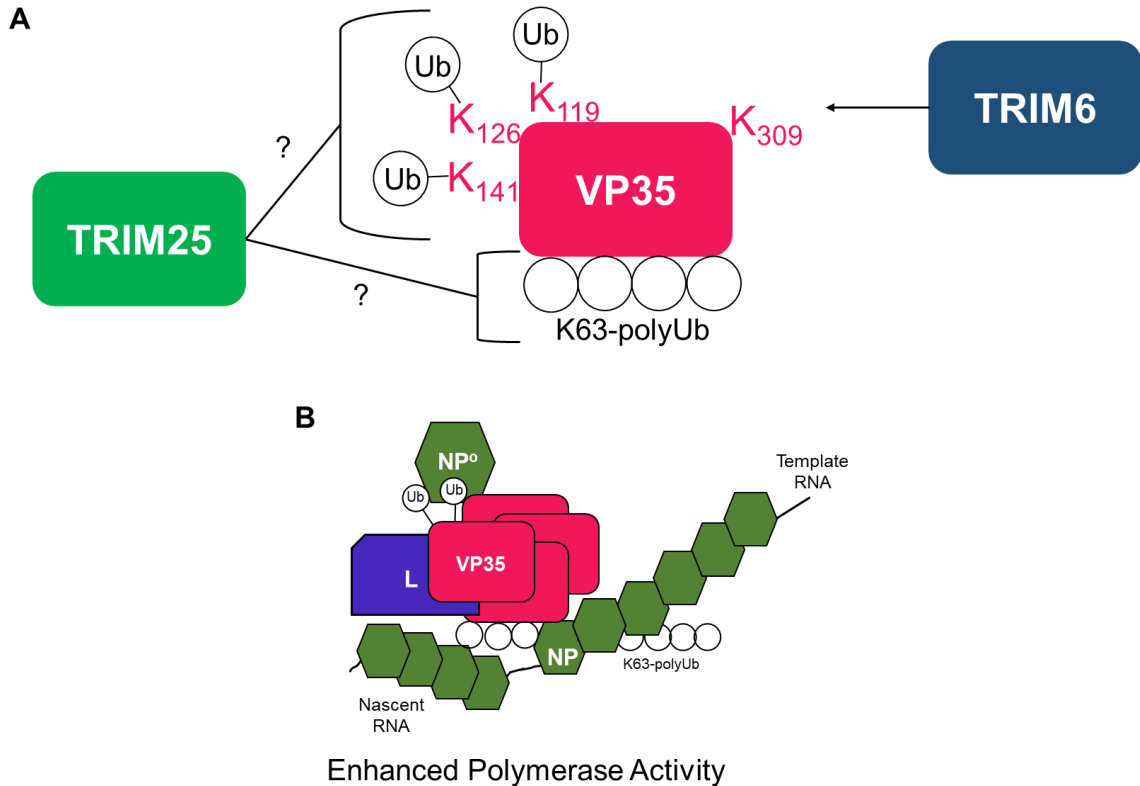


Figure 7.4 Ubiquitination of VP35 promotes Ebola virus' polymerase activity

(A) TRIM6 ubiquitinates VP35 at lysine (K) 309. Several K residues in VP35's N-terminus can be ubiquitinated, including K119, 126, and 141. VP35 interacts with unanchored K63-linked polyubiquitin (K63-polyUb) via its C-terminus. TRIM25 can enhance VP35 ubiquitination and non-covalent VP35-Ub interaction, and we suspect that TRIM25 may facilitate ubiquitination of VP35's N-terminal K residues and/or synthesize the K63-polyUb VP35 binds. (B) We found that interaction with K63-polyUb and the presence of Ks at K119, 126, and 141 is required for VP35's full polymerase co-factor activity. We propose that K63-polyUb could enhance polymerase co-factor activity by enhancing VP35's interaction with nucleoprotein (NP) which also binds with K63-polyUb. (Figure made by Sarah van Tol)

LIMITATIONS OF THE STUDY

Overall, our studies demonstrate the proviral roles of VP35 ubiquitination, but several limitations could be addressed to solidify our conclusions. Primary limitations discussed below include lack of an *in vivo* study for the rEBOV-VP35/K309 mutants, an *in vitro* polymerase model, assessment of VP35's helicase activity, rEBOV-VP35/N terminal K-to-R mutants, an EBOV infection model disrupting K63-polyUb formation or interaction with VP35, and infection in human-origin TRIM25-knockout cells.

Determining whether preventing VP35/K309 ubiquitination attenuates EBOV replication *in vivo* is important for establishing physiological relevance. Although we generated recombinant mouse-adapted (ma) EBOV-VP35/K309R and -G mutants, our attempt to infect wt and *Trim6*^{-/-} mice with these viruses and the wt ma-rEBOV did not result in consistent weight loss for infected animals. We detected viral RNA in the serum of one third of wt mice infected with wt ma-EBOV and none of the wt mice infected with either the K309R or -G mutants or any *Trim6*^{-/-} mice were qPCR positive. Further, we could not detect infectious virus in the serum from any of the mice regardless of the infecting virus or mouse genotype. The experiment should be repeated after optimizing an infectious dose for wt mice that results in weight loss for all of the mice. *In vivo* studies assessing the relevance of TRIM25 during infection are also needed.

A current constraint of our understanding of EBOV's polymerase is the absence of a structure and difficulties associated with reconstituting the polymerase *in vitro* to study the polymerase directly. The structures for several negative-sense RNA viruses viral polymerases, comprised of the RdRp with the phosphoprotein, have been solved^{178,179}, but we do not know how translatable the observed features are to filoviruses. Further, an EBOV

polymerase complex has been notoriously difficult to reconstitute due to the need for host proteins and the co-expression of VP35 and L ¹⁹⁰. The only reported successful recombinant EBOV polymerase system can only evaluate the polymerase's priming and short primer elongation ¹⁹⁰. In order to model the role of covalent and non-covalent ubiquitin in regulating the polymerase's processivity more directly, an *in vitro* model needs to be established where VP35, L, NP^o, NP-RNA, and relevant host proteins are present. Evaluation of polymerase activity with extracts collected from infected cells or cells expressing the minigenome components treated with recombinant K63-polyUb, (de)ubiquitinating enzymes, and other proteins of interest (i.e. TRIM6 and -25) in parallel with strand-specific qPCR could more clearly demonstrate the polymerase activity (i.e. replicase, transcriptase, and/or processivity) being regulated.

Although our experimental evidence strongly links TRIM6-mediated VP35/K309 to the observed attenuation, we cannot rule out that the K309R mutation impairs its helicase activity. Since K residues are typically linked to RNA helicases' ability to interact with and subsequently hydrolyze ATP ^{144,183,184} and our VP35/K309R/ and -G mutants retain their ATPase activity, we do not expect helicase activity to be disrupted. In the case the N-terminal K119.126.141 cluster, however, we need to test our K-to-R mutants for both their ATPase- and helicase-like activities to distinguish the potential contributions of ubiquitination from enzymatic activity.

A few of our observations also need to be validated in the context of virus infection to assess their functional relevance. Our N-terminal K-to-R mutations have not been introduced into recombinant virus, and an infection model is needed to assess whether the K119, -126, and/or -141-to-R mutations attenuate virus replication. Generally,

minigenome results tend to correlate with phenotype during infection, however, we cannot rule out that these mutations could also impact EBOV assembly and/or infectivity. Further, we have not been able to test the role of K63-polyUb during infection. IsoT is a potent enzyme, and its over-expression could have indirect effects on cell health and confound any observed impact on EBOV replication. Treatment of cells with an IsoT inhibitor ¹⁹¹ may allow for a better controlled approach in the context of a reconstituted polymerase. Alternatively, the identification of a small molecule that prohibits VP35's non-covalent interaction with Ub would be useful to evaluate the effects of their binding more directly. Introduction of VP35/R225A or -E mutation into rEBOV may be helpful, however, this mutant is devoid of minigenome activity ²² and its rescue may not be possible.

Finally, we need to confirm that TRIM25 plays a proviral role in human cells. Infection experiments with both rEBOV-eGFP and ma-EBOV both showed dramatic attenuation in *Trim25*^{-/-} MEFs, but we cannot rule out the possibility of species-specific differences. Sequencing of virus from cells lacking TRIM25 could identify mutations that allow escape from reliance on TRIM25 or adaptation to utilize an alternate E3 ligase. Elucidation of the specific regions within VP35's C-terminus and TRIM25's PRY-SPRY domain that interaction and the specific VP35 K residues that TRIM25 ubiquitinates is important when exploring the potential of targeting this interaction for therapeutic development. Exploring these interactions with TRIM25 orthologs from mouse, human, and other species may also illuminate the conservation of this interaction across species.

Chapter 8: Conclusions and Future Perspectives

CONCLUSIONS

Within EBOV-infected cells, the VP35 population includes both ubiquitinated and non-ubiquitinated forms. We expect that the ability to dynamically receive and lose these post-translational modifications and interact with unanchored, K63-polyUb cues VP35's interactions with other host and viral proteins to orchestrate VP35's engagement in its distinct functions (Figures 7.1 and 7.4). Although the lack of VP35/K309-ubiquitination does not prohibit the production of infectious virus, preventing this modification significantly dysregulates the viral life cycle. We propose that VP35/K309 ubiquitination facilitates a stable interaction with L to enhance viral transcription and prevents the premature packaging of immature nucleocapsids into progeny virions, and that a basic residue is needed for efficient IFN-I antagonism and interaction with VP24. We found that the retention of VP35's N-terminal K119.126.141 cluster as Ks is required for optimal polymerase co-factor activity, and we hypothesize that ubiquitination of and/or ATPase binding by these residues regulates VP35's helicase activity. We propose free, K63-polyUb acts as a scaffold for the EBOV polymerase to stabilize interactions between VP35's C-terminal first-basic patch and NP-encapsidated viral RNA. Packaging of free Ub into virus EBOV particles may thus provide an advantage to the virus upon uncoating, particularly if the polyUb is K63-linked and can facilitate the formation of the transcriptase to support primary transcription. TRIM25 is proviral in the context of EBOV infection, and we expect TRIM25-mediated ubiquitination of VP35's N-terminal K119.126.141 cluster and/or synthesis of unanchored, K63-polyUb enhances VP35's polymerase co-factor activity.

Overall, our results point to novel roles for host factor mediated VP35 ubiquitination in promoting multiple stages of EBOV replication.

CONSERVATION OF VP35 UBIQUITINATION ACROSS *FILOVIRIDAE*

Based on the universal presence of a K at the 309-equivalent position across all characterized *Filoviruses* (Figure 8.1), we expect ubiquitination at this site to be conserved across this virus family. Future studies are required to confirm VP35 ubiquitination at the corresponding residue. The retention of this PTM would make this an attractive target for a pan-filoviral antiviral therapeutic. Although we have not been able to confirm ubiquitination of the K119.126.141 cluster during EBOV infection, it is important to note that all three Ks are universally conserved across the six *Ebolavirus* species (Figure 8.1). Further, the K126 and 141 equivalent residues are conserved in Měnglà virus (MALV), Ravn virus (RAVN), and some MARVs isolated from *Rousettus aegyptiacus* bats, but the K126 equivalent residue is an R the Lake Victoria MARV isolates (Figure 8.1). Like K309, the K141 equivalent residue is universally conserved across *Filoviruses* including Llovium virus (LLOV) (Figure 8.1).

Interestingly, a filovirus VP35-like element encoded by *Myotis* bats (mIEFL35) encodes for a G at the K309 equivalent residue¹⁹²⁻¹⁹⁴. Analogous to our VP35/K309G mutant, the mIEFL35 has reduced potency in antagonism of IFN-I and impaired dsRNA-binding¹⁹². In the context of mIEFL35, which lacks conservation of the NPBP and FBP, predictably cannot interact with NP and loses polymerase co-factory activity despite retaining self-interact via its coiled-coil domain¹⁹³. The K126.141 are conserved¹⁹³, and it would be interesting to investigate the ubiquitination status and ATPase- and helicase-

like activities of mIELF35. There is contradicting evidence whether mIELF35 possesses a dominant negative effect on EBOV polymerase activity in the context of a minigenome system^{192,193}. Studying mIELF35 in the context of filovirus infection indicate whether this factor could negatively regulate the viral polymerase.

In addition to VP35 K residue conservation, it is important to investigate whether there are any tissue- and/or host-specific differences in the E3 ubiquitin ligase(s) that VP35 hijacks. Understanding the diversity of E3 ubiquitin ligases that can conjugate ubiquitin onto VP35/K309 or synthesize unanchored, K63-polyUb that promotes polymerase activity will aid in the design of potential therapeutics. Further, flexibility in which ubiquitin ligase can fulfill this role may allow the virus to evade therapeutic intervention.

BLOCKING VP35 UBIQUITINATION

The translation of our findings into a novel EBOV treatment is a long-term goal. Targeting VP35 ubiquitination and interaction with unanchored ubiquitin, TRIM6, and TRIM25 may be a potential therapeutic strategy. We are currently working with a collaborator to predict small molecule inhibitors that would block VP35's interaction with free Ub. A similar strategy could also be employed to model NP-Ub interactions once we identify which of NP's sub-domains facilitates the interaction. Structural data to model VP35's IID⁶⁵ and -TRIM25's B30.2/SPRY¹⁹⁵ interactions could aid in identifying or designing small molecules that could block VP35's interaction with TRIMs 6 and -25. The predicted inhibitors would then be screened with *in vitro* binding assays and tested with the minigenome system before testing with infectious EBOV.

PACKAGING OF FREE UBIQUITIN INTO EBOV PARTICLES

A novel finding of our studies was the packaging of ubiquitin into EBOV particles. Future studies are needed to elucidate the functional relevance. We could attempt to prevent or enhance the incorporation of free Ub into EBOV particles through over-expression or knockdown of IsoT in infected cells and purify virus from their supernatants. Studies are needed to identify whether any E3 ligases, such as TRIM25, is able to facilitate the synthesis of polyUb that is incorporated into the Ebola virus particles. Comparison of the amount of free Ub incorporated into EBOV particles collected from cells with various host factors knocked down or over-expressed could inform the mechanism of Ub packaging. Based on the study investigating Ub packaging into IAV particles, we speculate that the Ub may analogously facilitate uncoating of the nucleocapsid. Identifying the chain linkage topology of the packaged chains is needed to substantiate our speculation that the chains could promote primary transcription upon entry. We are also interested in investigating the conservation of free-Ub packaging across *Filoviridae* and other virus genera.

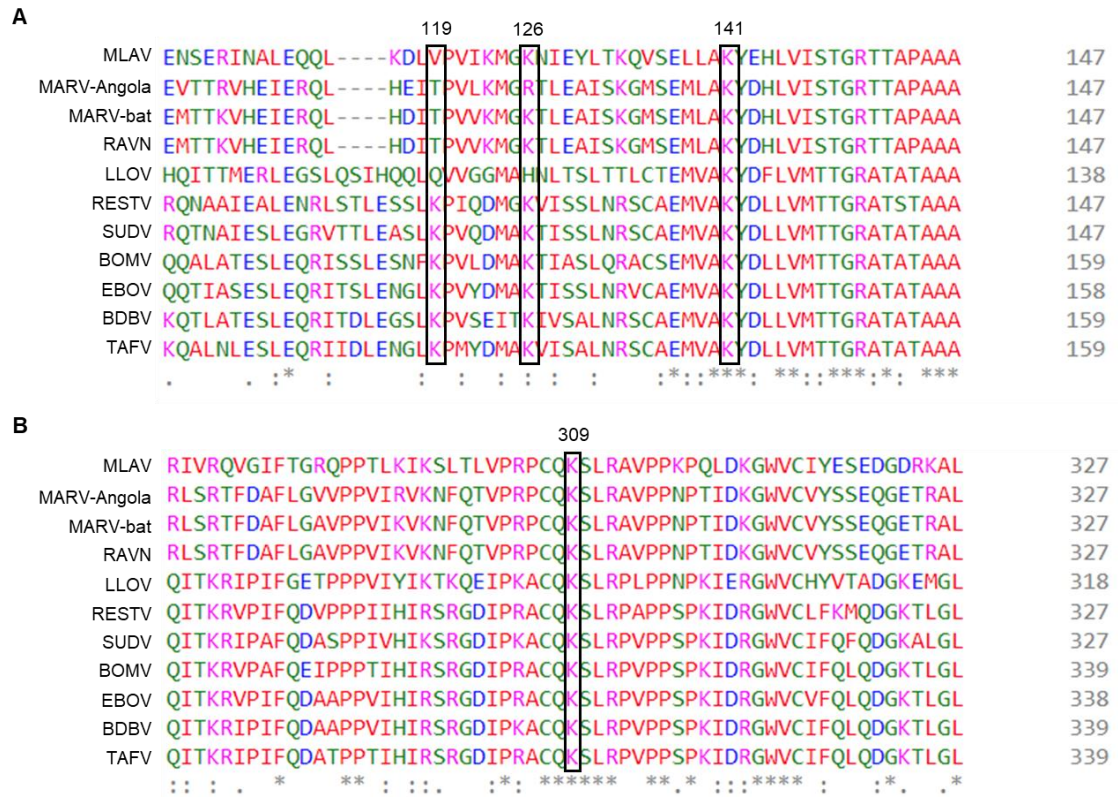


Figure 8.1 Alignment of Filovirus VP35

(A) Alignment of Filovirus VP35 for the region containing the K119.126.26 cluster (*Zaire ebolavirus* (EBOV) numbering). Boxes are placed around the EBOV equivalent 119, 126, and 141 residues. (B) Alignment of Filovirus VP35 for the region containing K309 (*Zaire ebolavirus* (EBOV) numbering). A box is placed around the EBOV equivalent 309 residue. (A-B) Alignments were done with EMBL-EBI CLUSTAL O(1.2.4) multiple sequence alignment. The following protein FASTA files from NCBI were used: YP_010087184.1 (*Mengla dianlovirus* – MLAV), Q1PD52.1 (*Marburg marburgvirus* Angola strain – MARV-Angola), QPJ58062.1 (MARV isolated from *Rouessetus aegyptiacus*), AAC40456.1 (Ravn virus –RAVN), YP_004928136.1 (*Lloviu cuevavirus* – LLOV), NP_690581.1 (RESTV), YP_138521.1 (SUDV), YP_009513275.1 (BOMV), NP_066244.1 (EBOV), YP_003815433.1 (BDBV), and YP_003815424.1 (TAFV). (Figure made by Sarah van Tol)

References

- 1 Kuhn, J. H. *et al.* ICTV Virus Taxonomy Profile: Filoviridae. *The Journal of general virology* **100**, doi:10.1099/jgv.0.001252 (2019).
- 2 Jacob, S. T. *et al.* Ebola virus disease. *Nat Rev Dis Primers* **6**, 13, doi:10.1038/s41572-020-0147-3 (2020).
- 3 CDC. *Ebola (Ebola Virus Disease) History of Ebola Outbreaks*, <https://www.cdc.gov/vhf/ebola/history/chronology.html#anchor_1526565058132> (2021).
- 4 Feldmann, H., Sprecher, A. & Geisbert, T. W. Ebola. *The New England journal of medicine* **382**, doi:10.1056/NEJMra1901594 (2020).
- 5 Iversen, P. L. *et al.* Recent successes in therapeutics for Ebola virus disease: no time for complacency. *The Lancet. Infectious diseases* **20**, doi:10.1016/S1473-3099(20)30282-6 (2020).
- 6 Muhlberger, E., Weik, M., Volchkov, V. E., Klenk, H. D. & Becker, S. Comparison of the transcription and replication strategies of marburg virus and Ebola virus by using artificial replication systems. *Journal of virology* **73**, 2333-2342 (1999).
- 7 Muhlberger, E. Filovirus replication and transcription. *Future Virol* **2**, 205-215, doi:10.2217/17460794.2.2.205 (2007).
- 8 Younan, P. *et al.* Ebola virus-mediated T-lymphocyte depletion is the result of an abortive infection. *PLoS pathogens* **15**, e1008068, doi:10.1371/journal.ppat.1008068 (2019).
- 9 Shabman, R. S. *et al.* Deep sequencing identifies noncanonical editing of Ebola and Marburg virus RNAs in infected cells. *mBio* **5**, doi:10.1128/mBio.02011-14 (2014).
- 10 Hume, A. J. & Mühlberger, E. Distinct Genome Replication and Transcription Strategies within the Growing Filovirus Family. *Journal of molecular biology* **431**, 4290-4320, doi:10.1016/j.jmb.2019.06.029 (2019).
- 11 Bharat, T. A. *et al.* Structural dissection of Ebola virus and its assembly determinants using cryo-electron tomography. *Proceedings of the National Academy of Sciences of the United States of America* **109**, 4275-4280, doi:10.1073/pnas.1120453109 (2012).
- 12 Huang, Y., Xu, L., Sun, Y. & Nabel, G. J. The assembly of Ebola virus nucleocapsid requires virion-associated proteins 35 and 24 and posttranslational modification of nucleoprotein. *Molecular cell* **10**, 307-316 (2002).
- 13 Takamatsu, Y., Kolesnikova, L., Schauflinger, M., Noda, T. & Becker, S. The Integrity of the YxxL Motif of Ebola Virus VP24 Is Important for the Transport of Nucleocapsid-Like Structures and for the Regulation of Viral RNA Synthesis. *Journal of virology* **94**, doi:10.1128/jvi.02170-19 (2020).
- 14 Mateo, M. *et al.* Knockdown of Ebola virus VP24 impairs viral nucleocapsid assembly and prevents virus replication. *The Journal of infectious diseases* **204 Suppl 3**, doi:10.1093/infdis/jir311 (2011).

- 15 Kruse, T. *et al.* The Ebola Virus Nucleoprotein Recruits the Host PP2A-B56 Phosphatase to Activate Transcriptional Support Activity of VP30. *Molecular cell* **69**, 136-145.e136, doi:10.1016/j.molcel.2017.11.034 (2018).
- 16 Biedenkopf, N., Hartlieb, B., Hoenen, T. & Becker, S. Phosphorylation of Ebola virus VP30 influences the composition of the viral nucleocapsid complex: impact on viral transcription and replication. *The Journal of biological chemistry* **288**, 11165-11174, doi:10.1074/jbc.M113.461285 (2013).
- 17 Biedenkopf, N., Schlereth, J., Grunweller, A., Becker, S. & Hartmann, R. K. RNA Binding of Ebola Virus VP30 Is Essential for Activating Viral Transcription. *Journal of virology* **90**, 7481-7496, doi:10.1128/jvi.00271-16 (2016).
- 18 Takamatsu, Y. *et al.* Serine-Arginine Protein Kinase 1 Regulates Ebola Virus Transcription. *mBio* **11**, doi:10.1128/mbio.02565-19 (2020).
- 19 Ilinykh, P. A. *et al.* Role of protein phosphatase 1 in dephosphorylation of Ebola virus VP30 protein and its targeting for the inhibition of viral transcription. *The Journal of biological chemistry* **289**, doi:10.1074/jbc.M114.575050 (2014).
- 20 Trunschke, M. *et al.* The L-VP35 and L-L interaction domains reside in the amino terminus of the Ebola virus L protein and are potential targets for antivirals. *Virology* **441**, 135-145, doi:10.1016/j.virol.2013.03.013 (2013).
- 21 Groseth, A. *et al.* The Ebola virus ribonucleoprotein complex: a novel VP30-L interaction identified. *Virus research* **140**, 8-14, doi:10.1016/j.virusres.2008.10.017 (2009).
- 22 Prins, K. C. *et al.* Basic residues within the ebolavirus VP35 protein are required for its viral polymerase cofactor function. *Journal of virology* **84**, 10581-10591, doi:10.1128/jvi.00925-10 (2010).
- 23 Leung, D. W. *et al.* An Intrinsically Disordered Peptide from Ebola Virus VP35 Controls Viral RNA Synthesis by Modulating Nucleoprotein-RNA Interactions. *Cell reports* **11**, 376-389, doi:10.1016/j.celrep.2015.03.034 (2015).
- 24 Kirchdoerfer, R. N., Abelson, D. M., Li, S., Wood, M. R. & Saphire, E. O. Assembly of the Ebola Virus Nucleoprotein from a Chaperoned VP35 Complex. *Cell reports* **12**, 140-149, doi:10.1016/j.celrep.2015.06.003 (2015).
- 25 Landeras-Bueno, S. *et al.* Sudan Ebolavirus VP35-NP Crystal Structure Reveals a Potential Target for Pan-Filovirus Treatment. *mBio* **10**, doi:10.1128/mBio.00734-19 (2019).
- 26 Zhu, T. *et al.* Crystal Structure of the Marburg Virus Nucleoprotein Core Domain Chaperoned by a VP35 Peptide Reveals a Conserved Drug Target for Filovirus. *Journal of virology* **91**, doi:10.1128/jvi.00996-17 (2017).
- 27 Reid, S. P., Cardenas, W. B. & Basler, C. F. Homo-oligomerization facilitates the interferon-antagonist activity of the ebolavirus VP35 protein. *Virology* **341**, 179-189, doi:10.1016/j.virol.2005.06.044 (2005).
- 28 Zinzula, L. *et al.* Structures of Ebola and Reston Virus VP35 Oligomerization Domains and Comparative Biophysical Characterization in All Ebolavirus Species. *Structure (London, England : 1993)* **27**, 39-54.e36, doi:10.1016/j.str.2018.09.009 (2019).
- 29 Chanthamontri, C. K. *et al.* Ebola Viral Protein 35 N-terminus is a Parallel Tetramer. *Biochemistry*, doi:10.1021/acs.biochem.8b01154 (2018).

- 30 Di Palma, F. *et al.* Relevance of Ebola virus VP35 homo-dimerization on the type I interferon cascade inhibition. *Antivir Chem Chemother* **27**, 2040206619889220, doi:10.1177/2040206619889220 (2019).
- 31 Moller, P., Pariente, N., Klenk, H. D. & Becker, S. Homo-oligomerization of Marburgvirus VP35 is essential for its function in replication and transcription. *Journal of virology* **79**, 14876-14886, doi:10.1128/jvi.79.23.14876-14886.2005 (2005).
- 32 Leung, D. W. *et al.* Structural basis for dsRNA recognition and interferon antagonism by Ebola VP35. *Nature structural & molecular biology* **17**, 165-172, doi:10.1038/nsmb.1765 (2010).
- 33 Luthra, P., Jordan, D. S., Leung, D. W., Amarasinghe, G. K. & Basler, C. F. Ebola Virus VP35 Interaction with Dynein LC8 Regulates Viral RNA Synthesis. *Journal of virology* **89**, 5148-5153, doi:10.1128/jvi.03652-14 (2015).
- 34 Lim, D., Shin, H. C., Choi, J. S., Kim, S. J. & Ku, B. Crystal structure of human LC8 bound to a peptide from Ebola virus VP35. *Journal of microbiology (Seoul, Korea)* **59**, doi:10.1007/s12275-021-0641-7 (2021).
- 35 Rodriguez Galvan, J. *et al.* Human Parainfluenza Virus 3 Phosphoprotein Is a Tetramer and Shares Structural and Interaction Features with Ebola Phosphoprotein VP35. *Biomolecules* **11**, doi:10.3390/biom11111603 (2021).
- 36 Shu, T. *et al.* Ebola virus VP35 has novel NTPase and helicase-like activities. *Nucleic Acids Res* **47**, 5837-5851, doi:10.1093/nar/gkz340 (2019).
- 37 Johnson, R. F., McCarthy, S. E., Godlewski, P. J. & Harty, R. N. Ebola virus VP35-VP40 interaction is sufficient for packaging 3E-5E minigenome RNA into virus-like particles. *Journal of virology* **80**, 5135-5144, doi:10.1128/jvi.01857-05 (2006).
- 38 Bharat, T. A. *et al.* Cryo-electron tomography of Marburg virus particles and their morphogenesis within infected cells. *PLoS biology* **9**, e1001196, doi:10.1371/journal.pbio.1001196 (2011).
- 39 Takeuchi, O. & Akira, S. Pattern recognition receptors and inflammation. *Cell* **140**, 805-820, doi:10.1016/j.cell.2010.01.022 (2010).
- 40 Ebner, P., Versteeg, G. A. & Ikeda, F. Ubiquitin enzymes in the regulation of immune responses. *Critical reviews in biochemistry and molecular biology*, 1-36, doi:10.1080/10409238.2017.1325829
10.1080/10409238.2017.1325829. (2017).
- 41 Liu, S. & Chen, Z. J. Expanding role of ubiquitination in NF-kappaB signaling. *Cell research* **21**, 6-21, doi:10.1038/cr.2010.170
10.1038/cr.2010.170. Epub 2010 Dec 7. (2010).
- 42 Hiscott, J. Convergence of the NF-kappaB and IRF pathways in the regulation of the innate antiviral response. *Cytokine & growth factor reviews* **18**, 483-490, doi:10.1016/j.cytogfr.2007.06.002 (2007).
- 43 Runge, S. *et al.* In vivo ligands of MDA5 and RIG-I in measles virus-infected cells. *PLoS pathogens* **10**, e1004081, doi:10.1371/journal.ppat.1004081
10.1371/journal.ppat.1004081. eCollection 2014 Apr. (2014).
- 44 Yoneyama, M. *et al.* The RNA helicase RIG-I has an essential function in double-stranded RNA-induced innate antiviral responses. *Nature immunology* **5**, 730-737, doi:10.1038/ni1087 (2004).

- 45 Hornung, V. *et al.* 5'-Triphosphate RNA is the ligand for RIG-I. *Science (New York, N.Y.)* **314**, 994-997, doi:10.1126/science.1132505 (2006).
- 46 Pichlmair, A. *et al.* RIG-I-mediated antiviral responses to single-stranded RNA bearing 5'-phosphates. *Science (New York, N.Y.)* **314**, 997-1001, doi:10.1126/science.1132998 (2006).
- 47 Kato, H. *et al.* Differential roles of MDA5 and RIG-I helicases in the recognition of RNA viruses. *Nature* **441**, 101-105, doi:10.1038/nature04734 (2006).
- 48 Chan, Y. K. & Gack, M. U. RIG-I-like receptor regulation in virus infection and immunity. *Current opinion in virology* **12**, 7-14, doi:10.1016/j.coviro.2015.01.004 (2015).
- 49 Jiang, X. *et al.* Ubiquitin-induced oligomerization of the RNA sensors RIG-I and MDA5 activates antiviral innate immune response. *Immunity* **36**, 959-973, doi:10.1016/j.immuni.2012.03.022 (2012).
- 50 Wu, B. *et al.* Structural basis for dsRNA recognition, filament formation, and antiviral signal activation by MDA5. *Cell* **152**, 276-289, doi:10.1016/j.cell.2012.11.048
10.1016/j.cell.2012.11.048. Epub 2012 Dec 27. (2013).
- 51 Seth, R. B., Sun, L., Ea, C. K. & Chen, Z. J. Identification and characterization of MAVS, a mitochondrial antiviral signaling protein that activates NF-kappaB and IRF 3. *Cell* **122**, 669-682, doi:10.1016/j.cell.2005.08.012 (2005).
- 52 Peisley, A., Wu, B., Yao, H., Walz, T. & Hur, S. RIG-I forms signaling-competent filaments in an ATP-dependent, ubiquitin-independent manner. *Molecular cell* **51**, 573-583, doi:10.1016/j.molcel.2013.07.024
10.1016/j.molcel.2013.07.024. Epub 2013 Aug 29. (2013).
- 53 Gack, M. U., Nistal-Villan, E., Inn, K. S., Garcia-Sastre, A. & Jung, J. U. Phosphorylation-mediated negative regulation of RIG-I antiviral activity. *Journal of virology* **84**, 3220-3229, doi:10.1128/jvi.02241-09
10.1128/JVI.02241-09. Epub 2010 Jan 13. (2010).
- 54 Oshiumi, H. *et al.* The ubiquitin ligase Riplet is essential for RIG-I-dependent innate immune responses to RNA virus infection. *Cell host & microbe* **8**, 496-509, doi:10.1016/j.chom.2010.11.008
10.1016/j.chom.2010.11.008. (2010).
- 55 Zeng, W. *et al.* Reconstitution of the RIG-I pathway reveals a signaling role of unanchored polyubiquitin chains in innate immunity. *Cell* **141**, 315-330, doi:10.1016/j.cell.2010.03.029
10.1016/j.cell.2010.03.029. (2010).
- 56 Arimoto, K. *et al.* Negative regulation of the RIG-I signaling by the ubiquitin ligase RNF125. *Proceedings of the National Academy of Sciences of the United States of America* **104**, 7500-7505, doi:10.1073/pnas.0611551104 (2007).
- 57 Arimoto, K., Konishi, H. & Shimotohno, K. UbcH8 regulates ubiquitin and ISG15 conjugation to RIG-I. *Molecular immunology* **45**, 1078-1084, doi:10.1016/j.molimm.2007.07.021 (2008).
- 58 Hou, F. *et al.* MAVS forms functional prion-like aggregates to activate and propagate antiviral innate immune response. *Cell* **146**, 448-461, doi:10.1016/j.cell.2011.06.041
10.1016/j.cell.2011.06.041. Epub 2011 Jul 21. (2011).

- 59 Liu, S. *et al.* MAVS recruits multiple ubiquitin E3 ligases to activate antiviral signaling cascades. *eLife* **2**, e00785, doi:10.7554/eLife.00785 (2013).
- 60 Xie, P. TRAF molecules in cell signaling and in human diseases. *Journal of molecular signaling* **8**, 7, doi:10.1186/1750-2187-8-7 (2013).
- 61 McNab, F., Mayer-Barber, K., Sher, A., Wack, A. & O'Garra, A. Type I interferons in infectious disease. *Nature reviews. Immunology* **15**, 87-103, doi:10.1038/nri3787 (2015).
- 62 Chau, T. L. *et al.* Are the IKKs and IKK-related kinases TBK1 and IKK-epsilon similarly activated? *Trends in biochemical sciences* **33**, 171-180, doi:10.1016/j.tibs.2008.01.002 (2008).
- 63 Juang, Y. T. *et al.* Primary activation of interferon A and interferon B gene transcription by interferon regulatory factor 3. *Proceedings of the National Academy of Sciences of the United States of America* **95**, 9837-9842 (1998).
- 64 Hartman, A. L., Towner, J. S. & Nichol, S. T. A C-terminal basic amino acid motif of Zaire ebolavirus VP35 is essential for type I interferon antagonism and displays high identity with the RNA-binding domain of another interferon antagonist, the NS1 protein of influenza A virus. *Virology* **328**, 177-184, doi:10.1016/j.virol.2004.07.006 (2004).
- 65 Leung, D. W. *et al.* Structure of the Ebola VP35 interferon inhibitory domain. *Proceedings of the National Academy of Sciences of the United States of America* **106**, 411-416, doi:10.1073/pnas.0807854106 (2009).
- 66 Zinzula, L., Esposito, F., Pala, D. & Tramontano, E. dsRNA binding characterization of full length recombinant wild type and mutants Zaire ebolavirus VP35. *Antiviral research* **93**, 354-363, doi:10.1016/j.antiviral.2012.01.005 (2012).
- 67 Cardenas, W. B. *et al.* Ebola virus VP35 protein binds double-stranded RNA and inhibits alpha/beta interferon production induced by RIG-I signaling. *Journal of virology* **80**, 5168-5178, doi:10.1128/jvi.02199-05 (2006).
- 68 Edwards, M. R. *et al.* Differential Regulation of Interferon Responses by Ebola and Marburg Virus VP35 Proteins. *Cell reports* **14**, 1632-1640, doi:10.1016/j.celrep.2016.01.049 (2016).
- 69 Prins, K. C. *et al.* Mutations abrogating VP35 interaction with double-stranded RNA render Ebola virus avirulent in guinea pigs. *Journal of virology* **84**, 3004-3015, doi:10.1128/jvi.02459-09 (2010).
- 70 Hartman, A. L. *et al.* Inhibition of IRF-3 activation by VP35 is critical for the high level of virulence of ebola virus. *Journal of virology* **82**, 2699-2704, doi:10.1128/jvi.02344-07 (2008).
- 71 Woolsey, C. *et al.* A VP35 Mutant Ebola Virus Lacks Virulence but Can Elicit Protective Immunity to Wild-Type Virus Challenge. *Cell reports* **28**, 3032-3046.e3036, doi:10.1016/j.celrep.2019.08.047 (2019).
- 72 Prins, K. C., Cardenas, W. B. & Basler, C. F. Ebola virus protein VP35 impairs the function of interferon regulatory factor-activating kinases IKKepsilon and TBK-1. *Journal of virology* **83**, 3069-3077, doi:10.1128/jvi.01875-08 (2009).

- 73 Basler, C. F. *et al.* The Ebola virus VP35 protein inhibits activation of interferon regulatory factor 3. *Journal of virology* **77**, 7945-7956, doi:10.1128/jvi.77.14.7945-7956.2003 (2003).
- 74 Chang, T. H. *et al.* Ebola Zaire virus blocks type I interferon production by exploiting the host SUMO modification machinery. *PLoS pathogens* **5**, e1000493, doi:10.1371/journal.ppat.1000493 (2009).
- 75 Jin, H. *et al.* The VP35 protein of Ebola virus impairs dendritic cell maturation induced by virus and lipopolysaccharide. *Journal of General Virology* **91**, 352-361, doi:10.1099/vir.0.017343-0 (2010).
- 76 Leung, L. W. *et al.* Ebolavirus VP35 suppresses IFN production from conventional but not plasmacytoid dendritic cells. *Immunol Cell Biol* **89**, 792-802, doi:10.1038/icb.2010.169 (2011).
- 77 Lubaki, N. M. *et al.* The lack of maturation of Ebola virus-infected dendritic cells results from the cooperative effect of at least two viral domains. *Journal of virology* **87**, 7471-7485, doi:10.1128/jvi.03316-12 (2013).
- 78 Yen, B., Mulder, L. C., Martinez, O. & Basler, C. F. Molecular basis for ebolavirus VP35 suppression of human dendritic cell maturation. *Journal of virology* **88**, 12500-12510, doi:10.1128/jvi.02163-14 (2014).
- 79 Bharaj, P. *et al.* The Host E3-Ubiquitin Ligase TRIM6 Ubiquitinates the Ebola Virus VP35 Protein and Promotes Virus Replication. *J Virol* **91**, doi:10.1128/jvi.00833-17 (2017).
- 80 Ivanov, A. *et al.* Global phosphoproteomic analysis of Ebola virions reveals a novel role for VP35 phosphorylation-dependent regulation of genome transcription. *Cellular and molecular life sciences : CMLS*, doi:10.1007/s00018-019-03303-1 (2019).
- 81 Zhu, L. *et al.* Ebola virus replication is regulated by the phosphorylation of viral protein VP35. *Biochemical and biophysical research communications* **521**, 687-692, doi:10.1016/j.bbrc.2019.10.147 (2020).
- 82 Yau, R. & Rape, M. The increasing complexity of the ubiquitin code. *Nature cell biology* **18**, 579-586, doi:10.1038/ncb3358 (2016).
- 83 Husnjak, K. & Dikic, I. Ubiquitin-binding proteins: decoders of ubiquitin-mediated cellular functions. *Annual review of biochemistry* **81**, 291-322, doi:10.1146/annurev-biochem-051810-094654
10.1146/annurev-biochem-051810-094654. Epub 2012 Apr 5. (2012).
- 84 Ye, Y. & Rape, M. Building ubiquitin chains: E2 enzymes at work. *Nature reviews. Molecular cell biology* **10**, 755-764, doi:10.1038/nrm2780
10.1038/nrm2780. (2009).
- 85 Shi, Y. *et al.* Ube2D3 and Ube2N are essential for RIG-I-mediated MAVS aggregation in antiviral innate immunity. *Nat Commun* **8**, 15138, doi:10.1038/ncomms15138
10.1038/ncomms15138. (2017).
- 86 Rajsbaum, R., Garcia-Sastre, A. & Versteeg, G. A. TRIMmunity: the roles of the TRIM E3-ubiquitin ligase family in innate antiviral immunity. *Journal of molecular biology* **426**, 1265-1284, doi:10.1016/j.jmb.2013.12.005
10.1016/j.jmb.2013.12.005. Epub 2013 Dec 12. (2013).

- 87 Versteeg, G. A., Benke, S., Garcia-Sastre, A. & Rajsbaum, R. InTRIMsic immunity: Positive and negative regulation of immune signaling by tripartite motif proteins. *Cytokine & growth factor reviews* **25**, 563-576, doi:10.1016/j.cytogfr.2014.08.001
10.1016/j.cytogfr.2014.08.001. Epub 2014 Aug 13. (2014).
- 88 Hicke, L., Schubert, H. L. & Hill, C. P. Ubiquitin-binding domains. *Nature reviews. Molecular cell biology* **6**, 610-621, doi:10.1038/nrm1701 (2005).
- 89 Rajsbaum, R. *et al.* Unanchored K48-linked polyubiquitin synthesized by the E3-ubiquitin ligase TRIM6 stimulates the interferon-IKepsilon kinase-mediated antiviral response. *Immunity* **40**, 880-895, doi:10.1016/j.immuni.2014.04.018
10.1016/j.immuni.2014.04.018. Epub 2014 May 29. (2014).
- 90 Fletcher, A. J., Mallery, D. L., Watkinson, R. E., Dickson, C. F. & James, L. C. Sequential ubiquitination and deubiquitination enzymes synchronize the dual sensor and effector functions of TRIM21. *Proceedings of the National Academy of Sciences of the United States of America* **112**, 10014-10019, doi:10.1073/pnas.1507534112
10.1073/pnas.1507534112. Epub 2015 Jul 6. (2015).
- 91 Han, Z. *et al.* Ubiquitin Ligase WWP1 Interacts with Ebola Virus VP40 to Regulate Egress. *Journal of virology*, doi:10.1128/jvi.00812-17 (2017).
- 92 Han, Z. *et al.* ITCH E3 Ubiquitin Ligase Interacts with Ebola Virus VP40 To Regulate Budding. *Journal of virology* **90**, 9163-9171, doi:10.1128/jvi.01078-16 (2016).
- 93 Harty, R. N., Brown, M. E., Wang, G., Huibregtse, J. & Hayes, F. P. A PPxY motif within the VP40 protein of Ebola virus interacts physically and functionally with a ubiquitin ligase: implications for filovirus budding. *Proceedings of the National Academy of Sciences of the United States of America* **97**, 13871-13876, doi:10.1073/pnas.250277297 (2000).
- 94 Urata, S. & Yasuda, J. Regulation of Marburg virus (MARV) budding by Nedd4.1: a different WW domain of Nedd4.1 is critical for binding to MARV and Ebola virus VP40. *The Journal of general virology* **91**, 228-234, doi:10.1099/vir.0.015495-0 (2010).
- 95 Yasuda, J., Nakao, M., Kawaoka, Y. & Shida, H. Nedd4 regulates egress of Ebola virus-like particles from host cells. *Journal of virology* **77**, 9987-9992 (2003).
- 96 Okumura, A. *et al.* Suppressor of Cytokine Signaling 3 Is an Inducible Host Factor That Regulates Virus Egress during Ebola Virus Infection. *Journal of virology* **89**, 10399-10406, doi:10.1128/jvi.01736-15 (2015).
- 97 Shepley-McTaggart, A. *et al.* Ubiquitin Ligase SMURF2 Interacts with Filovirus VP40 and Promotes Egress of VP40 VLPs. *Viruses* **13**, doi:10.3390/v13020288 (2021).
- 98 Han, Z. *et al.* Small-molecule probes targeting the viral PPxY-host Nedd4 interface block egress of a broad range of RNA viruses. *Journal of virology* **88**, 7294-7306, doi:10.1128/jvi.00591-14 (2014).
- 99 Loughran, H. M. *et al.* Quinoxaline-based inhibitors of Ebola and Marburg VP40 egress. *Bioorganic & medicinal chemistry letters* **26**, 3429-3435, doi:10.1016/j.bmcl.2016.06.053 (2016).

- 100 Okumura, A., Pitha, P. M. & Harty, R. N. ISG15 inhibits Ebola VP40 VLP budding in an L-domain-dependent manner by blocking Nedd4 ligase activity. *Proceedings of the National Academy of Sciences of the United States of America* **105**, 3974-3979, doi:10.1073/pnas.0710629105 (2008).
- 101 Baz-Martinez, M. *et al.* Regulation of Ebola virus VP40 matrix protein by SUMO. *Scientific reports* **6**, 37258, doi:10.1038/srep37258 (2016).
- 102 Vidal, S. *et al.* Regulation of the Ebola Virus VP24 Protein by SUMO. *Journal of virology* **94**, doi:10.1128/JVI.01687-19 (2019).
- 103 Batra, J. *et al.* Protein Interaction Mapping Identifies RBBP6 as a Negative Regulator of Ebola Virus Replication. *Cell* **175**, 1917-1930.e1913, doi:10.1016/j.cell.2018.08.044 (2018).
- 104 Lun, C. M., Waheed, A. A., Majadly, A., Powell, N. & Freed, E. O. Mechanism of Viral Glycoprotein Targeting by Membrane-Associated RING-CH Proteins. *mBio* **12**, doi:10.1128/mBio.00219-21 (2021).
- 105 Yu, C. *et al.* MARCH8 Inhibits Ebola Virus Glycoprotein, Human Immunodeficiency Virus Type 1 Envelope Glycoprotein, and Avian Influenza Virus H5N1 Hemagglutinin Maturation. *mBio* **11**, doi:10.1128/mBio.01882-20 (2020).
- 106 Ozato, K., Shin, D. M., Chang, T. H. & Morse, H. c. TRIM family proteins and their emerging roles in innate immunity. *Nature reviews. Immunology* **8**, doi:10.1038/nri2413 (2008).
- 107 Uchil, P. D. *et al.* TRIM protein-mediated regulation of inflammatory and innate immune signaling and its association with antiretroviral activity. *Journal of virology* **87**, 257-272, doi:10.1128/jvi.01804-12
10.1128/JVI.01804-12. Epub 2012 Oct 17. (2012).
- 108 Uchil, P. D., Quinlan, B. D., Chan, W. T., Luna, J. M. & Mothes, W. TRIM E3 ligases interfere with early and late stages of the retroviral life cycle. *PLoS pathogens* **4**, doi:10.1371/journal.ppat.0040016 (2008).
- 109 Versteeg, G. A. *et al.* The E3-ligase TRIM family of proteins regulates signaling pathways triggered by innate immune pattern-recognition receptors. *Immunity* **38**, 384-398, doi:10.1016/j.immuni.2012.11.013
10.1016/j.immuni.2012.11.013. (2013).
- 110 Giraldo, M. I. *et al.* Envelope protein ubiquitination drives entry and pathogenesis of Zika virus. *Nature* **585**, doi:10.1038/s41586-020-2457-8 (2020).
- 111 Reymond, A. *et al.* The tripartite motif family identifies cell compartments. *The EMBO journal* **20**, 2140-2151, doi:10.1093/emboj/20.9.2140 (2001).
- 112 Esposito, D., Koliopoulos, M. G. & Rittinger, K. Structural determinants of TRIM protein function. *Biochemical Society transactions* **45**, 183-191, doi:10.1042/bst20160325
10.1042/BST20160325. (2017).
- 113 Koliopoulos, M. G., Esposito, D., Christodoulou, E., Taylor, I. A. & Rittinger, K. Functional role of TRIM E3 ligase oligomerization and regulation of catalytic activity. *The EMBO journal* **35**, 1204-1218, doi:10.15252/embj.201593741
10.15252/embj.201593741. Epub 2016 May 6. (2016).

- 114 Sanchez, J. G. *et al.* The tripartite motif coiled-coil is an elongated antiparallel hairpin dimer. *Proceedings of the National Academy of Sciences of the United States of America* **111**, 2494-2499, doi:10.1073/pnas.1318962111
10.1073/pnas.1318962111. Epub 2014 Feb 3. (2014).
- 115 Dawidziak, D. M., Sanchez, J. G., Wagner, J. M., Ganser-Pornillos, B. K. & Pornillos, O. Structure and catalytic activation of the TRIM23 RING E3 ubiquitin ligase. *Proteins* **85**, doi:10.1002/prot.25348 (2017).
- 116 Diaz-Griffero, F. *et al.* A B-box 2 surface patch important for TRIM5alpha self-association, capsid binding avidity, and retrovirus restriction. *Journal of virology* **83**, doi:10.1128/JVI.01307-09 (2009).
- 117 Li, X. & Sodroski, J. The TRIM5alpha B-box 2 domain promotes cooperative binding to the retroviral capsid by mediating higher-order self-association. *Journal of virology* **82**, doi:10.1128/JVI.01548-08 (2008).
- 118 Streich, F. C., Jr., Ronchi, V. P., Connick, J. P. & Haas, A. L. Tripartite motif ligases catalyze polyubiquitin chain formation through a cooperative allosteric mechanism. *The Journal of biological chemistry* **288**, 8209-8221, doi:10.1074/jbc.M113.451567 (2013).
- 119 Yudina, Z. *et al.* RING Dimerization Links Higher-Order Assembly of TRIM5alpha to Synthesis of K63-Linked Polyubiquitin. *Cell reports* **12**, 788-797, doi:10.1016/j.celrep.2015.06.072
10.1016/j.celrep.2015.06.072. Epub 2015 Jul 23. (2015).
- 120 Short, K. M. & Cox, T. C. Subclassification of the RBCC/TRIM superfamily reveals a novel motif necessary for microtubule binding. *The Journal of biological chemistry* **281**, 8970-8980, doi:10.1074/jbc.M512755200 (2006).
- 121 Sardiello, M., Cairo, S., Fontanella, B., Ballabio, A. & Meroni, G. Genomic analysis of the TRIM family reveals two groups of genes with distinct evolutionary properties. *BMC evolutionary biology* **8**, 225, doi:10.1186/1471-2148-8-225
10.1186/1471-2148-8-225. (2008).
- 122 Shi, M. *et al.* Negative regulation of NF-kappaB activity by brain-specific TRIPartite Motif protein 9. *Nat Commun* **5**, 4820, doi:10.1038/ncomms5820
10.1038/ncomms5820. (2014).
- 123 Chikuma, S., Suita, N., Okazaki, I. M., Shibayama, S. & Honjo, T. TRIM28 prevents autoinflammatory T cell development in vivo. *Nature immunology* **13**, 596-603, doi:10.1038/ni.2293
10.1038/ni.2293. (2012).
- 124 Ichimura, T. *et al.* 14-3-3 proteins sequester a pool of soluble TRIM32 ubiquitin ligase to repress autoubiquitylation and cytoplasmic body formation. *Journal of cell science* **126**, 2014-2026, doi:10.1242/jcs.122069
10.1242/jcs.122069. Epub 2013 Feb 26. (2013).
- 125 Diaz-Griffero, F. *et al.* Rapid turnover and polyubiquitylation of the retroviral restriction factor TRIM5. *Virology* **349**, 300-315, doi:10.1016/j.virol.2005.12.040 (2006).
- 126 Sugiura, T. The cellular level of TRIM31, an RBCC protein overexpressed in gastric cancer, is regulated by multiple mechanisms including the ubiquitin-

- proteasome system. *Cell biology international* **35**, 657-661,
doi:10.1042/cbi20100772
- 10.1042/CBI20100772. (2011).
- 127 Meroni, G. Genomics and evolution of the TRIM gene family. *Advances in experimental medicine and biology* **770**, 1-9 (2012).
- 128 Han, K., Lou, D. I. & Sawyer, S. L. Identification of a genomic reservoir for new TRIM genes in primate genomes. *PLoS genetics* **7**, e1002388,
doi:10.1371/journal.pgen.1002388
- 10.1371/journal.pgen.1002388. Epub 2011 Dec 1. (2011).
- 129 Bell, J. L. *et al.* TRIM16 acts as an E3 ubiquitin ligase and can heterodimerize with other TRIM family members. *PloS one* **7**, e37470,
doi:10.1371/journal.pone.0037470
- 10.1371/journal.pone.0037470. Epub 2012 May 21. (2012).
- 130 Carthagen, L. *et al.* Human TRIM gene expression in response to interferons. *PloS one* **4**, e4894, doi:10.1371/journal.pone.0004894
- 10.1371/journal.pone.0004894. Epub 2009 Mar 17. (2009).
- 131 Gao, B., Xu, W., Wang, Y., Zhong, L. & Xiong, S. Induction of TRIM22 by IFN-gamma Involves JAK and PC-PLC/PKC, but Not MAPKs and p13K/Akt/mTOR Pathways. *Journal of interferon & cytokine research : the official journal of the International Society for Interferon and Cytokine Research* **33**, 578-587,
doi:10.1089/jir.2012.0170
- 10.1089/jir.2012.0170. Epub 2013 May 9. (2013).
- 132 Sjostrand, M. *et al.* Expression of the immune regulator tripartite-motif 21 is controlled by IFN regulatory factors. *Journal of immunology (Baltimore, Md. : 1950)* **191**, 3753-3763, doi:10.4049/jimmunol.1202341
- 10.4049/jimmunol.1202341. Epub 2013 Aug 23. (2013).
- 133 Rajsbaum, R., Stoye, J. P. & O'Garra, A. Type I interferon-dependent and -independent expression of tripartite motif proteins in immune cells. *European journal of immunology* **38**, 619-630, doi:10.1002/eji.200737916 (2008).
- 134 Hu, M. M. *et al.* TRIM38 Negatively Regulates TLR3/4-Mediated Innate Immune and Inflammatory Responses by Two Sequential and Distinct Mechanisms. *Journal of immunology (Baltimore, Md. : 1950)* **195**, 4415-4425,
doi:10.4049/jimmunol.1500859
- 10.4049/jimmunol.1500859. Epub 2015 Sep 21. (2015).
- 135 Narayan, K. *et al.* TRIM13 is a negative regulator of MDA5-mediated type I interferon production. *Journal of virology* **88**, 10748-10757,
doi:10.1128/jvi.02593-13
- 10.1128/JVI.02593-13. Epub 2014 Jul 9. (2014).
- 136 Jiang, M. X. *et al.* Expression profiling of TRIM protein family in THP1-derived macrophages following TLR stimulation. *Scientific reports* **7**, 42781,
doi:10.1038/srep42781
- 10.1038/srep42781. (2017).
- 137 McNab, F. W., Rajsbaum, R., Stoye, J. P. & O'Garra, A. Tripartite-motif proteins and innate immune regulation. *Current opinion in immunology* **23**,
doi:10.1016/j.coi.2010.10.021 (2011).

- 138 Manocha, G. D. *et al.* Regulatory role of TRIM21 in the type-I interferon pathway in Japanese encephalitis virus-infected human microglial cells. *Journal of neuroinflammation* **11**, doi:10.1186/1742-2094-11-24 (2014).
- 139 Laurent-Rolle, M. *et al.* The interferon signaling antagonist function of yellow fever virus NS5 protein is activated by type I interferon. *Cell host & microbe* **16**, doi:10.1016/j.chom.2014.07.015 (2014).
- 140 Manokaran, G. *et al.* Dengue subgenomic RNA binds TRIM25 to inhibit interferon expression for epidemiological fitness. *Science (New York, N.Y.)* **350**, doi:10.1126/science.aab3369 (2015).
- 141 Bharaj, P. *et al.* The Matrix Protein of Nipah Virus Targets the E3-Ubiquitin Ligase TRIM6 to Inhibit the IKKepsilon Kinase-Mediated Type-I IFN Antiviral Response. *PLoS pathogens* **12**, e1005880, doi:10.1371/journal.ppat.1005880 10.1371/journal.ppat.1005880. eCollection 2016 Sep. (2016).
- 142 Gack, M. U. *et al.* Influenza A virus NS1 targets the ubiquitin ligase TRIM25 to evade recognition by the host viral RNA sensor RIG-I. *Cell host & microbe* **5**, 439-449, doi:10.1016/j.chom.2009.04.006 10.1016/j.chom.2009.04.006. (2009).
- 143 Rajsbaum, R. & García-Sastre, A. Viral evasion mechanisms of early antiviral responses involving regulation of ubiquitin pathways. *Trends in microbiology* **21**, doi:10.1016/j.tim.2013.06.006 (2013).
- 144 Hage, A. *et al.* The RNA helicase DHX16 recognizes specific viral RNA to trigger RIG-I-dependent innate antiviral immunity. *Cell reports* **38**, doi:10.1016/j.celrep.2022.110434 (2022).
- 145 van Tol, S. *et al.* VAMP8 contributes to TRIM6-mediated type-I interferon antiviral response during West Nile virus infection. *Journal of virology*, doi:10.1128/jvi.01454-19 (2019).
- 146 Lang, X. *et al.* TRIM65-catalyzed ubiquitination is essential for MDA5-mediated antiviral innate immunity. *The Journal of experimental medicine* **214**, 459-473, doi:10.1084/jem.20160592 (2017).
- 147 Yan, J., Li, Q., Mao, A. P., Hu, M. M. & Shu, H. B. TRIM4 modulates type I interferon induction and cellular antiviral response by targeting RIG-I for K63-linked ubiquitination. *Journal of molecular cell biology* **6**, 154-163, doi:10.1093/jmcb/mju005 10.1093/jmcb/mju005. (2014).
- 148 Gack, M. U. *et al.* in *Nature* Vol. 446 916-920 (2007).
- 149 Oshiumi, H., Matsumoto, M. & Seya, T. Ubiquitin-mediated modulation of the cytoplasmic viral RNA sensor RIG-I. *Journal of biochemistry* **151**, 5-11, doi:10.1093/jb/mvr111 10.1093/jb/mvr111. Epub 2011 Sep 2. (2011).
- 150 Castanier, C. *et al.* MAVS ubiquitination by the E3 ligase TRIM25 and degradation by the proteasome is involved in type I interferon production after activation of the antiviral RIG-I-like receptors. *BMC biology* **10**, 44, doi:10.1186/1741-7007-10-44 10.1186/1741-7007-10-44. (2012).

- 151 Pauli, E. K. *et al.* The ubiquitin-specific protease USP15 promotes RIG-I-mediated antiviral signaling by deubiquitylating TRIM25. *Science signaling* **7**, ra3, doi:10.1126/scisignal.2004577
10.1126/scisignal.2004577. (2014).
- 152 Xu, C., Evensen, O. & Munang'andu, H. M. De Novo Transcriptome Analysis Shows That SAV-3 Infection Upregulates Pattern Recognition Receptors of the Endosomal Toll-Like and RIG-I-Like Receptor Signaling Pathways in Macrophage/Dendritic Like TO-Cells. *Viruses* **8**, 114, doi:10.3390/v8040114
10.3390/v8040114. (2016).
- 153 Miranzo-Navarro, D. & Magor, K. E. Activation of duck RIG-I by TRIM25 is independent of anchored ubiquitin. *PLoS one* **9**, e86968, doi:10.1371/journal.pone.0086968
10.1371/journal.pone.0086968. eCollection 2014. (2014).
- 154 Rajsbaum, R. *et al.* Species-specific inhibition of RIG-I ubiquitination and IFN induction by the influenza A virus NS1 protein. *PLoS pathogens* **8**, e1003059, doi:10.1371/journal.ppat.1003059
10.1371/journal.ppat.1003059. Epub 2012 Nov 29. (2012).
- 155 Feng, Z. Q. *et al.* Molecular characterization, tissue distribution and expression analysis of TRIM25 in Gallus gallus domesticus. *Gene* **561**, 138-147, doi:10.1016/j.gene.2015.02.025
10.1016/j.gene.2015.02.025. Epub 2015 Feb 13. (2015).
- 156 Gonçalves-Carneiro, D., Takata, M. A., Ong, H., Shilton, A. & Bieniasz, P. D. Origin and evolution of the zinc finger antiviral protein. *PLoS pathogens* **17**, doi:10.1371/journal.ppat.1009545 (2021).
- 157 Ludwig, S. & Wolff, T. Influenza A virus TRIMs the type I interferon response. *Cell host & microbe* **5**, 420-421, doi:10.1016/j.chom.2009.05.004
10.1016/j.chom.2009.05.004. (2009).
- 158 Heikel, G., Choudhury, N. R. & Michlewski, G. The role of Trim25 in development, disease and RNA metabolism. *Biochemical Society transactions* **44**, 1045-1050, doi:10.1042/bst20160077
10.1042/BST20160077. (2016).
- 159 Sanchez-Aparicio, M. T., Ayllon, J., Leo-Macias, A., Wolff, T. & Garcia-Sastre, A. Subcellular Localizations of RIG-I, TRIM25, and MAVS Complexes. *Journal of virology* **91**, doi:10.1128/jvi.01155-16
10.1128/JVI.01155-16. Print 2017 Jan 15. (2016).
- 160 Hu, Y. *et al.* The Severe Acute Respiratory Syndrome Coronavirus Nucleocapsid Inhibits Type I Interferon Production by Interfering with TRIM25-Mediated RIG-I Ubiquitination. *Journal of virology* **91**, doi:10.1128/jvi.02143-16
10.1128/JVI.02143-16. Print 2017 Apr 15. (2017).
- 161 Santiago, F. W. *et al.* Hijacking of RIG-I signaling proteins into virus-induced cytoplasmic structures correlates with the inhibition of type I interferon responses. *Journal of virology* **88**, 4572-4585, doi:10.1128/jvi.03021-13
10.1128/JVI.03021-13. Epub 2014 Jan 29. (2014).
- 162 Sanchez-Aparicio, M. T., Feinman, L. J., Garcia-Sastre, A. & Shaw, M. L. Paramyxovirus V Proteins Interact with the RIG-I/TRIM25 Regulatory Complex

- and Inhibit RIG-I Signaling. *Journal of virology* **92**, doi:10.1128/jvi.01960-17 (2018).
- 163 Towner, J. S. *et al.* Generation of eGFP expressing recombinant Zaire ebolavirus for analysis of early pathogenesis events and high-throughput antiviral drug screening. *Virology* **332**, doi:10.1016/j.virol.2004.10.048 (2005).
- 164 Bray, M., Davis, K., Geisbert, T., Schmaljohn, C. & Huggins, J. A mouse model for evaluation of prophylaxis and therapy of Ebola hemorrhagic fever. *The Journal of infectious diseases* **178**, doi:10.1086/515386 (1998).
- 165 Ran, F. A. *et al.* Genome engineering using the CRISPR-Cas9 system. *Nature protocols* **8**, doi:10.1038/nprot.2013.143 (2013).
- 166 Qiu, L. Q., Lai, W. S., Stumpo, D. J. & Blackshear, P. Mouse Embryonic Fibroblast Cell Culture and Stimulation. *Bio-protocol* **6**, doi:10.21769/BioProtoc.1859 (2016).
- 167 Madaan, A., Verma, R., Singh, A., T. , Swatantra, K. J. & Manu, J. A stepwise procedure for isolation of murine bone marrow and generation of dendritic cells. *Journal of Biological Methods* **1**, doi:https://jbmeth.org/jbm/article/view/12 (2014).
- 168 Watanabe, S., Noda, T., Halfmann, P., Jasenosky, L. & Kawaoka, Y. Ebola virus (EBOV) VP24 inhibits transcription and replication of the EBOV genome. *The Journal of infectious diseases* **196 Suppl 2**, doi:10.1086/520582 (2007).
- 169 Neumann, G., Feldmann, H., Watanabe, S., Lukashevich, I. & Kawaoka, Y. Reverse genetics demonstrates that proteolytic processing of the Ebola virus glycoprotein is not essential for replication in cell culture. *Journal of virology* **76**, doi:10.1128/jvi.76.1.406-410.2002 (2002).
- 170 Schneider, C. A., Rasband, W. S. & Eliceiri, K. W. NIH Image to ImageJ: 25 years of image analysis. *Nature methods* **9**, doi:10.1038/nmeth.2089 (2012).
- 171 Leung, D. W. *et al.* Structural basis for dsRNA recognition and interferon antagonism by Ebola VP35. *Nature structural & molecular biology* **17**, 165-172, doi:10.1038/nsmb.1765 (2010).
- 172 Tao, W., Gan, T., Guo, M., Xu, Y. & Zhong, J. Novel Stable Ebola Virus Minigenome Replicon Reveals Remarkable Stability of the Viral Genome. *Journal of virology* **91**, doi:10.1128/JVI.01316-17 (2017).
- 173 Frias-Staheli, N. *et al.* Ovarian tumor domain-containing viral proteases evade ubiquitin- and ISG15-dependent innate immune responses. *Cell host & microbe* **2**, doi:10.1016/j.chom.2007.09.014 (2007).
- 174 Giraldo, M. I. *et al.* K48-linked polyubiquitination of dengue virus NS1 protein inhibits its interaction with the viral partner NS4B. *Virus research* **246**, doi:10.1016/j.virusres.2017.12.013 (2018).
- 175 Reyes-Turcu, F. E. *et al.* The ubiquitin binding domain ZnF UBP recognizes the C-terminal diglycine motif of unanchored ubiquitin. *Cell* **124**, doi:10.1016/j.cell.2006.02.038 (2006).
- 176 Banerjee, I. *et al.* Influenza A virus uses the aggresome processing machinery for host cell entry. *Science (New York, N.Y.)* **346**, 473-477, doi:10.1126/science.1257037 (2014).

- 177 Ogino, T. & Green, T. J. RNA Synthesis and Capping by Non-segmented
Negative Strand RNA Viral Polymerases: Lessons From a Prototypic Virus.
Frontiers in microbiology **10**, 1490, doi:10.3389/fmicb.2019.01490 (2019).
- 178 Pan, J. *et al.* Structure of the human metapneumovirus polymerase
phosphoprotein complex. *Nature* **577**, 275-279, doi:10.1038/s41586-019-1759-1
(2020).
- 179 Gilman, M. S. A. *et al.* Structure of the Respiratory Syncytial Virus Polymerase
Complex. *Cell* **179**, 193-204.e114, doi:10.1016/j.cell.2019.08.014 (2019).
- 180 Sugita, Y., Matsunami, H., Kawaoka, Y., Noda, T. & Wolf, M. Cryo-EM
structure of the Ebola virus nucleoprotein-RNA complex at 3.6 Å resolution.
Nature **563**, 137-140, doi:10.1038/s41586-018-0630-0 (2018).
- 181 Du Pont, K. E., McCullagh, M. & Geiss, B. J. Conserved motifs in the flavivirus
NS3 RNA helicase enzyme. *Wiley interdisciplinary reviews. RNA* **13**,
doi:10.1002/wrna.1688 (2022).
- 182 Xia, H. *et al.* Human Enterovirus Nonstructural Protein 2CATPase Functions as
Both an RNA Helicase and ATP-Independent RNA Chaperone. *PLoS pathogens*
11, doi:10.1371/journal.ppat.1005067 (2015).
- 183 Rozen, F., Pelletier, J., Trachsel, H. & Sonenberg, N. A lysine substitution in the
ATP-binding site of eucaryotic initiation factor 4A abrogates nucleotide-binding
activity. *Molecular and cellular biology* **9**, doi:10.1128/mcb.9.9.4061-4063.1989
(1989).
- 184 Raney, K. D., Byrd, A. K. & Aarattuthodiyil, S. Structure and Mechanisms of SF1
DNA Helicases. *Advances in experimental medicine and biology* **767**,
doi:10.1007/978-1-4614-5037-5_2 (2013).
- 185 Xia, Z. P. *et al.* Direct activation of protein kinases by unanchored polyubiquitin
chains. *Nature* **461**, 114-119, doi:10.1038/nature08247
10.1038/nature08247. Epub 2009 Aug 12. (2009).
- 186 Di Rienzo, M. *et al.* Autophagy induction in atrophic muscle cells requires ULK1
activation by TRIM32 through unanchored K63-linked polyubiquitin chains.
Science advances **5**, doi:10.1126/sciadv.aau8857 (2019).
- 187 McEwan, W. A. *et al.* Intracellular antibody-bound pathogens stimulate immune
signaling via the Fc receptor TRIM21. *Nature immunology* **14**, 327-336,
doi:10.1038/ni.2548
10.1038/ni.2548. Epub 2013 Mar 3. (2013).
- 188 Rajsbaum, R. & Garcia-Sastre, A. Virology. Unanchored ubiquitin in virus
uncoating. *Science (New York, N.Y.)* **346**, 427-428, doi:10.1126/science.1261509
(2014).
- 189 Fang, J. *et al.* Functional interactomes of the Ebola virus polymerase identified by
proximity proteomics in the context of viral replication. *Cell reports* **38**,
doi:10.1016/j.celrep.2022.110544 (2022).
- 190 Tchesnokov, E. P., Raesisimakiani, P., Ngure, M., Marchant, D. & Gotte, M.
Recombinant RNA-Dependent RNA Polymerase Complex of Ebola Virus.
Scientific reports **8**, 3970, doi:10.1038/s41598-018-22328-3 (2018).
- 191 Mann, M. K. *et al.* Discovery of Small Molecule Antagonists of the USP5 Zinc
Finger Ubiquitin-Binding Domain. *Journal of medicinal chemistry* **62**,
doi:10.1021/acs.jmedchem.9b00988 (2019).

- 192 Edwards, M. R. *et al.* Conservation of Structure and Immune Antagonist Functions of Filoviral VP35 Homologs Present in Microbat Genomes. *Cell reports* **24**, 861-872.e866, doi:10.1016/j.celrep.2018.06.045 (2018).
- 193 Kondoh, T. *et al.* Putative endogenous filovirus VP35-like protein potentially functions as an IFN antagonist but not a polymerase cofactor. *PloS one* **12**, doi:10.1371/journal.pone.0186450 (2017).
- 194 Taylor, D. J., Dittmar, K., Ballinger, M. J. & Bruenn, J. A. Evolutionary maintenance of filovirus-like genes in bat genomes. *BMC evolutionary biology* **11**, doi:10.1186/1471-2148-11-336 (2011).
- 195 D'Cruz, A. A. *et al.* Crystal structure of the TRIM25 B30.2 (PRYSPRY) domain: a key component of antiviral signalling. *The Biochemical journal* **456**, doi:10.1042/BJ20121425 (2013).

VITA

Sarah Rose van Tol was born on December 12th, 1991, in Belleville, IL to Peter and Donna van Tol. She is the younger sister to Matthew and Mark van Tol. From an early age, her affinity toward animals steered her toward a career in science. From collecting beetles as a five-year old to working at a veterinary office, her early life nurtured her interest in the life sciences. Sarah graduated from Belleville Township High School-East in 2010.

After high school, Sarah attended Iowa State University in Ames, IA and majored in Animal Ecology and Biology with minors in Emerging Global Disease and Microbiology. While at Iowa State, Sarah was introduced to research as first-year student in the honors research mentorship program, where she worked with Dr. Donald Beitz studying cattle nutrition. The following summer, Sarah volunteered as an assistant on a longitudinal habitat assessment project at Lapalala Game Reserve in South Africa. On this trip, Sarah learned about the threat bovine tuberculosis posed to wildlife which sparked her interest in one health. Her new-found fascination with wildlife diseases strongly influenced the courses she selected for her science electives, including registering for “Insects and Our Health”. While learning about arboviruses and complex parasite life cycles, Sarah’s curiosity of the molecular mechanisms underlying host-pathogen interactions directed her toward virology and immunology courses as well as graduate school applications. In her senior year, Sarah joined Dr. Susan Carpenter’s molecular virology lab studying porcine reproductive and respiratory syndrome virus immune escape variants. Her time in Dr. Carpenter’s lab solidified her desire to study molecular microbiology, and she accepted her

offer to attend Johns Hopkins Bloomberg School of Public Health's Department of Molecular Microbiology and Immunology as a master's student.

Sarah conducted her master's thesis research in Dr. George Dimopolous' lab studying how an entomopathogenic bacterium influenced a malaria vector (*Anopheles gambiae*) mosquito's fitness and midgut microbiome. While at Johns Hopkins, Sarah's interest in zoonotic viruses matured, and she became interested in how natural reservoir hosts tolerate infection with virulent viruses. After graduating in 2016, Sarah matriculated into the Graduate School of Biomedical Sciences at the University of Texas Medical Branch as a Presidential Scholar. Here, Sarah joined the labs of her co-mentors Dr. Alexander Freiberg and Dr. Ricardo Rajsbaum to study Ebola virus VP35 ubiquitination and pteropine bat-henipaviral interactions. Throughout her time in the program, Sarah has been awarded two NIH fellowships: T32 biodefense training and a F31 Ruth L. Kirschstein Predoctoral Individual NRSA. Sarah plans to pursue a career as an academic researcher studying reservoir host-zoonotic virus relationships to better understand how to treat people and animals infected with virulent viruses.

EDUCATION

B.S., May 2014, Iowa State University, Ames, Iowa

M.S., May 2016, Johns Hopkins Bloomberg School of Public Health, Baltimore,
Maryland

PUBLICATIONS

- Hage, A., Bharaj, P., **van Tol, S.**, Giraldo, M. I., Gonzalez-Orozco, M., Valerdi, K. M., Warren, A. N., Aguilera-Aguirre, L., Xia, X., Widen, S. G., Moulton, H. M., Lee, B., Johnson, J. R., Krogan, N. J., García-Sastre, A., Shi, P-Y., Freiberg, A. N., Rajsbaum, R. (2022). The RNA Helicase DHX16 Recognizes Specific Viral RNA to Trigger RIG-I-dependent Innate Antiviral Immunity. *Cell Reports* Mar 8;38(10):110434. doi: 10.1016/j.celrep.2022.110434.
- Valerdi, K. M., Hage, A., **van Tol, S.**, Rajsbaum, R., Giraldo, M. I. (2021). The Role of the Host Ubiquitin System in Promoting Replication of Emergent Viruses. *Viruses* 13(3): 369. doi: 10.3390/v13030369.
- Moustaqil, M., Ollivier, E., Chiu, H-P., **van Tol, S.**, Rudolffi-Soto, P., Stevens, C., Bhumkar, A., Hunter, D. J.B., Freiberg, A., Jacques, D., Lee, B., Sierecki, E., Gambin, Y. (2020). SARS-CoV-2 proteases cleave IRF3 and critical modulators of inflammatory pathways (NLRP12 and TAB1): implications for disease presentation across species and the search for reservoir hosts. *Emerging Microbes and Infections* 10(1): 1-27. doi: 10.1080/22221751.2020.1870414.
- Giraldo, M.I., Hage, A., **van Tol, S.**, Rajsbaum, R. (2020). TRIM Proteins in Host Defense and Viral Pathogenesis. *Current Clinical Microbiology Reports*. doi: 10.1007/s40588-020-00150-8.
- Giraldo, M.I., Hongjie, X., Aguilera-Aguirre, L., Hage, A., **van Tol, S.**, Shan, C., Xie, X., Sturdevant, G.S., Robertson, S.J., McNally, K.L., Meade-White, K., Azar, S.R., Rossi, S.L., Maury, W., Woodson, M., Ramage, H., Johnson, J.R., Krogan, N.J., Morais, M.C., Best, S.M., Shi, P-Y., Rajsbaum, R. (2020). Envelope Protein Ubiquitination Drives Zika Virus Entry and Pathogenesis. *Nature*. doi: 10.1038/s41586-020-2457-8.

- van Tol, S.***, Atkins, C.*, Bharaj, P., Rajsbaum, R., Freiberg, A.N. (2020). VAMP8 contributes to TRIM6-mediated type-I interferon antiviral response during West Nile virus infection. *Journal of Virology* 94(2). doi: 10.1128/JVI.01454-19. PMC6955268 (* denotes equal contribution)
- Short, S.M., **van Tol, S.**, Smith, B., Dong, Y., Dimopoulos, G. (2018). The mosquito adulticidal *Chromobacterium* sp. Panama causes transgenerational impacts on fitness parameters and elicits xenobiotic gene responses. *Parasites & Vectors*, 11(1): 229. doi: 10.1186/s13071-018-2822-8.
- Short, S. M., **van Tol, S.**, MacLeod, H. J., & Dimopoulos, G. (2018). Hydrogen cyanide produced by the soil bacterium *Chromobacterium* sp. Panama contributes to mortality in *Anopheles gambiae* mosquito larvae. *Sci Rep*, 8(1), 8358. doi:10.1038/s41598-018-26680-2.
- van Tol, S.***, Hage, A.*, Giraldo, M. I., Bharaj, P., Rajsbaum, R. (2017). The TRIMendous Role of TRIMs in Virus-Host Interactions. *Vaccines*, 5(3): E23. doi: 10.3390/vaccines5030023.
- Evans, A. B., Loyd, H., Dunkelberger, J. R., **van Tol, S.**, Bolton, M.J., Dorman, K.S., Dekkers, J.C.M., Carpenter, S. (2017). Antigenic and Biological Characterization of ORF2-6 Variants at Early Times Following PRRSV Infection. *Viruses*, 9(5): 113.
- van Tol, S.**, Dimopoulos, G. Influences of the Mosquito Microbiota on Vector Competence. In A.S. Raikhel (Ed.): *Progress in Mosquito Research*, Vol 51, AIPP, pp. 243-291. UK: Academic Press, 2016.

Permanent address: 7840 S. Kostner Ave, Chicago, IL 60652

This dissertation was typed by Sarah Rose van Tol